DUKE POWER COMPANY

McGUIRE NUCLEAR STATION
CATAWBA NUCLEAR STATION

NUCLEAR PHYSICS METHODOLOGY FOR RELOAD DESIGN

DPC-NF-2010

April, 1984

Nuclear Production Department
Nuclear Engineering

MCGUIRE NUCLEAR STATION
CATAWBA NUCLEAR STATION

NUCLEAR PHYSICS METHODOLOGY FOR RELOAD DESIGN

DPC-NF-2010
APRIL, 1984

L. H. FLORES
W. G. JEFFERIES
J. H. RANDLES
D. E. BORTZ
R. H. CLARK

DUKE POWER COMPANY
NUCLEAR PRODUCTION DEPARTMENT
NUCLEAR ENGINEERING
NUCLEAR DESIGN

STATEMENT OF DISCLAIMER

This report was prepared by Duke Power Company ("Duke Power") for filing with the United States Nuclear Regulatory Commission ("USNRC") for the sole purpose of obtaining approval of Duke Power's PWR nuclear design methods at McGuire and Catawba. Duke Power makes no warranty or representation and assumes no obligation, responsibility, or liability with respect to the contents of this report or its accuracy or completeness. Any use of or reliance on the report or the information contained in this report is at the sole risk of the party using or relying on it.

ABSTRACT

This Technical Report describes Duke Power Company's Nuclear Design Methodology for the McGuire and Catawba Nuclear Station. The nuclear design process consists of mechanical properties used as nuclear design input, the nuclear code system and methodology Duke Power intends to use to perform design calculations and to provide operational support, and the development of statistical reliability factors.

TABLE OF CONTENTS

TABLE OF CONTENTS (Contd.)

TABLE OF CONTENTS (Contd.)

TABLE OF CONTENTS (Contd.)

TABLE OF CONTENTS (Contd.)

LIST OF TABLES

LIST OF TABLES (Contd.)

LIST OF FIGURES

LIST OF FIGURES (Contd.)

1. Introduction

1.1 Introduction

A commercial Pressurized Water Reactor (PWR) is designed to hold a constant number of nuclear fuel assemblies which are generally identical mechanically, but differ in the amount of fissile material content. During cycles subsequent to the initial cycle, fuel assemblies differ in burnup as well. Refueling occurs at intervals of 6 to 18 months, depending on the utility's operational requirements. At refueling, a predetermined number of irradiated fuel assemblies are discharged and the same number are loaded as fresh (reload region) or possibly irradiated assemblies. The fuel management scheme determines the locations of all fresh and irradiated assemblies.

This report describes some of the various aspects of nuclear design with principal emphasis placed upon development of a core loading pattern and nuclear calculations performed to evaluate safety and operational parameters. The following sections provide detailed discussion, including descriptions, of design methods, analytical formulations, and calculational procedures involved in the various nuclear design tasks for the McGuire and Catawba Nuclear Stations. The nuclear design is essentially a series of analytical calculations with the objective of designing the reload core in such a manner that the reactor can be operated up to a specified power level for a specified number of days within acceptable safety and operating limits. It consists of the development of the basic specifications of the reload region (fuel enrichment, number of assemblies, uranium loading, etc.); it sets forth the number and identity of each residual fuel assembly, selects the location of each fuel assembly in the core for the new fuel cycle, establishes the core characteristics. The nuclear design used in conjunction with the thermal hydraulic and safety analyses establishes the operating limits, control rod limits, and protection system setpoints.

In arriving at the final nuclear design, the designer tries to meet the

requirements imposed by the operational considerations, fuel economics considerations, and safety considerations. These requirements are called nuclear design criteria and are as follows:

1. Initial core excess reactivity will be sufficient to enable full power operation for the desired length of the cycle.

2. The fuel assemblies to be discharged at the end of the fuel cycle will attain maximum permissible burnup so that maximum energy extraction consistent with the fuel mechanical integrity criteria is achieved.

3. Values of important core parameters (moderator temperature coefficient, Doppler coefficient, ejected rod worth, boron worth, control rod worth, maximum linear heat rate of the fuel pin at various elevations in the core, and shutdown margin) predicted for the cycle are conservative with respect to their values assumed in the safety analysis of various postulated accidents, and if they are not conservative, acceptable reevaluation or reanalysis of applicable accidents is performed.

4. The power distributions within the reactor core for all possible (or permissible) core conditions that could exist during the operation of the cycle will not lead to exceeding the thermal design criteria of the fuel or exceeding the LOCA-limited peaking factors.

5. Fuel management will produce fuel rod power and burnup consistent with the mechanical integrity analysis of the fuel rod.

The nuclear design process described in this report consists of mechanical properties used as nuclear design input, the nuclear code system and methodology Duke Power intends to use to perform design calculations and to provide operational support, and the development of statistical reliability factors.

1.2 Definition of Terms

The terms and symbols used in this report will be consistent with those employed by Westinghouse for its nuclear engineering reports. Presented below are terms which will be needed throughout the text of the report:

a/o atom percent
ARI all rods in
ARO all rods out

axial offset (A.O.)	$\frac{P_T - P_B}{P_T + P_B}$, where P_T is the integrated power in the top half of the core, and P_B is the integrated power in the bottom half of the core
β_i	delayed neutron fraction for group i
β_{eff}	effective delayed neutron fraction in core
BOL	beginning of life
BP	burnable poison
BU	fuel burnup
C_B	Chemical shim boron concentration in the main coolant
CZP	cold zero power
EOL	end of cycle life
EQXE	equilibrium xenon condition
GWD/MTU	Gigawatt days per metric ton of initial uranium metal, 1 GWD/MTU is 1000 MWD/MTU
HFP	hot full power
HZP	hot zero power

$\bar{I}$	delayed neutron importance factor
ΔI or Axial Flux Difference (A.F.D.)	flux difference between the top and bottom halves of the core; in this report, ΔI is a calculated value, rather than a difference between measured signals from the excore detectors
K(z)	F_Q^T normalized to the maximum value allowed at any core height
ℓ^*	prompt neutron lifetime
MOL	middle of cycle life
MWD/MTU	measure of energy extracted per unit weight of initial uranium metal fuel; is equal to 1 megawatt times 1 day, divided by 1 metric ton of uranium
pcm	percent mille (a reactivity change that equals 10^{-5} $\Delta\rho$)
ppm	parts per million by weight; which specifies the amount of chemical shim boron present by weight in the main coolant system
radial local	ratio of assembly maximum rod to assembly average x-y power
RCCA	rod cluster control assembly; the type of control rod assembly used in McGuire and Catawba. (All RCCA are full length absorbers for both plants.)
ρ	reactivity
$\Delta\rho$	$\frac{K_1 - K_2}{K_1 \times K_2}$, where K_1 and K_2 are eigenvalues obtained from two calculations where only one parameter was varied
shutdown margin	amount of negative reactivity (ρ) by which a reactor core is maintained in a HZP subcritical condition after a control rod trip
step	unit of control rod travel equal to 0.625 inch
T_{MOD}	moderator temperature; defined as the temperature corresponding to the average water enthalpy of the core
T_{res}	resonance temperature of the fuel
w/o	weight percent

Power distributions will be quantified in terms of hot channel factors. These factors are a measure of the peak pellet power and the energy produced in the coolant. The factors are:

Power density	thermal power produced per unit volume of the core (KW/liter)
Linear Power Density	thermal power produced per unit length of active fuel (KW/ft)
Average Linear Power Density	total thermal power produced in the core divided by the total active fuel length of all fuel rods in the core
Local Heat Flux	local heat flux on the cladding surface ($BTU/ft^2/hr$)
Rod Power or Integral Power	is the length integrated linear power density in one rod (KW)

Various hot channel factors are:

F_Q^T, Heat Flux Hot Channel Factor, the maximum local heat flux on the surface of a fuel rod divided by the average fuel rod flux, including conservatisms for fuel pellet and rod dimensional uncertainties.

F_Q^N, Nuclear Heat Flux Hot Channel, is defined as the maximum local fuel rod linear power density divided by the average linear power density, assuming nominal fuel rod and pellet dimensions.

F_Q^E, Engineering Heat Flux Hot Channel, is the allowance on heat flux required for manufacturing tolerances. The engineering factor allows for local variations in enrichment, pellet density and diameter. Combined statistically the net effect is a factor of 1.03 to be applied to calculated KW/ft.

$F_{\Delta H}^N$, Nuclear Enthalpy Rise Hot Channel Factor, is defined as the ratio of the integral of linear power along the rod with the highest integrated power to the average rod power.

It is convenient, for the purposes of discussion, to define subfactors of F_Q^T; however, design limits are set in terms of the total peaking factor.

F_Q^T = Total peaking factor or Heat Flux Hot Channel Factor

$$= \frac{\text{Maximum KW/ft}}{\text{Average KW/ft}}$$

without densification effects

$$F_Q^T = F_Q^N \times F_Q^E$$

$$= \max \left[F_{XY}^N (Z) \times P (Z)\right] \times F_Q^R \times F_Q^E$$

where:

F_Q^N and F_Q^E are defined above.

F_Q^R = 95/95 Relability factor for F_Q (Section 6.2.1.2)

F_{XY}^N (Z) = ratio of peak power density to average power density in the horizontal plane at elevation Z

P(Z) = ratio of the power per unit core height in the horizontal plane at elevation Z to the average value of power per unit core height

including densification allowance

$$F_Q^T = \max \left[F_{XY}^N (Z) \times P(Z) \times S(Z)\right] \times F_Q^R \times F_Q^E$$

where

S(Z) = the allowance made for densification effects at height Z in the core.

2. Fuel Description

The fuel is described as a composition of fuel assembly (material selection, fuel rod lattice), spacer grid (material selection, number of spacer grids and interface with internals), and fuel rod (rod dimensions, cladding type and dimensions, pellet density and dimensions, fuel stack height, fill gas pressure and composition).

2.1 Fuel Pellet

The fuel pellets are right circular cylinders consisting of slightly enriched uranium dioxide powder which has been compacted by cold pressing and then sintered to the required density. The ends of each pellet are dished slightly to allow greater axial expansion at the center of the pellets.

2.2 Fuel Rod

The fuel rods consist of uranium dioxide ceramic pellets contained in slightly cold worked Zircaloy-4 tubing which is plugged and seal welded at the ends to encapsulate the fuel.

Void volume and clearances are provided within the rods to accommodate fission gases released from the fuel, differential thermal expansion between the cladding and the fuel, and fuel density changes during irradiation, thus, avoiding overstressing of the cladding or seal welds. Shifting of the fuel within the cladding during handling or shipping prior to core loading is prevented by a stainless steel helical spring which bears on top of the fuel. During assembling of these rods, the pellets are stacked in the cladding to the required fuel height, the spring is then inserted into the top end of the fuel tube and the end plugs are pressed into the ends of the tube and welded. All fuel rods are internally pressurized with helium during the welding process in order to minimize compressive cladding stresses and prevent clad flattening due to coolant operating pressure.

2.3 Fuel Assembly

Each fuel assembly consists of 264 fuel rods, 24 guide thimble tubes and 1 instrumentation thimble tube all arranged within a supporting structure. The fuel assembly structure consists of a bottom nozzle, top nozzle, guide and instrument thimbles and grids.

The instrumentation thimble is located in the center position and provides a channel for insertion of an incore neutron detector, if the fuel assembly is located in an instrumented core position. This tube is a constant diameter and is expanded at the top and midgrids to force the thimble and sleeve outward to a predetermined diameter, thus joining the two components.

The guide thimbles are structural members which provide channels for the neutron absorber rods, burnable poison rods, neutron source or thimble plug assemblies. Each thimble is fabricated from Zircaloy-4 tubing having two different diameters. The tube diameter at the top sections provides the annular area necessary to permit rapid control rod insertion during a reactor trip. The lower portion of the guide thimble is swaged to a smaller diameter to reduce diametral clearances and produce a dashpot action near the end of the control rod travel during normal trip operation. Holes are provided on the thimble tube above the dashpot to reduce the rod drop time. The dashpot is closed at the bottom by means of an end plug which is provided with a small flow port to avoid fluid stagnation in the dashpot volume during normal operation.

The bottom nozzle serves as the bottom structural element of the fuel assembly and directs the coolant flow distribution to the assembly. The square nozzle is fabricated from Type 304 stainless steel and consists of a perforated plate and four angle legs with bearing plates. These legs form a plenum for the inlet coolant flow to the fuel assembly. The plate also prevents accidental downward ejection of the fuel rods from the fuel assembly. The bottom nozzle is fastened to the fuel assembly guide thimbles by weld-locked screws which penetrate through the nozzle and mate with a threaded plug in each guide thimble.

The top nozzle assembly functions as the upper structural element of the fuel assembly and provides a partial protective housing for the rod cluster control assembly or other core components. It consists of an adapter plate, enclosure, top plate and pads. The springs and bolts are made of Inconel 718, whereas the top nozzle is made of Type 304 stainless steel. The square adapter plate is provided with round penetrations and semi-circular ended slots to permit the flow of coolant upward through the top nozzle. Other round holes are provided to accept sleeves which are welded to the adaptor plate and mechanically attached to the thimble tubes. The top plate has a large square hole in the center to permit access for the control rods and the control rod spiders.

Holddown springs are mounted on the top plate of the top nozzle assembly and are fastened in place by bolts and clamps located at two diagonally opposite corners. On the other two corners integral pads are positioned which contain alignment holes for locating the upper end of the fuel assembly.

The fuel rods are supported at intervals along their length, by grid assemblies which maintain the lateral spacing between the rods. Each fuel rod is supported within each grid by the combination of support dimples and springs. The magnitude of the grid restraining force on the fuel rod is set high enough to minimize possible fretting, without overstressing the cladding at the point of contact between the grids and the fuel rods. The grid assemblies also allow axial thermal expansion of the fuel rods without imposing restraints sufficient to develop buckling or distortion of the fuel rods.

Two types of grid assemblies are used in each fuel assembly. Both types consist of individual slotted straps interlocked into an "egg-crate" arrangement. One type, with mixing vanes projecting from the edges of the straps into the coolant stream, is used in the high heat flux region of the fuel assemblies to promote mixing of the coolant. The second type, located at the ends of the assembly, does not contain mixing vanes on the internal straps. The outside straps on all grids contain mixing vanes which, in addition to their mixing function, aid in guiding the grids and

fuel assemblies past projecting surfaces during handling or during loading and unloading of the core.

As identified in Table 2-2, the optimized fuel assembly (OFA) design uses a Zircaloy-4 material for the intermediate grids. This material is primarily chosen for its low neutron absorption properties. The material used for the end grids is Inconel-718, chosen for its corrosion resistance and high strength properties. This design is compared to the standard fuel assembly design which utilizes Inconel-718 for all grid assemblies.

Because of the considerable design, engineering and testing needed to incorporate a new fuel design into a reload core, it is usually not considered unless there is sufficient economic, engineering or regulatory justification. If, however, sufficient justification exists, the new fuel design is typically documented in a generic topical report and the reload report would reference this topical report.

2.4 Core Component Data

The basic physical dimensions and materials of the fuel pellet, fuel rod, fuel assembly, rod cluster control assembly, burnable poison assembly, and neutron source assembly are used in the fuel cycle design, thermal-hydraulic design and fuel mechanical performance. Table 2-1 presents a summary of this data for the Westinghouse standard fuel assembly design. In addition, Table 2-2 is presented to identify the significant differences between Westinghouse standard and optimized fuel assembly design. All data presented is intended as an example.

TABLE 2-1

WESTINGHOUSE
SYSTEM AND COMPONENT DATA
OPTIMIZED FUEL ASSEMBLY DESIGN

Active Core

Equivalent Diameter, in.	132.7
Core Average Active Fuel Height, First Core, in. (cold dimensions)	144
Height-to-Diameter Ratio	1.09
Total Cross-Section Area, ft^2	96.06
H_2O/U Molecular Ratio, Lattice (Cold)	2.73

Fuel Assemblies

Number	193
Rod Array	17 x 17
Rods per Assembly	264
Rod Pitch, in.	0.496
Overall Transverse Dimensions, in.	8.426 x 8.426
Fuel Weight (as UO_2), lbs.	204,200
Zircaloy Weight, lbs. (active core)	45,352
Number of Grids per Assembly	two - R type six - Z type
Composition of grids	two INC718 End Grids six ZIRC4 Spacer Grids
Weight of Grids (Effective in Core) lbs.	INC - 332 Zirc - 2985
Number of Guide Thimbles per Assembly	24
Composition of Guide Thimbles	Zircaloy 4
Diameter of Guide Thimbles (upper part), in.	0.442 I.D. x 0.474 O.D.
Diameter of Guide Thimbles (lower part), in.	0.397 I.D. x 0.429 O.D.
Diameter of Instrument Guide Thimbles, in.	0.442 I.D. x 0.474 O.D.

TABLE 2-1 (Continued)

Fuel Rods	
Number Per Assembly	264
Outside Diameter, in.	0.360
Diametral Gap, in.	0.0062
Clad Thickness, in.	0.0225
Clad Material	Zircaloy-4
Fuel Pellets	
Material	UO_2 Sintered
Density (percent of Theoretical)	95
Diameter, in.	0.3088
Length, in.	0.510
Mass of UO_2 per Foot of Fuel Rod, lb/ft	0.334
Hybrid Rod Cluster Control Assemblies	
Neutron Absorber	B_4C
B_4C Diameter, in.	0.294
Density, lbs/in^3	0.064
Tip Material	Ag-In-Cd
Composition	80%, 15%, 5%
AgInCd Diameter, in.	0.301
Length, in.	40
Density, lbs/in^3	0.367
Cladding Material	Type 304, Cold Worked Stainless Steel
Clad Wall Thickness, in.	0.0385
Number of Clusters	
Full Length	53
Number of Absorber Rods per Cluster	24
Full Length Assembly Weight (dry), lb.	90

TABLE 2-1 (Continued)

Burnable Poison Rods

Material	Borosilicate Glass
Outside Diameter, in.	0.381
Inner Tube, O.D., in.	.1815
Clad Material	Stainless Steel
Inner Tube Material	Stainless Steel
Boron Loading (w/o B_2O_3 in glass rod)	12.5
Weight of Boron - 10 per foot of rod, lb/ft	.000419

Ag-In-Cd Rod Cluster Control Assemblies

Neutron Absorber	Ag-In-Cd
Composition	80%, 15%, 5%
Diameter, in.	0.341
Length, in.	142.0
Density, lbs/in^3	0.367
Cladding Material	Type 304, Cold Worked Stainless Steel
Clad Wall Thickness, in.	0.0185
Number of Absorber Rods per Cluster	24

TABLE 2-2

COMPARISON OF 17 x 17 OPTIMIZED ASSEMBLY
AND 17 x 17 STANDARD ASSEMBLY DESIGN PARAMETERS

Parameter	Optimized Assembly Design	Standard Design
Fuel Ass'y. Length, in.	159.8	159.8
Fuel Rod Length, in.	151.6	151.6
Assembly Envelope, in.	8.426	8.426
Compatible with core internals	Yes	Yes
Compatible w/Movable In-Core Detector System	Yes	Yes
Fuel Tube Material	Zircaloy-4	Zircaloy-4
Fuel Rod Clad OD, in.	0.360	0.374
Fuel Rod Clad Thickness, in.	0.0225	0.0225
Fuel/Clad Gap, mil	6.2	6.5
Fuel Pellet dia. in.	0.3088	0.3225
Relative UO_2/Rod	0.92	1.0
Guide Thimble Material	Zircaloy-4	Zircaloy-4
Guide Thimble OD, in.	0.474	0.482
Guide Thimble Wall Thickness, in.	0.016	0.016
Spacer Grid Structural Mat'l. inner grid (6)	Zircaloy-4	Inconel-718
Spacer Grid Structural Mat'l. end grid (2)	Inconel-718	Inconel-718
Grid Support for Fuel Rods	6 Point; 2 Springs + 4 Dimples	6 Point; 2 Springs + 4 Dimples
Grid Height, inch, less vanes/inner straps	2.25	1.32
Grid Fabrication Method	Laser welded joining of interlocking stamped straps	Brazed joining of interlocking stamped straps
Grid/Guide Thimble Attach.	Thimbles bulged together with sleeves laser prewelded onto grid straps	Thimbles bulged together with sleeves prebrazed onto grid straps

3. Nuclear Code System

3.1 Introduction

Nuclear design calculations performed for Westinghouse reactors employ the EPRI-ARMP code system[1] and the CASMO-2 code[2]. A summary description of each code is given in Appendix A. The ARMP/CASMO-2 code sequence has been reviewed and approved by the NRC for use in the design of reload cores for Oconee Nuclear Station by Duke Power[3]. Presented in this section will be a description of the sequence, cross section preparation and parameterization, PDQØ7[4] modeling procedures, and EPRI-NODE-P[5] modeling procedures.

The nuclear calculational system enables the nuclear engineer to numerically model and simulate the reactor core. The system used by Duke Power for McGuire and Catawba is outlined in Figure 3-1.

3.2 Sources of Input Data

The determination of nuclear fuel loading patterns and core physics characteristics requires an accurate database consisting of:

1. Core operating conditions
2. Dimensional characteristics
3. Composite materials and mechanical properties
4. Nuclear cross sections

The FSAR, supplemented by vendor reports and open literature, is the primary source of data for items 1 to 3. These data are used as input to the cross section generators and core simulators. A secondary data source for the core simulators are estimates of fuel pellet volume-averaged temperatures which are calculated by a fuel performance code, such as COMETHE-IIIK[6] or TACO-2[7], as functions of power and burnup.

The cross section generators CASMO-2 and EPRI-CELL[8] use processed ENDF/B libraries unique to each code.

EPRI-CELL is a unit cell lattice code which is used to calculate few-group cross sections for fuel and nonfuel compositions as shown in Table 3-1.

CASMO-2 uses a processed version[9] of the ENDF/B-3 library. Group cross sections of σ_a, σ_f, $\nu\sigma_f$, σ_{tr}, scattering kernels, resonance integrals, and fission product data are among the data contained in this library. The 69 group library is divided into 14 fast, 13 resonance, and 42 thermal energy range groups. A 25 group version of this library is also used.

The EPRI-CELL library is derived from the ENDF/B-4 library[10]. The 97 energy groups are divided into 62 fast groups and 35 thermal groups.

3.3 Cross Section Preparation

In order to model the neutronics of a reload core, it is necessary to generate a set of cross sections for use in a diffusion theory code. Two cross section generators are currently used at Duke Power: Table 3.1 shows the core materials or compositions which are parameterized by CASMO-2 and EPRI-CELL.

Inputs which are provided to both codes are: lattice materials and geometry, temperatures for fuel, clad, and moderator, effective resonance temperature, fuel enrichment, soluble boron concentration, number of depletion steps, length of depletion steps, etc.

3.3.1 Fuel Calculations

Calculations for fuel regions employ fixed fuel and moderator temperatures for the cell depletion. Restart calculations are performed at various burnups to parameterize fuel cell cross sections at varying moderator and fuel temperatures.

The output of EPRI-CELL and CASMO-2 consists of sets of broad group cross sections which characterize the regions of interest. Cross sections are then formatted into PDQØ7 tableset structure using either NUPUNCHER[11] (1-dimensional parameterization), or MULTIFIT[12] (2 and 3 dimensional parameterization or g-factors). Cross sections from CASMO-2 are similarly formatted using CHART.[13]

3.3.2 Non-Fuel Calculations

Cross sections for empty control rod guide tubes, reflector, instrument thimble, and the water gap are calculated with either EPRI-CELL or CASMO-2. Separate cross section sets are generated for various moderator temperatures.

Strong absorbers such as RCCA and BP require reaction rate matching to obtain diffusion theory eqivalent cross sections. Calculations using CASMO-2 are performed for these strong absorbers where first a transport theory method determines absorption rates, and then a series of diffusion theory iterations are performed to calculate a g-factor such that the absorption rates agree between both types of flux solutions. These g-factors are then incorporated in the tabulated cross sections.

RCCA cross sections are evaluated at BOL HFP conditions, while BP cross sections are evaluated with an HFP depletion calculation.

In both types of g-factor calculations, lattices with expected core average enrichments are used. Core baffle cross sections are also calculated with CASMO-2. A lattice geometry is employed, with the baffle material density modified to reflect real versus modeled thickness in the quarter core PDQØ7 discrete pin model.

3.4 PDQØ7 Models

The PDQØ7 few-group diffusion-depletion code is employed for core modeling. Two different models are used currently.

The first is the assembly colorset model, which is used for calculating k_∞ and M^2 data for EPRI-NODE-P 3-D simulations. The second model is the quarter-core model, which is used for X-Y power distribution calculations and for normalization of EPRI-NODE-P radial power distributions.

Aspects which are common to both PDQØ7 models are:

1. Discrete pin representation
2. Two-group cross sections
3. Mixed Number Density thermal group constants

4. Improved Removal Treatment removal cross sections
5. Microscopic cross section parameterization for uranium, plutonium, burnable absorber, soluble boron, xenon, samarium, and lumped fission products
6. Thermally expanded geometry - pin pitch and assembly pitch

3.4.1 Colorset PDQØ7 Modeling

The colorset PDQØ7 model consists typically of four quarter assemblies arranged such that a representative neutron spectrum is obtained. Figure 3-2 shows a typical colorset geometry.

To accommodate asymmetric burnable poison rod loadings, full or half assembly geometries are used. The EPRI-ARMP PWR Procedures[14] are used for modeling, and most of the conventions and guidelines are employed.

Fuel types are determined according to enrichment and BPRA loading. K_∞ and M^2 data for each fuel type are calculated by performing the following operations:

I. BOL Cases - 0 MWD/MTU
   - A. k_∞ and M^2 - unrodded vs. T_{mod} (Inlet, Average, Outlet)
   - B. k_∞ and M^2 - rodded vs. T_{mod} (Inlet, Average, Outlet)
   - C. Boron worth
   - D. Doppler worth

II. Depletion Data - Exposure dependent data
   - A. Nominal HFP depletion at constant T_{mod}, T_{fuel}
   - B. Branch cases from depletion
     1. Boron worth
     2. Control rod worth
     3. Equilibrium Xenon worth
     4. Doppler worth
     5. Moderator temperature worth

In the above PDQØ7 branch calculations, only one parameter is varied, allowing a partial derivative of reactivity with respect to that parameter to be calculated.

The parameterization procedure involves approximately 150-200 cases, depending on the number of depletion steps.

The output from the PDQØ7 colorset cases is written to PDQØ7 integral files which in turn are processed by the linking codes EPRI-FIT[15] and SUPERLINK[16] to yield B-constant data for EPRI-NODE-P.

3.4.2 Quarter Core PDQØ7 Model

Two-dimensional X-Y core simulations are performed with a discrete pin PDQØ7 model. Assembly average and maximum pin powers are calculated, along with critical boron concentrations and other reactivity parameters. Moderator and doppler feedbacks are incorporated in this model.

The geometry employed utilizes thermally expanded dimensions. Figure 3-3 shows a geometry of a fuel assembly and water gaps. Figure 3-4 shows the complete quarter core mesh layout.

The plane of solution used in quarter core analyses is the axial midplane or the six foot level of the active fuel. Moderator and doppler feedbacks are employed as described in Reference 17.

The depletion calculation is used to determine burnup dependent parameters. The soluble boron concentration is modified at each timestep such that the reactor is approximately critical.

Timesteps are taken using point depletion so that the core average exposure advances by: 150, 500, 1000, 2000, ..., N * 2000 MWD/MTU until end of life (EOL) is reached. EOL is typically defined as that exposure where the critical boron at hot full power, equilibrium xenon conditions is 10 ppmB.

PDQØ7 depletion calculations are used to determine the following parameters:

1. Assembly average and maximum pin powers
2. Core reactivity

3. Nuclide reaction rates: Fission and absorption
4. Nuclide inventories
5. Neutron flux distributions

Other calculations performed with the quarter core model may include:

1. RCCA bank worths
2. Boron and xenon worths
3. Power deficits
4. Moderator and doppler temperature coefficients

Cases 2, 3, and 4 are usually performed with a nodal code; however, these are shown to demonstrate the quarter core model's flexibility.

3.5 EPRI-NODE-P Model

EPRI-NODE-P is the nodal code employed for three-dimensional analyses and reactivity studies. A summary description of EPRI-NODE-P is given in Appendix A. Typical calculations which are performed with the Duke Power EPRI-NODE-P model are:

1. Full core ejected rod worths
2. Power deficits
3. Differential rod worths
4. Axial xenon transients
5. Three-dimensional power distributions, etc.

The quarter core model uses one radial node per assembly and eighteen axial nodes.

Each unique combination of enrichment and BPRA loading comprises a separate fuel type. The fuel type is parameterized by sets of fitting coefficients which determine reactivity due to control rods, exposure, soluble boron, xenon, etc. Doppler and moderator feedbacks are explicitly treated.

EPRI-NODE-P radial power distributions are normalized near the beginning of cycle. Assembly average powers are adjusted to match quarter core PDQØ7 calculations with radial albedoes - α_H and an internal leakage factor - g_H. The axial power distribution, is adjusted using vertical leakage

factors α_v determined from comparisons of calculated and measured axial power distributions from benchmark core follow calculations.

Sections 5, 6, 7, and 9 discuss indepth calculational procedures of EPRI-NODE-P. Sections 10 and 11 address benchmarking of EPRI-NODE-P and PDQØ7 calculations to measured power and reactivity data.

TABLE 3-1

Codes Employed for Cross Section
Calculation by Composition

1. EPRI-CELL

   a. Uranium Fuel
   b. Empty Control Rod Guide Tube/Instrument Tube
   c. Reflector
   d. Water Gap

2. CASMO-2

   a. Burnable Poison Rod Assembly
   b. Gadolinia doped Uranium Fuel
   c. Control Rod - AgInCd or B_4C
   d. Baffle

Figure 3–1

NUCLEAR FLOW CHART

FOR EPRI–ARMP

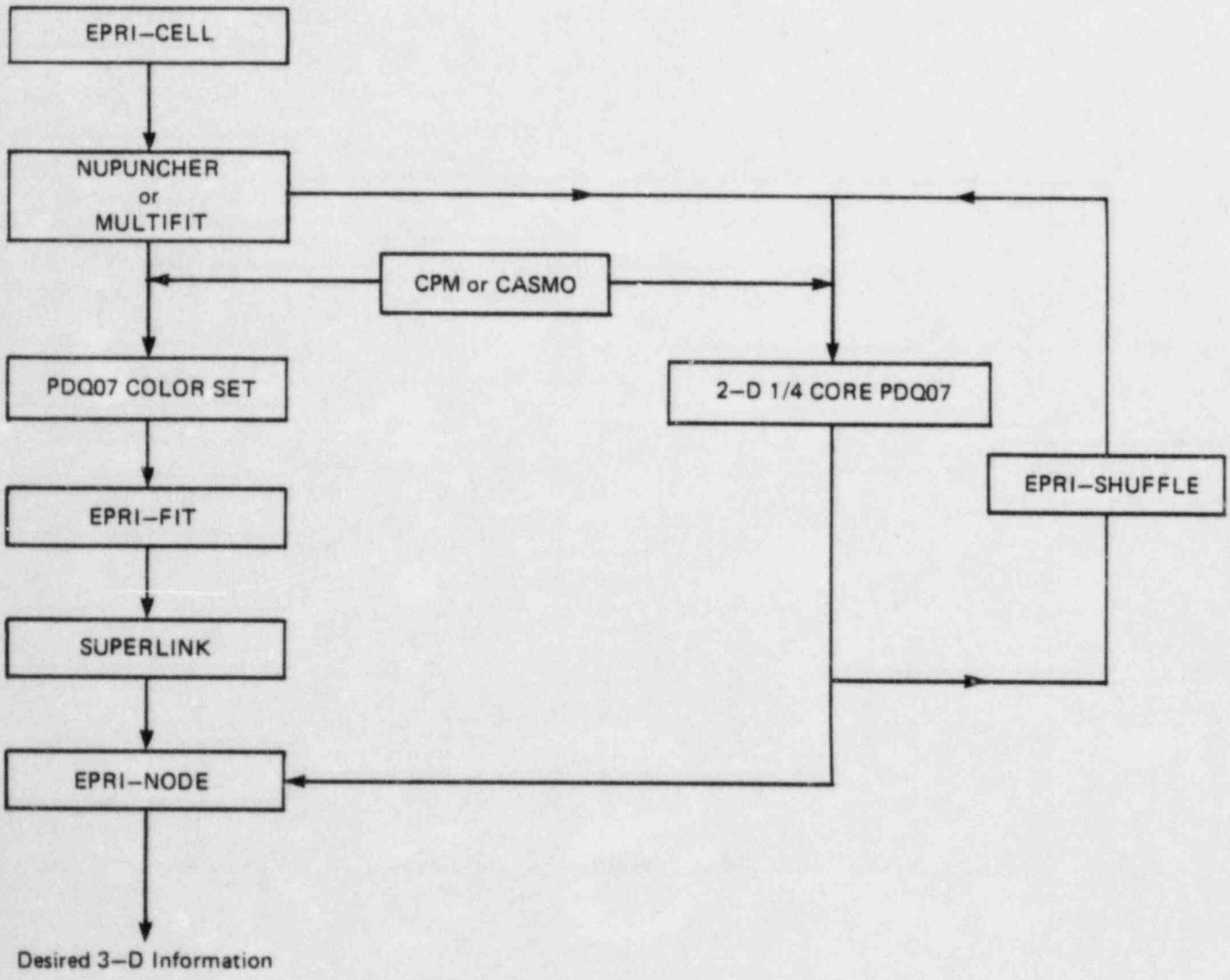

FIGURE 3-2

17X17 ASSEMBLY PDQ07

COLORSET GEOMETRY

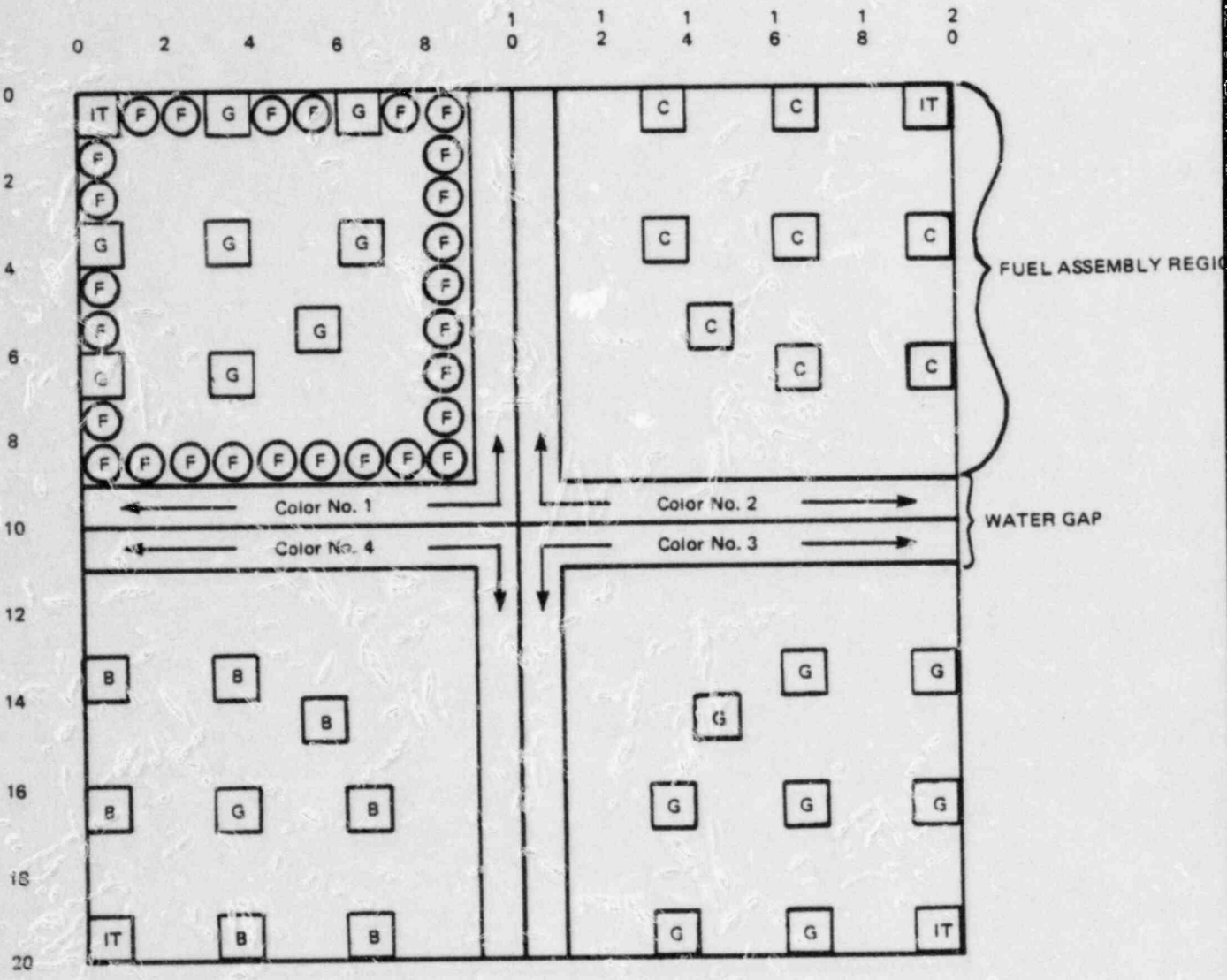

LEGEND:

IT INSTRUMENT TUBE
C GUIDE TUBE WITH CONTROL ROD
G EMPTY GUIDE TUBE
B GUIDE TUBE WITH BURNABLE POISON ROD
F FUEL ROD

FIGURE 3–3

PDQ07 QUARTER CORE MODEL

ASSEMBLY GEOMETRY

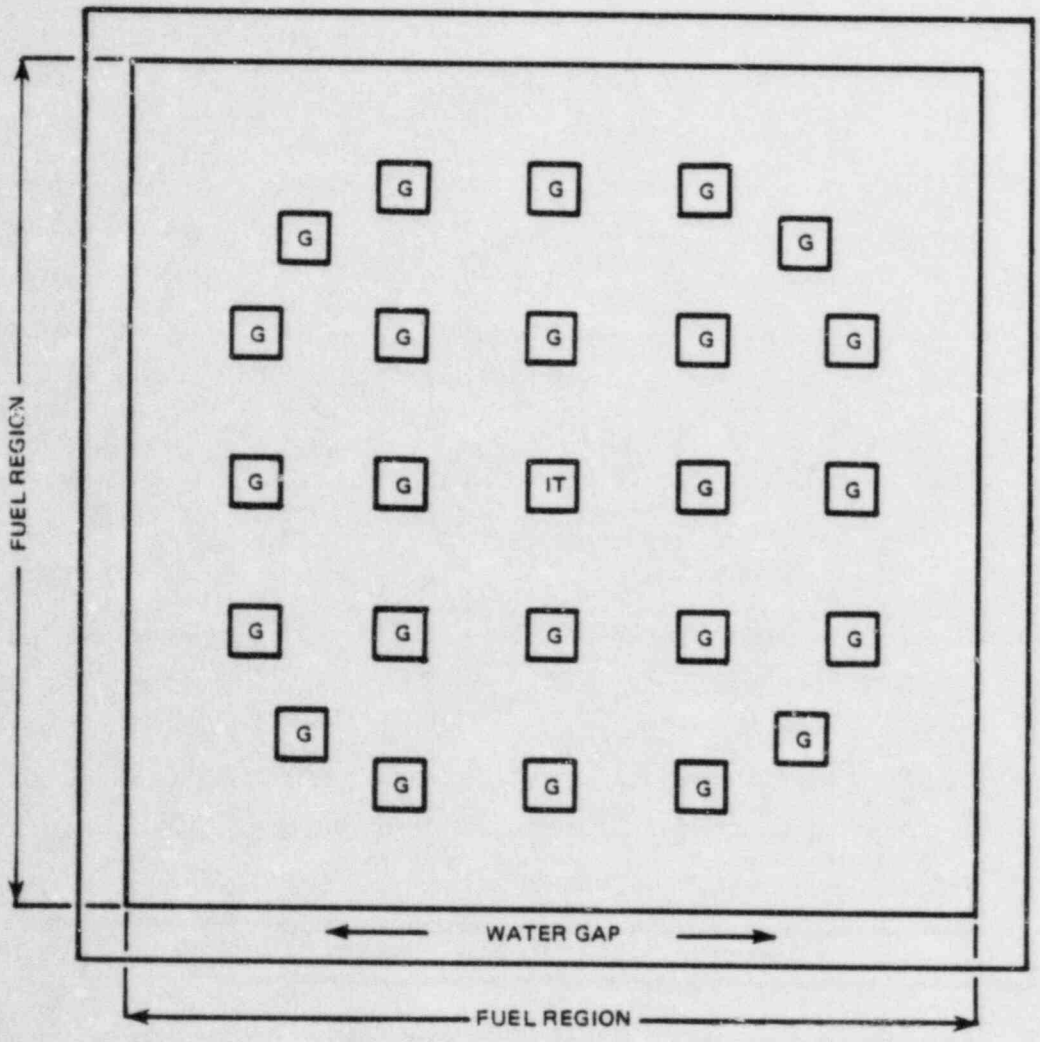

LEGEND:

IT: INSTRUMENT TUBE
G: CONTROL ROD GUIDE TUBE

FIGURE 3–4

PDQ07 QUARTER CORE

17X17 GEOMETRY

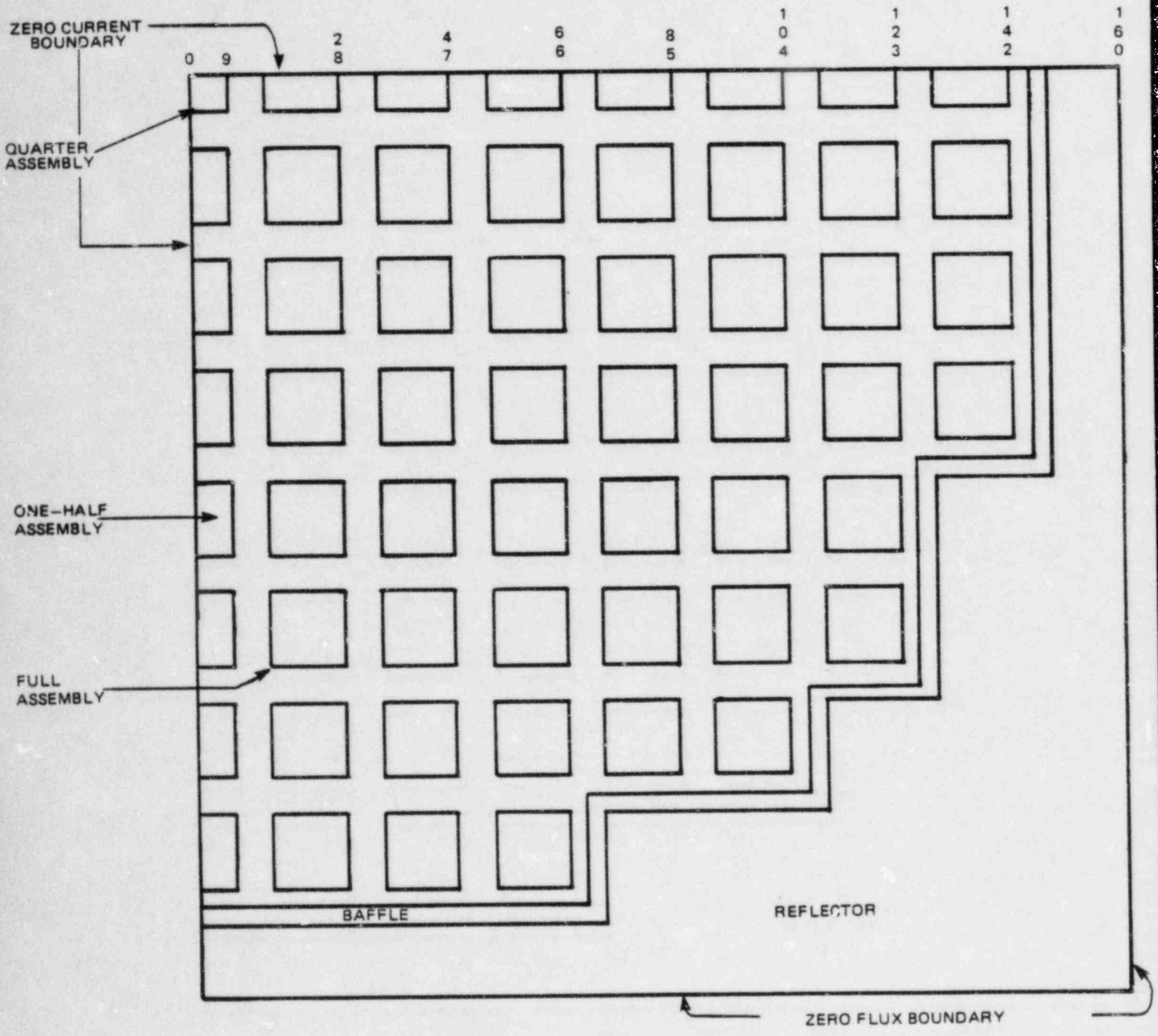

4. Fuel Cycle Design

4.1 Preliminary Fuel Cycle Design - Initialization

To commence the design of a reload, an initialization procedure is used. Core operation requirements along with planned changes in reactor primary or secondary systems are assembled. A preliminary loading pattern is designed which meets operational requirements. Physics data from the preliminary design are compared with core operating requirements to determine the adequacy of the reload design. Likewise, physics data are compared to Technical Specifications to verify that the preliminary design will conform to existing limits.

4.1.1 Review of Design Basis Information

The preliminary design procedure requires assembly of design basis information which in turn will determine the cycle's operational capabilities. Typical design basis data are shown on Table 4-1.

Table 4-1 and other pertinent nuclear design data are assembled and reviewed for consistency with previous sets of design basis data.

4.1.2 Determination of Cycle-Specific Operating Requirements

Design basis data from Table 4-1 uniquely determines expected operating requirements and capabilities. For instance, a longer than annual cycle may require a low leakage loading pattern and the use of burnable absorber rods. A larger energy requirement than can be provided by normal operation with a given reload enrichment may require a planned power coastdown at end of cycle. Similarly, other design bases will govern the rest of the cycle-specific operational characteristics.

4.1.3 Preliminary Loading Pattern and Reload Region Determination

The purpose of a preliminary loading pattern analysis is to determine the uranium and separative work requirements to meet a desired cycle lifetime. The cycle lifetime is either estimated by the BOL excess reactivity (ρ_{exc}) or by a reload core depletion with a coarse mesh PDQØ7 or a nodal (EPRI-NODE-P) model. If the number of new fuel assemblies and their enrichment is known, this analysis will yield an estimate of the cycle lifetime.

When uranium requirements are to be determined, an iterative series of BOL calculations are performed in which:

1. A loading pattern is developed with a reasonable radial power distribution.
2. The BOL excess reactivity (ρ_{exc}) is calculated when ρ_{exc} is defined below.
3. If ρ_{exc} is sufficient to meet design cycle burnup, the chosen fixed enrichment and number of assemblies is used.
4. If ρ_{exc} is not sufficient, the enrichment/number of assemblies are modified and Step 1 is again performed.

The analysis of BOL excess reactivity uses the following definitions of ρ_{exc}:

$$\rho_{exc} = \frac{K'_{eff} - 1}{K'_{eff}}$$

where: K'_{eff} is the HFP, EQXE, equilibrium SM, at BOL at BOL and 0 PPMB.

For out-in reloads, ρ_{exc} is a fairly linear function of burnup. Therefore, for this type of reload, an estimate of cycle lifetime can be made with a high degree of confidence.

However, for cores which use low leakage loading patterns, the cycle lifetime is usually confirmed by using either a coarse mesh PDQØ7 model or a NODE-P model depletion of the reload core.

4.2 Final Fuel Cycle Design

Having determined the number and enrichment of the fuel assemblies during the PFCD, the final fuel cycle design (FFCD) concentrates on optimizing the placement of fresh and burned assemblies and burnable poison assemblies (if any) to result in an acceptable fuel cycle design. It must meet the following design criteria with appropriate reductions to account for calculational uncertainties:

1. $F^N_{\Delta H}$ - See Table 4-3.

2. Moderator Temperature Coefficient must meet Technical Specification requirements for all operating modes.
3. Maximum pellet burnup $\leq$ 50,000 MWD/MTU.
4. Shutdown Margin must meet Technical Specification requirements for all operating modes.
5. Maximum linear rod power $\leq$ 12.9 Kw/ft at 102% power.
6. Ejected rod F_Q and worth to be within limits of FSAR.
7. Dropped rod maximum $F^N_{\Delta H}$ to be within FSAR limits.

During the FFCD, nuclear calculations are performed to generate these parameters for input to fuel mechanical performance analyses, thermal and thermal-hydraulic analyses, and maneuvering analyses.

4.2.1 Fuel Shuffle Optimization and Cycle Depletion

BOC power distribution calculations are performed using combinations of EPRI-SHUFFLE and PDQ07. Initial runs start with the fuel shuffle scheme developed in the PFCD and the shuffle scheme (fuel assembly loading pattern) is modified to minimize power peaking. This is accomplished by a trial and error type search until an acceptable BOC power distribution results.

The reload design's "burnup window" is assessed at BOC to ensure that preliminary safety criteria are met. That is, in the design of cycle N, effects of tolerances in core burnup achieved during cycle N-1 are examined. At the lower cycle N-1 core burnup, the moderator temperature coefficient is calculated to ensure that Technical Specification limits are met. At the higher cycle N-1 burnup, the power distribution is calculated to verify that power peaking is not excessive. This analysis ensures that the design of cycle N is adequate at BOC, given a predetermined tolerance on the core burnup for cycle N-1.

The cycle is then depleted in steps corresponding to 0, 150, 500, 1000, 2000, 4000...MWD/MTU to verify that power peaking versus burnup remains acceptable. The shuffling variations include rearranging the location

of the burned or fresh fuel assemblies, BP placement, and rotation of the spent fuel assemblies. These calculations are typically performed assuming quarter core symmetry.

The shuffle pattern determined by optimizing power distribution may later need to be modified based upon results obtained in the remaining nuclear calculations.

4.2.2 Rod Worth Calculations

Control rods serve several functions in the McGuire reactor. The primary function is to provide adequate shutdown capability during normal and accident conditions. They are also used to maintain criticality during power maneuvers and to maintain the Axial Flux Difference (AFD) within Technical Specification limits. Since the presence of control rods influences both power distributions and criticality, it is necessary in many calculations to evalute not only the reactivity effect but also the perturbation that a given rod configuration has on the power distribution.

McGuire and Catawba are typically operated in the ARO or feed and bleed mode. All RCCA have full length absorber rods. During full power operation, control bank D is typically inserted about six inches (215 steps withdrawn) in the active core. Bank D is used to control power during load follow maneuvers and, in conjunction with banks B and C, to achieve criticality during startup.

Calculations of control rod worth and power peaking (F_Q) are used in the safety analysis of the reload core. The calculations discussed in subsequent sections include the following:

1. Control Rod Worths
2. Shutdown Margin
3. Ejected Rod Analysis
4. Dropped Rod Analysis

4.2.2.1 Control Rod Worths

RCCA bank locations in McGuire and Catawba usually are fixed and do not change from cycle to cycle. The worth of each control bank (A, B, C, D) is calculated in quarter core geometry using either PDQØ7 or EPRI-NODE at BOC and EOC, at HFP and HZP. The total rod worth (ARI) is calculated at BOC, EOC, and any limiting burnup at HZP only for use in the shutdown margin calculation.

4.2.2.2 Shutdown Margin

Searches for the highest worth stuck rod are performed at BOC, EOC, or any limiting burnup for HZP conditions using full core EPRI-NODE and/or PDQØ7 calculations.

Table 4-2 summarizes the results of a shutdown margin calculation. The total rod worth described in section 4.2.2.1 is shown as Item 1. Item 2 is the worth of the highest stuck rod. The total worth reduced by the stuck rod worth is shown as the net worth (Item 3). A calculational uncertainty of 10% is subtracted off in Step 4, and Step 5 shows the available rod worth.

The required rod worth is calculated next in Steps 6-9. The power deficit obtained by running an EPRI-NODE or PDQØ7 cases at HFP and HZP (using constant Boron and Xenon) and subtracting the reactivities is shown as item 6. This reactivity insertion accounts for Doppler and Moderator deficits. The maximum allowable inserted rod worth, item 7, is obtained from the allowable rod insertion and the integral rod worth curve for that insertion (generated by EPRI-NODE). This accounts for the maximum allowed rod insertion at HFP. An axial flux redistribution occurs when the power level is reduced from HFP to HZP. This redistribution causes an increase in reactivity. If Item 6 is calculated using a 3-D code such as EPRI-NODE, no additional penalty is required here. However, if Item 6 was calculated using 2-D PDQØ7, an additional reactivity penalty is assessed as Item 8. The sum of these required worths (Item 9) is the total required worth.

The shutdown margin is shown as Item 10 and is defined as the total available worth minus the total required worth. For McGuire and Catawba, the Technical Specification requirements are 1.3% $\Delta\rho$ for $T_{AVG} \geq 200°F$ and 1.0% $\Delta\rho$ for $T_{AVG} < 200°F$.

4.2.2.3 Rod Insertion Limit Verification

As part of the reload design procedure, the current Rod Insertion Limits are verified for applicability in the reload core. (See Section 5.4.)

4.2.2.4 Ejected Rod Analysis

The Final Safety Analysis Report[18,19] (FSAR) presents two limiting criteria for the ejected rod accident: hot channel factor (F_Q) and reactivity insertion. The accident has been analyzed at HFP and HZP conditions at BOL and EOL.

Ejected rod calculations are performed on a Unit-specific basis to verify that reactivity insertions and hot channel factors do not exceed original FSAR accident analysis values.

Calculational limits are established by reducing FSAR values of reactivity insertion 10% and hot channel factor by 15%.

To verify that the ejected rod parameters are within calculational limits, ejected rod calculations are performed at BOC and EOC or at other limiting times in cycle life at both HFP and HZP.

The calculation of ejected rod parameters is accomplished using full core two dimensional pin mesh PDQØ7 or EPRI-NODE calculations. The HZP ejected rod calculations are performed with control banks B and C at their insertion limits in the core and with bank D fully inserted.

Single rods in banks D, C, and B are removed in subsequent cases and the worth of the ejected rod is calculated by subtracting the reactivities of the cases before and after the rod was removed. The fuel

and moderator temperature is held constant and equal to the HZP moderator temperature for these calculations. The highest worth calculated by the above procedure is the worst ejected rod at HZP. If the ejected rod worth exceeds the calculational limit, rod insertion limits are revised.

The HFP ejected rod worths are performed in a similar manner to the HZP calculations with the exceptions that only bank D is inserted at the HFP insertion limit and that the fuel temperature and moderator temperatures correspond to those of HFP conditions. The HFP ejected rod worths are performed without thermal feedback to be conservative. If the ejected rod worth exceeds the calculational limit, rod insertion limits are revised.

A parallel analysis, addressing F_Q, is performed at the same time as the rod worth analyses.

4.2.2.5 Dropped Rod Analysis

The calculation of the rod drop peaking factor is required to determine the DNBR resulting from the rod drop. Full core calculations using EPRI-NODE are performed with thermal-hydraulic feedback.

Search cases are run where single RCCA are inserted until the maximum $F^N_{\Delta H}$ and rod worth have been determined. RL factors, determined from PDQØ7 discrete pin calculations, are combined with nodal power data from EPRI-NODE with the NUC-MARGINS Code. NUC-MARGINS then calculates $F^N_{\Delta H}$ using the above data and additional factors to account for conservatism, tilt, and other parameters which would affect the value of $F^N_{\Delta H}$. This dropped rod $F^N_{\Delta H}$ and worth are used as input to the accident analysis evaluation.

4.2.3 Fuel Burnup Calculations

One of the current design criteria is that maximum pellet burnup is $\leq$ 50,000 MWD/MTU. This criterion is confirmed during the final fuel cycle design. Depletion calculations from 2-D quarter core pin mesh PDQØ7 models yield core, assembly average, and single fuel rod burnups. From these values a maximum ratio of single rod to assembly average

burnup can be calculated for each assembly. This data is then used in conjunction with 3-D EPRI-NODE depletion calculations (where the axial burnup distribution is calculated) to arrive at a local burnup limit which can be compared to the design limit of 50,000 MWD/MTU.

Generally, the assembly average burnups are in the 36,000 MWD/MTU range and sufficient margin to the 50,000 MWD/MTU limit exists to make the detailed calculation described above unnecessary.

As a result of DOE and EPRI extended burnup programs, along with fuel assembly design improvements, future relaxation of the burnup limit is expected.

4.2.4 Reactivity Coefficients and Defects

Reactivity coefficients define the reactivity insertion for small changes in reactor parameters such as moderator temperature, fuel temperature, and power level. These parameters are input to the safety analysis and used in modeling the reactor response during accidents and transients. Whereas reactivity coefficients represent reactivity effects over small changes in reactor parameters, reactivity defects usually apply to reactivity inserted from larger changes typical of HFP to HZP. An example of a reactivity deficit is the power defect from HFP to HZP used in the shutdown margin calculation. A different way of looking at the terms is that the coefficient when integrated over a given range yields the defect, or the coefficient is the partial derivative of reactivity with respect to one specific parameter.

Coefficients of reactivity are calculated using PDQØ7 or EPRI-NODE. First a nominal case is established at some reference conditions. Then one parameter of interest is varied up and/or down by a fixed amount in another calculation and the resulting change in core reactivity divided by the parameter change is the reactivity coefficient.

4.2.4.1 Doppler Coefficient

The Doppler Coefficient (DC) is the change in core reactivity produced by a small change in fuel temperature.

The major component of the Doppler Coefficient arises from the behavior of the Uranium-238 and Plutonium-240 resonance absorption cross sections. As the fuel temperature increases, the resonances broaden increasing the chance that a neutron will be absorbed and thus decreasing the core reactivity.

If Case 1 represents the reference case with an effective fuel temperature T_1 (and K^1 effective) and Case 2 represents a second case where the fuel temperature has been increased or decreased by approximately 50°F and is T_2, (and K^2 effective) the Doppler Coefficient is mathematically calculated from the following equation:

$$\alpha_D = \frac{\frac{K^1_{eff} - K^2_{eff}}{K^1_{eff} \times K^2_{eff}}}{T_1 - T_2} \times 10^5 = \Delta \text{ (pcm)/°F}$$

In the final fuel cycle design, both HFP and HZP Doppler Coefficients are calculated with either EPRI-NODE or PDQØ7.

4.2.4.2 Moderator Temperature Coefficient

The Moderator Temperature Coefficient (MTC) is the change in reactivity produced by a small change in moderator temperature. In McGuire and Catawba, the average core moderator temperature increases linearly as power is escalated from 0 to 100% HFP. At 100% HFP, the core average moderator temperature is approximately 592°F. Therefore, for accident and transient analyses it is necessary to know the moderator temperature coefficient over a range of moderator temperatures for CZP to HFP.

These analyses can be performed with either EPRI-NODE and/or PDQØ7 by effecting a change in the core average moderator temperature. Cases are run with the moderator temperature at 5°F above and at the reference temperatures. If these cases and the resulting $K_{effective}$'s are identified as Case 1

($TMOD_1$, K^1_{eff}) and Case 2 ($TMOD_2$, K^2_{eff}), the

moderator temperature coefficient is calculated from the following equation:

$$\alpha_{Tmod} = \frac{\frac{K^1_{eff} - K^2_{eff}}{K^1_{eff} \times K^2_{eff}}}{(TMOD_1 - TMOD_2)} \times 10^5 = \Delta\rho(pcm)/°F$$

Since the reload core is designed with a predetermined flexibility (burnup window), the MTC is verified to be within its design limit at the short end of the window as well as at the nominal BOC burnup.

4.2.4.3 Isothermal Temperature Coefficient

The fractional change in reactivity due to a small change in core temperature is defined as the isothermal temperature coefficient (ITC) of reactivity. This is equal to the sum of the moderator and Doppler temperature coefficients and may be explicitly calculated at HZP for isothermal conditions ($T_{FUEL}=T_{MOD}$) by setting both the fuel and moderator temperatures approximately 5°F above and at the reference HZP moderator temperature. This calculation may be performed with PDQØ7 and/or EPRI-NODE.

4.2.4.4 Power Coefficient and Power Defect

The power coefficient of reactivity is the core reactivity change resulting from an incremental change in core power level. The power defect is usually the total reactivity change associated with a power level change from HZP to HFP.

The power coefficient is defined by the following equation:

$$\alpha_P = \frac{\frac{K^1_{eff} - K^2_{eff}}{K^1_{eff} \times K^2_{eff}}}{P_1 - P_2} \times 10^5 = \Delta\rho(pcm)/\%\ power$$

where: K^1_{eff} is K-effective for the core at power P_1 (%)

K^2_{eff} is K-effective for the core at power P_2 (%)

Neglecting second order effects this equation is equivalent to the following:

$$\alpha_P = \alpha_{TMOD} \frac{\Delta TMOD}{\Delta P} + \alpha_D \frac{\Delta TFUEL}{\Delta P}$$

where: α_{TMOD} is the moderator temperature coefficient and α_D is the Doppler temperature coefficient.

Since the power coefficient should include flux redistribution effects resulting from axial variations in burnup and isotopics as well as non-uniform fuel temperature distributions, it should be performed using a 3-D simulator with thermal hydraulic feedback. If the calculation is performed using a 2-D model then it should be corrected for the 3-D effects.

A typical power coefficient calculation for HFP would proceed in the following manner: The HFP case is run using EPRI-NODE and the core K_{eff} is calculated (K^1_{eff}). Then a second EPRI-NODE case is run with the core power level reduced 5% while holding everything else constant. The K_{eff} from this case, K^2_{eff}, is used along with the results from the reference case to calculate the power coefficient:

$$\alpha_P = \frac{\frac{K^1_{eff} - K^2_{eff}}{K^1_{eff} \times K^2_{eff}} \times 10^5}{P_1 - P_2} = \frac{\Delta\rho(pcm)}{\% \text{ POWER}}$$

The power defect is calculated for use in the shutdown margin calculation (see Section 4.3.2.2) and is the reactivity change from HZP to HFP. This calculation should be performed in three dimensions to satisfactorily model the axial flux redistribution, however, a two dimensional calculation may be performed and corrected for this flux redistribution phenomenon.

Two EPRI-NODE or PDQØ7 runs are made to calculate the power defect. The first is made at 100% HFP and the second at HZP. These calculations are usually performed at BOC and EOC.

Both HFP and the HZP cases should have the equilibrium xenon concentration corresponding to HFP. The power defect is calculated from the following equation:

$$\text{Power Defect}_{\text{HFP} \rightarrow \text{HZP}} = \frac{K^1_{eff} - K^2_{eff}}{K^1_{eff} \times K^2_{eff}} \times 10^5 = \Delta\rho(\text{pcm})$$

where: $K^1_{effective}$ is core Keffective at HZP and

$K^2_{effective}$ is core Keffective at HFP.

4.2.4.5 Miscellaneous Coefficients

For reload design, certain coefficients of reactivity are not routinely calculated. These include moderator density coefficient, moderator pressure coefficient, and moderator void coefficient. These coefficients are calculated in an analogous manner by varying the appropriate core reactivity parameters.

4.2.4.6 Boron Related Parameters

Critical boron concentrations for various core conditions during cycle lifetime are calculated using PDQØ7 and/or EPRI-NODE. Table 4-4 lists conditions that critical boron concentrations and boron worths are calculated. In addition to these, an ARO critical boron letdown curve is generated for HFP EQXE.

4.2.4.7 Xenon Worth

The HFP equilibrium xenon worth is calculated at BOC (4 EFPD) and at EOC.

Calculations using either PDQØ7 or EPRI-NODE are performed for HFP equilibrium xenon conditions. If PDQØ7 is being used, a second no xenon case is run by either zeroing out the xenon number density or zeroing out the xenon cross section. If EPRI-NODE is being used, the power level on the xenon card can be set to zero and the time in hours set to 40.0 to obtain a no xenon concentration.

The difference in reactivities between the equilibrium and no xenon cases is the xenon worth. The xenon worth is used primarily for plant operation, i.e., startup after trip, rather than as a safety parameter.

4.2.4.8 Kinetics Parameters

The kinetics behavior of the nuclear reactor is often described in terms of solutions to the Inhour equation for six effective groups of delayed neutrons. Transient and accident analyses often involve kinetic modeling of the reactor core. The rate of change in power from a given reactivity insertion can be calculated by solving the kinetics equations if the six group effective delayed neutron fractions, the six group precursor decay constants, and the prompt neutron lifetime are known.

The computer codes used to calculate these parameters are PDQØ7 and DELAY. The method employed here is identical to that reviewed and approved by the NRC in Reference 20 for Oconee Reload Design. PDQØ7 is used to obtain spatially averaged isotopic fission rates as a function of burnup, and DELAY calculates kinetics parameters and then uses these parameters to solve the Inhour equation and thereby relate the stable reactor period to the reactivity insertion. This information is also needed for startup physics testing. Calculations are performed at BOL and EOL. The sum of the six group β_i effective, β effective, for the new reload cycle is compared to those values used in the FSAR.

4.2.5 Assessment of FFCD

Once the FFCD calculations are performed, the resultant data are assessed for validity and consistency with core operation requirements and safety limits.

The validation assessment consists of two different methods:

1. Comparison of calculations for reasonable agreement with previous data for similar conditions (i.e., comparison of BOL stuck rod worths for cycle N+1 to cycle N when both cycles have similar reload designs).
2. Checks of assumptions, intermediate calculations for code inputs, code input data and output are performed to insure calculational accuracy.

The assessment of consistency with requirements is also a two step procedure:

1. The calculated results must be within bounding values as determined by the Final Safety Analysis Report, or be proven to be non-limiting by way of a separate safety analysis or safety evaluation.
2. Calculated results must also show that core operational requirements are satisfied.

A complete discussion of requirements for documentation and quality assurance for safety related calculations is presented in Section 4.8 of the Duke Power Administrative Policy Manual for Nuclear Stations[21].

Table 4-1

Nuclear Design Basis Data
For Reload Design

1. Power operation mode: load follow or base load.
2. Vessel internal or core component modifications.
3. Expected minimum and maximum cycle burnups.
4. Feed enrichment (if already contracted for).
5. Number and design of feed assemblies.
6. RCS hydraulic conditions.

Table 4-2

Shutdown Margin Calculation

	BOC, % Δρ
Available Rod Worth	
1. Total rod worth, HZP	6.46
2. Maximum stuck rod, HZP	-1.39
3. Net Worth	5.07
4. Less 10% uncertainty	-.51
5. Total available worth	4.56
Required Rod Worth	
6. Power defect, HFP to HZP	.88
7. Max allowable inserted rod worth	.36
8. Flux redistribution	.63
9. Total required worth	1.87
10. Shutdown Margin (total avail. worth minus total required worth)	2.69

NOTE: Required shutdown margin is 1.30% Δρ for $T_{avg} \geq 200°F$.

Table 4-3

Maximum $F^N_{\Delta H}$ Factors for Design DNB

Assembly Type	Formulation[1]
17 x 17 Standard Design (Mixed OFA and STD)	1.49 (1 + .3 (1-P))
17 x 17 Optimized Design (Mixed OFA and STD)	1.49 (1 + .3 (1-P))
17 x 17 Optimized Design (All OFA)	1.49 (1 + .3 (1-P))

[1]Note: The value of 1.49 is a Technical Specification limit on the measured $F^N_{\Delta H}$. P is the normalized core power and is 1.0 at full power.

For reload design purposes, the calculational limit for $F^N_{\Delta H}$ is 1.435.

Table 4-4

Boron Parameters

Critical Boron - ppm

HZP, ARO, BOC, No Xenon

HZP, Bank D inserted, BOC, No Xenon

HZP, Bank D + C inserted, BOC, No Xenon

HFP, ARO, EQXE vs exposure

Boron Worth - ppm/%$\Delta\rho$

HFP, EQXE, ARO vs. exposure

HZP, NOXE, ARO vs. exposure

Boron Worth Versus Boron Concentration - HZP, NOXE

BOC

EOC

5. Nodal Analysis Methodology

5.1 Purpose and Introduction

Nodal analysis allows for modeling of the reactor core in three-dimensions and for performing calculations which because of either code restraints or economic restraints cannot be performed by any other means. Examples of nodal code capabilities include:

1. Calculations which need a three-dimensional geometry such as differential rod worths, axial xenon transients and three-dimensional power distributions.

2. Calculations which need a full-core geometry such as stuck and ejected rod worths.

This section addresses the role of a nodal code in performing cycle depletions, generating rod worth data, determining shutdown margins and shutdown boron concentrations, setting control rod insertion limits, and determining trip reactivity worths and shapes.

A nodal code is also used to calculate many of the startup test parameters and core physics parameters described in Section 9 of this report.

The nodal code used for McGuire and Catawba analyses is EPRI-NODE-P. (See descriptions in Section 3 and Appendix A). This code was approved by NRC for use in Oconee reload design in Reference 4. EPRI-NODE-P can be run with either a quarter-core or a full-core geometry. The McGuire and Catawba models utilize one radial node per assembly and twelve to eighteen axial nodes. EPRI-NODE-P radial powers are normalized to the two-dimensional PDQ07 assembly powers near the beginning of each cycle.

5.2 Fuel Cycle Depletion - Nodal Code

A fuel cycle depletion is performed for each cycle using nodal analysis. The nodal radial powers are normalized to the two-dimensional quarter-core PDQ07 powers at HFP conditions with equilibrium xenon and samarium at approximately 1000 MWD/MTU (25 EFPD) into the cycle. The nodal core

model is then depleted from BOC to EOC in steps corresponding to 0, 150, 500, 1000, 2000, 4000....MWD/MTU. This depletion is performed in the critical boron search mode, with nominal rod insertion (usually 215 SWD) and equilibrium xenon.

History files are saved at each burnup step throughout the cycle depletion. These history files contain records of the power, exposure and xenon concentration for each node in the core.

As a result of the nodal core depletion, the following data is obtained:

1. Two and three-dimensional power distributions at each burnup step.

2. A boron letdown curve, i.e., critical boron concentrations as a function of burnup.

3. Axially-dependent parameters such as offset or axial flux difference as a function of burnup.

4. Assembly exposures as a function of core-averaged burnup.

5. History files at approximately every 2000 MWD/MTU throughout the cycle saved for later use.

5.3 Rod Worth Analysis

Nodal analysis is used to calculate various rod worths which require three-dimensional capabilities. These calculations include differential rod worths and integral rod worths.

5.3.1 Differential Rod Worth Analysis

Differential rod worths are calculated as a function of rod insertion. The differential rod worth is defined as the change in reactivity associated with a small change in rod position. This rod worth is determined by running two EPRI-NODE-P cases at different rod insertions with all other parameters held constant (power, burnup, xenon, boron) and then by dividing the reactivity difference by bank height difference.

Differential rod worths for the control banks are calculated at HZP and HFP, at BOC and EOC, and at no xenon, equilibrium xenon, and peak xenon conditions. The rod banks are inserted both sequentially and in 50% overlap.

5.3.2 Integral Rod Worth Analysis

Integral rod worths are defined as the integral of the differential rod worth data. Integral rod worths are determined using EPRI-NODE-P by summing up the reactivities resulting from the differential rod worth analysis. Total integral rod worths for a rod bank can be calculated either with a two-dimensional or three-dimensional code by subtracting the reactivities resulting from cases where the rod bank is out and then in (other parameters held constant). However, in order to get the integral rod worth as a function of rod position, i.e., the shape of the rod worth curve, the three-dimensional nodal code is used.

Integral rod worth calculations for the control banks are performed at HZP and HFP, at BOC and EOC, and at no xenon, equilibrium xenon, and peak xenon conditions. The rod banks are inserted sequentially with 50% overlap. The total rod worth (ARI) is calculated at BOC, EOC, and any limiting burnup at HZP for use in the shutdown margin calculation.

5.4 Shutdown Margin Analysis

5.4.1 Shutdown Margin

Shutdown margin calculations are performed using EPRI-NODE-P. Section 4.2.2.2 describes the general shutdown margin methodology. Table 4-2 summarizes the results of a shutdown margin calculation.

EPRI-NODE-P is used specifically to calculate:

1. The total rod worth (ARI) at HZP, BOC, and EOC (Item 1 in Table 4-2). This worth is determined by running EPRI-NODE-P cases at ARO and ARI (with constant boron and xenon) and subtracting the reactivities.

2. The maximum stuck rod worth at HZP, BOC, and EOC (Item 2 in Table 4-2). EPRI-NODE-P utilizes its full-core capabilities in determining the worst case stuck rod. The worth of the stuck rod is determined by subtracting the reactivities between two EPRI-NODE-P cases, one with ARI, the other with ARI and the stuck rod out.

3. The power deficit from HFP to HZP, at BOC and EOC (Item 6 in Table 4-2. This deficit is determined by running EPRI-NODE-P cases at HFP and HZP (with constant boron and xenon) and subtracting the reactivities. This reactivity insertion accounts for Doppler and Moderator deficits, and for axial flux redistribution.

4. The maximum allowable inserted rod worth at HFP, BOC, and EOC (Item 7 in Table 4-2). This worth is obtained by reading the integral rod worth curve at the rod insertion limits (See Section 5.3.2).

5.4.2 Shutdown Boron Concentration

The shutdown boron concentration is another parameter that is determined using three-dimensional nodal analysis. Since the shutdown margin is determined based on the worst case stuck rod out of the core with all other rods in, the full-core capability of EPRI-NODE-P is needed.

EPRI-NODE-P is first used to determine the worst case stuck rod by calculating the worth of various rods in the core. After the worse case stuck rod is determined, an EPRI-NODE-P boron search case is performed at the ARI-stuck rod out conditions. This boron concentration is adjusted based on boron worth results until the core reactivity reflects the appropriate margin (1.3% $\Delta\rho$ for temperatures greater than 200°F, 1.0% $\Delta\rho$ for temperatures less than or equal to 200°F). The resulting boron concentration is the shutdown boron concentration required for the conditions modeled in the nodal code. This calculated boron concentration is conservatively increased by 100 ppm.

A shutdown boron concentration can be determined for any moderator temperature provided the input cross sections remain valid. Typical average moderator temperatures for which shutdown boron concentrations are provided are 68°F, 200°F, 500°F, and the HZP average moderator temperature (approximately 557°F).

5.5 Rod Insertion Limit Assessment

Control rod insertion limits define how deep the control rods may be inserted into the core during normal operation as a function of the power level. It is a Technical Specification requirement that the rods never be inserted deeper than the established limits. This analysis is usually a verification that the Rod Insertion Limits from cycle N-1 are adequate for cycle N.

5.5.1 Rod Insertion Limit-Criteria

The control rod insertion limits are determined based on:

1. Maintaining the required minimum shutdown margin throughout the cycle life.

   a. 1.3% $\Delta\rho$ for T > 200°F
   b. 1.0% $\Delta\rho$ for T $\leq$ 200°F

2. Maintaining the maximum calculated enthalpy rise peaking factor to: $F^N_{\Delta H} \leq 1.435\ (1 + .3[1-P])$.

3. The worst case consequences of a Rod Ejection, Rod Drop, or Rod Misalignment accident being acceptable, i.e., verifying that reactivity insertions and hot channel factors (F_Q) don't exceed the currently approved accident analysis values.

5.5.2 Rod Insertion Limit - Nodal Analysis

Determining control rod insertion limits involves an iterative process based on satisfying the above criteria. This process begins with insertion limits from the previous cycle.

The first requirement for insertion limits is that of satisfying the reactivity constraints, i.e., maintaining the required shutdown margin. The insertion limits from the previous cycle, along with integral rod worth curves for control banks in 50% overlap for the current cycle, are used to calculate the maximum allowable inserted rod worth for input into the shutdown margin calculation. The shutdown margin is

calculated at BOC, EOC, and any limiting burnup in order to determine if the control rod insertion limits are acceptable. If the shutdown margin criteria is not satisfied, the insertion limits are adjusted until satisfactory margin is obtained.

The insertion limits also have to satisfy the peaking factor constraints. The nodal powers are synthesized with discrete pin PDQØ7 pin powers to give values of $F^N_{\Delta H}$ at various power levels from HZP to HFP. The values of $F^N_{\Delta H}$ are then compared to the Technical Specification limits. If the Technical Specification limits are not satisfied, the control rod insertion limits are adjusted until satisfactory values of $F^N_{\Delta H}$ are obtained. (It may be found that to satisfy the Technical Specification limits on $F^N_{\Delta H}$ the loading pattern scheme needs to be altered. See Section 4.2).

In addition to satisfying reactivity and peaking factor constraints during normal operation, the control rod insertion limits may need to be modified based on the worst case consequences of an ejected RCCA, a dropped RCCA or a statically misaligned RCCA. Evaluations are performed with the nodal code to identify the worst case rod configuration during a withdrawal or misalignment event, that is, to identify the single RCCA which produces the maximum $F^N_{\Delta H}$ (control rods held at insertion limits). The results of the three-dimensional nodal analysis with these worst case rod configurations are compared to the design criteria associated with each event. The acceptability of the control rod insertion limits is dependent on the criteria being satisfied. (Sections 4.2.2.3 and 4.2.2.4 address specifically ejected rod and dropped rod analyses.)

5.6 Trip Reactivity Analysis

The minimum trip reactivity and the shape of the trip reactivity insertion curve (inserted rod worth as a function of rod position) are both generated using nodal analysis. These parameters are needed to perform the safety analysis for a loss of flow accident or an uncontrolled RCCA bank withdrawal or ejection event at power.

5.6.1 Minimum Trip Reactivity

The minimum trip reactivity is the minimum amount of reactivity available to be inserted into the core in the event of a reactor trip. It is evaluated for each reload core to ensure that the previously set limits are still valid.

The minimum trip reactivity at or near full power is calculated by subtracting the entire rod insertion allowance and the difference between the control rod requirements at 90% FP and 100% FP from the minimum available N-1 rod worth (most reactive rod stuck out of core). The rod insertion allowance is the amount of reactivity associated with the control rod insertion limits. It is the difference in reactivity between an ARO case and one with control rods at their insertion limits.

The minimum trip reactivity calculation is performed at both BOC and EOC. A sample BOC calculation is shown in Table 5-1.

5.6.2 Trip Reactivity Shape

The shape of the trip reactivity insertion curve defines the inserted rod worth as a function of rod position. The most limiting shape is the one which defines the minimum inserted rod worth as a function of rod position. This most limiting shape is evaluated each reload cycle to ensure that the values for the minimum inserted rod worth vs. rod position used in the safety analysis are still applicable.

The most limiting trip reactivity shape typically corresponds to the most bottom-skewed axial power shape. HFP axial power distributions are examined from BOC to EOC, with control rods at the full power rod insertion limits and the most reactive rod stuck out of the core. After the most limiting power shape is found, the N-1 control rods are inserted into the core in a stepwise manner. The results of this insertion yield the minimum inserted rod worth vs. rod position curve.

5.7 Assessment of Nodal Analyses

Once the nodal calculations are performed, the resultant data are assessed for validity and consistency with core operation requirements and safety limits.

The validation assessment consists of two different methods:

1. Comparison of calculations for reasonable agreement with previous data for similar conditions.

2. Checks of assumptions, intermediate calculations for code inputs, code input data and output are performed to insure calculational accuracy.

The assessment of consistency with requirements is also a two step procedure:

1. The calculated results must be within bounding values as determined by the Final Safety Analysis Report, or be proven to be non-limiting by way of a separate safety analysis or safety evaluation.

2. Calculated results must also show that core operational requirements are satisfied.

A complete discussion of requirements for documentation and quality assurance for safety related calculations is presented in Section 4.8 of the Duke Power Administrative Policy Manual for Nuclear Stations.[21]

Table 5-1

BOC Trip Reactivity Calculation

CRA Requirements	BOC Worths at 100% FP (% Δp)	BOC Worths at 90% FP (% Δp)
Power Defect*	2.12	1.96
Rod Insertion Allowance	1.13	1.13
Total CRA Requirement	3.25	3.09

Trip Reactivity	BOC Worths (% Δp)
Minimum Available N-1 Rod Worth	6.18
Rod Insertion Allowance	-1.13
Difference between CRA Requirements at 100% FP and 90% FP	-.16
Minimum Trip Reactivity	4.89

* The Power Defect includes doppler, variable T_{MOD} and redistribution effects.

6. Calculation of Safety Related Physics Parameters

6.1 Reload Specific Safety Related Physics Parameters

With a reload of fresh fuel, a reactor core's physics characteristics are altered in three major areas:

1. Power distribution
2. Control rod worths
3. Kinetics

Each of the above has its own subset of specific parameters which are addressed individually. Also, non-fuel-related changes, such as a revised T_{avg} program, are accounted for in calculations of cycle specific safety parameters. Table 6.1 lists these parameters.

This section identifies safety parameters which are examined during a reload analysis for the McGuire and Catawba cores and outlines analysis methods for determining values.

6.2 Calculational Methodology

6.2.1 Power Distributions

Core power distributions are calculated in two dimensions with PDQØ7 and in three dimensions with EPRI-NODE. Radial local assembly factors are derived from PDQØ7 calculations and used with EPRI-NODE nodal powers to verify that the reload core operates within design F_Q and $F^N_{\Delta H}$ versus power limits.

6.2.1.1 Radial Power Peaking

PDQØ7 calculations are performed for several different operating conditions:

1. ARO Nominal Depletion at HFP EQXE
2. Control Bank D inserted - HFP
3. HZP Sequential bank insertions: BOL and EOL
4. HFP Xe, Sm, or soluble boron variations from nominal

Conditions 1, 2, and 3 are primarily power peaking calculations; while condition 4 calculations provide reactivity data for the reactor's Operator Aid Computer (OAC).

The PDQEDIT[22] code post-processes PDQØ7 data files to produce:

1. Maps of assembly power, burnup, and isotopics
2. Summaries of core average, maxima, and minima
3. Assembly radial local factors
4. Data for the offline measured power program - (See Section 11.2.2)

6.2.1.2 Total Power Peaking

The quarter core EPRI-NODE model, described in Section 3, is used with the analysis techniques of Section 5 to evaluate a broad spectrum of power distributions. A full core model is used for evaluating non-symmetric power distributions, such as the dropped rod configuration.

Like the PDQØ7 model, the EPRI-NODE model has moderator, doppler, and xenon feedbacks. Nodal powers are multiplied by the respective assembly radial local factor to yield F_Q^C as formulated in equation 6-1:

$$F_Q^C = \text{Max} \left(F_{i,\ell}^{NODE} \times RL_\ell\right) \qquad (6\text{-}1)$$

Where:

RL_ℓ = Radial local for assembly ℓ.

$F_{i,\ell}^{NODE}$ = Nodal power calculated at axial location i and for assembly ℓ.

Reliability factors as described in Section 11 are applied to PDQØ7 and EPRI-NODE calculations such that with a 95 percent confidence level, 95 percent of the calculated powers will be greater than or equal to measured powers. These factors are defined as:

$F_{\Delta H}^R$ = 95/95 Reliability factor for $F_{\Delta H}^N$

F_Q^R = 95/95 Reliability factor for F_Q

An additional multiplier, F_Q^E, is applied to F_Q to account for manufacturing tolerances (See Section 1.2). Power distributions which are used to verify the reload design employ the following formulations:

$$F_{\Delta H}^T = F_{\Delta H}^R \times F_{\Delta H}^C \qquad (6\text{-}2)$$

$$F_Q^T = F_Q^R \times F_Q^E \times F_Q^C \qquad (6\text{-}3)$$

6.2.2 Control Rod Worth

Individual and bank RCCA worths vary with each reload. Safety parameters which pertain to RCCA worth are:

1. Shutdown margin
2. Maximum differential bank worth
3. Ejected RCCA worth
4. Dropped RCCA worth
5. Trip reactivity

Control rod worths are evaluated with either PDQØ7 or EPRI-NODE. Sections 4 and 5 describe the calculational procedure for the shutdown margin.

6.2.2.1 Shutdown Margin

There are two shutdown margins which are required:

1. 1.3% ΔK/K for $T_{avg} > 200°F$
2. 1.0% ΔK/K for $T_{avg} \leq 200°F$

The 1.3% shutdown margin is based on an analysis of a steam-line break accident at EOL and HZP conditions. The 1.0% margin is an industry standard.

The shutdown margin is evaluated at BOL, EOL, and at any intermediate burnup where the margin is seen to be more limiting. (See Section 4.2.2.2.)

6.2.2.2 Maximum Differential Rod Worth

The uncontrolled RCCA withdrawal accident requires an estimate of the maximum differential bank worth at HZP. Two control banks are assumed withdrawn simultaneously with no overlap. The maximum worth (pcm/inch) is determined by a series of EPRI-NODE calculations simulating two-bank withdrawal for various pairs of sequential RCCA banks, e.g., C_B and C_C. Calculations are performed at BOL and EOL. When the maximum differential bank worth has been determined, a 10% conservatism factor is then applied. This conservative worth is compared to the FSAR value.

6.2.2.3 Ejected Rod Worth

The ejected RCCA worth is evaluated using EPRI-NODE with a full core model. Calculations are performed at BOL and EOL and at HFP and HZP conditions.

In all calculations, control banks D, C, and B are inserted at their respective insertion limits, depending on core power.

Due to the short duration of this accident, adiabatic conditions are assumed - no moderator or doppler feedbacks. The ejected rod is simulated by fully withdrawing an inserted rod from a rodded location and calculating the resultant reactivity and power distribution. The ejected rod worth is then:

$$\Delta\rho \text{ (pcm)} = \frac{K_A^{ej} - K_A^{R}}{K_A^{ej} \times K_A^{R}} \times 10^5 \qquad (6\text{-}4)$$

Where:

A - Initial condition, e.g., HFP and BOL

R - Denotes control banks at insertion limits

ej - Denotes ejected rod

K - K_{eff} calculated by EPRI-NODE

Although Doppler feedback is not used in the power distribution calculation, the Doppler Coefficient is an input to the safety evaluation of this accident.

6.2.2.4 Dropped Rod Worth

The dropped RCCA is modeled with a full core EPRI-NODE calculation. It is assumed that no trip signal is generated, and therefore all other RCCA remain at their current positions. Search cases are performed in which single RCCAs are fully inserted into the core. Calculations are performed at full power and equilibrium xenon with Doppler and moderator feedbacks. The results of these cases are examined for both reactivity insertion and power peaking.

6.2.2.5 Trip Reactivity

Trip reactivity insertion and the shape of the trip curve are calculated with EPRI-NODE. (See Section 5.5.)

A full core model is used to evaluate:

1. N-1 reactivity insertion rate at constant acceleration.
2. Net reactivity insertion at trip (N-1).

The N-1 trip assumes that the most reactive control rod is stuck. The calculated trip worth is then conservatively reduced by the 100 to 90% power defect.

6.2.3 Kinetics

Kinetics parameters of each reload design are evaluated to verify that design limits of the FSAR are met. Table 6-2 lists these safety parameters and the codes which are used to evaluate them. Reactivity coefficients and their respective calculational procedures have been discussed in Sections 4 and 5.

The DELAY code, which was reviewed and approved by the NRC in Reference 4, uses data extracted from PDQØ7 calculations to derive β_i, λ_i, and ℓ^*. The prompt neutron lifetime is calculated using the formulation:

$$\ell^* = \frac{1}{V_1 \Sigma_{T1}} + \frac{K_2}{V_2 \Sigma_{T2}} \qquad (6\text{-}5)$$

Where:

$V_1 = 8.448 \times 10^6 \div \sigma_a^1 (B^{10})$

$V_2 = 2.2 \times 10^5$

$\Sigma_{T1} = \nu\Sigma_F^1/K_1$

$\Sigma_{T2} = (\Sigma_R^1/\Sigma_{T1}) \times (\nu\Sigma_F^2/K_2)$

$K_{eff} = K_1 + K_2$

(For a two-group formulation with group 2 being Mixed Number Density)

An isotopic fission rate weighting procedure is used to derive the delayed neutron fractions, β_i, and the precursor half-lives, λ_i. Reactor period and reactivity versus doubling time are calculated using the Inhour equation.

DELAY calculations are performed at BOL, MOL, and EOL. Calculated data from DELAY are also used for measuring rod worths during startup.

6.3 Comparison of Cycle Specific Safety Related Physics Parameters

After the safety parameters have been calculated for the reload core, a comparison to FSAR or other current safety analysis values is performed. If the comparison shows that the safety related physics parameters are conservative with respect to the current safety analysis limits, then no additional safety analyses are required.

However, if a safety related parameter is non-conservative, then a safety evaluation is performed to determine the need for a new safety analysis, or the core is redesigned to yield conservative safety parameters.

TABLE 6-1

Reload Safety Related Physics Parameters

1. Power Distribution
   - A. Fuel assembly and fuel rod powers (Two-Dimensional, nominal conditions) - $F^N_{\Delta H}$
   - B. Maximum local rod power (F_q)
     1. Nominal operation - for Rod Insertion Limits
     2. Transient - load follow, axial xenon redistribution, rod ejection

2. Control Rod Worths
   - A. Individual Bank Worth
   - B. Stuck Rod Worth
   - C. Shutdown Margin
   - D. Dropped Rod Worth
   - E. Differential Worth of two banks in 100% overlap at HZP
   - F. Trip reactivity

3. Kinetics
   - A. Moderator Temperature Coefficient
   - B. Doppler Power Coefficient
   - C. Boron Worth
   - D. β_i - Effective and λ_i
   - E. Prompt Neutron Lifetime
   - F. Time-dependent Reactivity

TABLE 6-2

Reload Safety Related Kinetics Parameters

and Computer Codes

	Parameter	Computer Code
1.	Moderator Temperature Coefficient	EPRI-NODE or PDQØ7
2.	Doppler Only Power Coefficient	EPRI-NODE or PDQØ7
3.	Total Rod Worth	EPRI-NODE or PDQØ7
4.	Maximum Differential Rod Worth of Two Banks Moving Together	EPRI-NODE
5.	Ejected Rod Worth	EPRI-NODE
6.	Dropped Rod Worth	EPRI-NODE
7.	Prompt Neutron Lifetime, ℓ^*	DELAY
8.	Delayed Neutron Fraction, β	DELAY

7. 3-D Power Peaking Analysis

7.1 Power Peaking Criteria

Once a loading pattern has been developed, as in Section 4, using two-dimensional analyses, power peaking behavior is examined with three-dimensional analyses. The three-dimensional analysis is used to establish operational power-axial flux difference limits. These limits are such that the initial conditions used in the ECCS and Loss-of-Flow transients are satisfied. Currently, the LOCA F_Q limits and DNB limits of these transients are determined by Westinghouse.

Similarly, the three dimensional analysis is used to establish power peaking information for setting RPS limits through the OTΔT and OPΔT trip functions. The fuel limits to which the design calculations are compared are centerline fuel melt and DNBR.

7.2 CAOC Power Peaking Control

Local power peaking (F_Q) is controlled with the Constant Axial Offset Control (CAOC) procedure[23] in Westinghouse reactors. This method minimizes power peaking by maintaining the AO within a band about a target value. The band width is typically +3 and -12% for reload cores. The target AO is measured at approximately HFP, ARO EQXE conditions. The band width does not vary; however, the target AO changes approximately linearly with exposure. Technical specifications allow only short duration (less than one hour in twenty-four) exceptions to AO limits. In this way, xenon maldistributions are minimized.

Xenon maldistributions, combined with RCCA bank motions during power maneuvers, are the primary cause of severe F_Qs. Typical power maneuvers used at McGuire and Catawba are:

1. Minimum boron duty - Power maneuver is accomplished primarily by control bank motion. Boron requirements are minimized to accommodate bank motion and AO control. See Figure 7-1 for comparative plots of RCCA position, boron concentration, reactor power, and AO during this maneuver.

2. Maximum return to power - AO is maintained near appropriate upper (lower) limits such that bank motion for power change will result in the AO staying within its band. Near the end of the cycle, when boration/dilution abilities are limited, the core average moderator temperature is reduced, thus giving a net positive reactivity insertion to increase power. When full power is reached, the inlet temperature is returned to its programmed value. Figure 7-2 illustrates system parameters during this transient.

During the above power maneuvers, the AO is controlled using the CAOC strategy.

7.3 Power Peaking and Verification

Verification of a reload design, using 3-D calculations, consists of simulating a series of power maneuvers and evaluating the margin to the design F_Q where:

$$\text{Margin} = \frac{(F_Q^{\text{Design}} - F_Q^T)}{F_Q^{\text{Design}}}$$

and:

F_Q^{Design} = design limit F_Q

F_Q^T = calculated F_Q with all allowances and conservatisms

Power maneuvers are performed at BOL and EOL, usually with three separate power levels from 100% power and subsequent power ascension.

Load follow maneuvers are simulated, using a series of EPRI-NODE calculations. Initial HFP conditions are assumed. Core power is reduced via a step change in control bank location, along with a simultaneous step power change. A series of one-hour timesteps are used to calculate and update xenon, Iodine, and core power distributions. Core power is maintained at a reduced level until peak xenon conditions are reached, typically 6 to 9 hours. Figure 7.1 qualitatively displays important core parameters during the power maneuver.

The method of F_Q calculation is identical to that for the LOCA total peak, as described in Reference 3. It is assumed that assembly radial local factors are constant during the transient. Allowances are made for:

1. Model uncertainty
2. Engineering hot channel factor
3. Power spike
4. Quadrant tilt
5. Others, as applicable

The nodal powers and PDQØ7 radial local factors are combined in the NODE Utility Code[24] to calculate margins to the LOCA F_Q. Core height-dependent LOCA F_Q limits are presented in Table 7-1. F_Q margins are evaluated at:

1. Transient initiation - control bank insertion
2. Peak xenon - after bank withdrawal
3. Xenon undershoot

F_Q margins for the power maneuver in Figure 7-1 are shown on Table 7-2, where the McGuire 2 Cycle 1 core was analyzed.

7.4 Advanced Maneuverability

To improve the core's power flexibility, the CAOC "bands" from Section 7.2 can be widened by an extensive power peaking analysis. This analysis is performed using EPRI-NODE and methods similar to the "rods-out" maneuvering analysis of Sections 5 and 7 in Reference 3 are performed.

Unlike the Oconee methodology, penalty functions, $f(\Delta I)$, are used in the reactor trip system functions to prevent CFM, or DNB problems. These functions are parameterized to cover a wide range of operating conditions, including skewed axial power shapes. A more complete description of these functions, $OT\Delta T$ and $OP\Delta T$, can be found in the Bases for Section 2.0 section of the McGuire Units 1 and 2 Technical Specifications.

The primary design criterion in developing the widened power - AFD operating band is that the core can be operated such that the design LOCA Kw/ft limits are not violated. The resultant operating limits for a typical reload core are shown in Figure 7-3.

7.4.1 Analysis Procedure

Several assumptions are made in deriving the power - AFD window:

1. Control bank insertion as a function of power is limited to the Rod Insertion Limits.
2. Azimuthal and radial power transients are effectively dampened. (However, allowance for quadrant power tilt is made.)
3. Axially skewed power distributions are limited to Condition I (normal) operation which might maldistribute the core xenon distribution. Condition II events - rod ejection, rod drop, etc., are analyzed separately in the accident analysis.
4. Xenon distributions are core and cycle specific. The radial xenon distribution is consistent with assembly radial power.

At various times in reactor life, axial xenon transients are induced by either load follow transients or return to power from an equilibrium xenon state at a lower power level. Core xenon conditions include, but are not limited to: equilibrium, maximum, and minimum states.

The above states are used as input to control bank scan calculations using EPRI-NODE. The nodal powers are converted, using PDQØ7 along with other factors (F_Q^E, quadrant tilt, F_Q^R, etc.), to F_Q^T with appropriate conservatisms and allowances. From the control bank scan calculations at various power levels - down to 50% full power, a flyspeck plot of margins (see Section 7.3) then determines the power - AFD operating limits.

TABLE 7-1
Design Limit F_Q

Fraction of Core Height	McGuire First Core	McGuire Transition Cores*	Catawba All Cores
0.0	2.32	2.15	2.32
0.50	2.32	2.15	2.32
0.90	2.18	2.02	2.18
1.0	1.50	1.40	1.50

* These limits apply to cores with a mixture of 17x17 Standard and 17x17 Optimized fuel assemblies. These values are subject to change pending any future LOCA reanalyses.

TABLE 7-2
F_Q Margin to LOCA

Time (hours)	Power Level (% Full Power)	Minimum Margin To LOCA (%)
1-12	100	18.27
13	50	54.69
14	50	54.17
15	50	53.49
16	50	53.76
17	50	52.14
18	50	51.63
19	50	51.27
20	50	51.08
21	100	14.37
22	100	15.74
23	100	16.80
24	100	16.75
25	100	15.75
26	100	15.26
27	100	15.17
28	100	15.29
29	100	15.62
30	100	16.14
31	100	16.78
32	100	17.39
33	100	17.99

Figure 7-1

Design Load Follow Maneuver

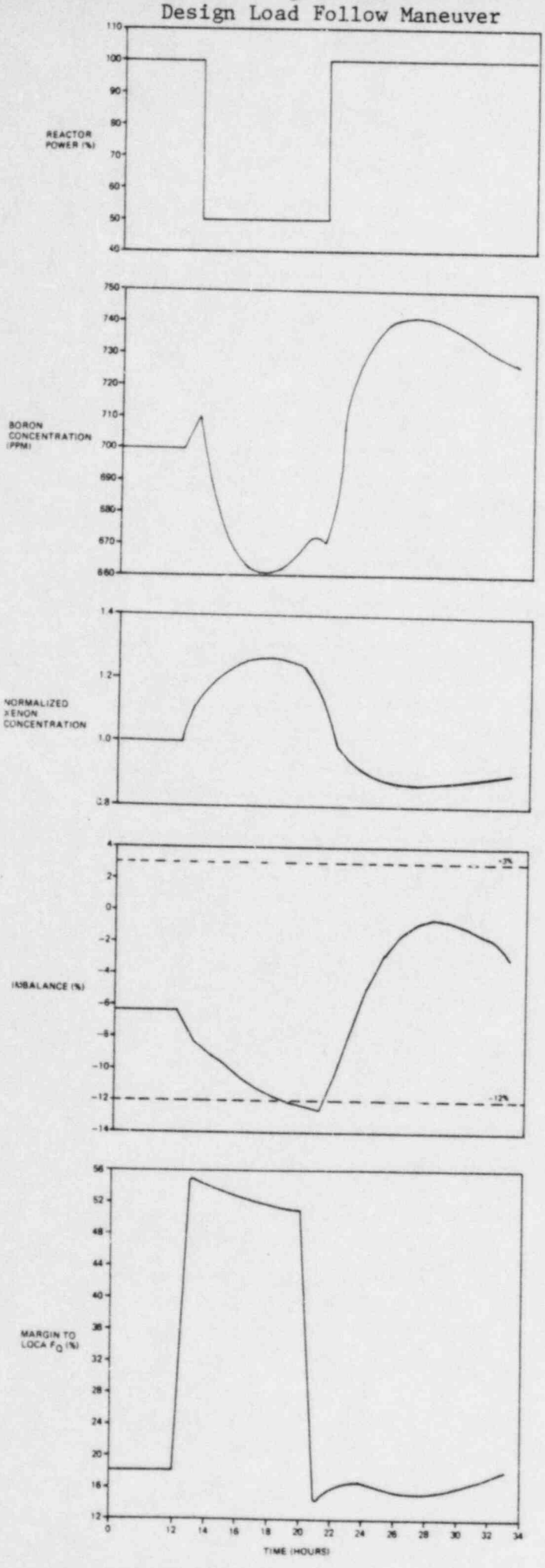

Figure 7-2

REDUCED TEMPERATURE
RETURN TO POWER

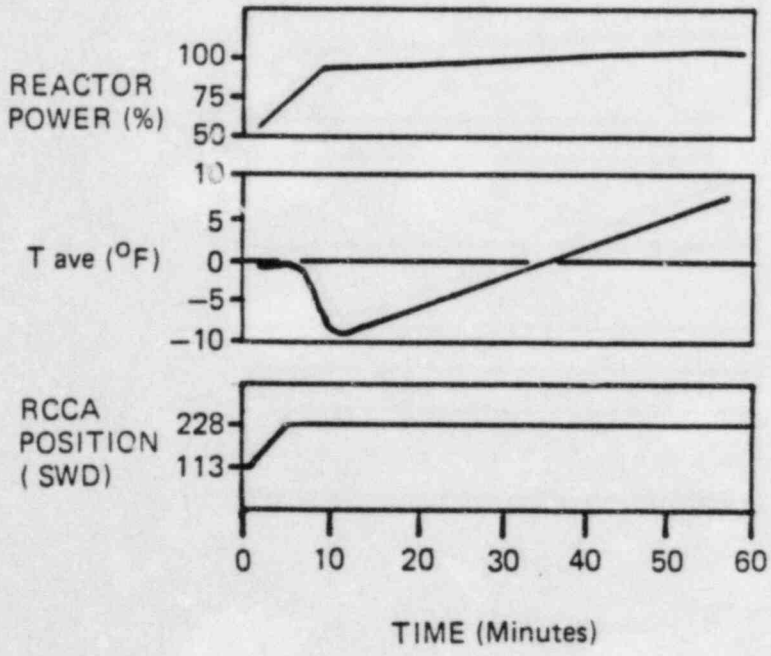

FIGURE 7–3

POWER – AXIAL FLUX DIFFERENCE
OPERATING LIMITS – TYPICAL

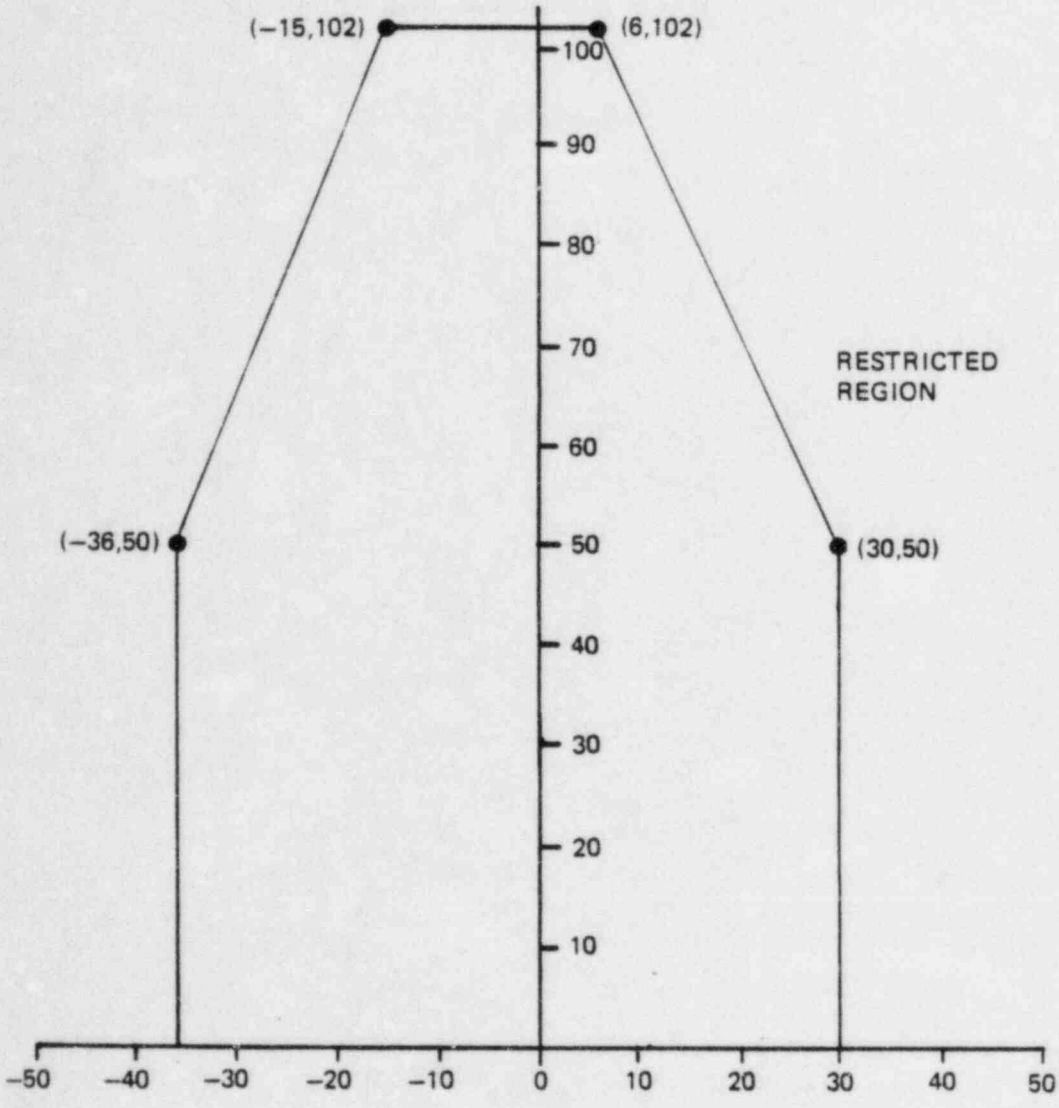

8. Radial Local Analysis

8.1 Background

The local radial is an important factor in fuel cycle design because of its significant influence on LOCA and DNB analysis. The premise for performing this analysis is to evaluate the ability of PDQØ7 to predict the radial local. The radial local is defined as the ratio of the maximum pin power, to the assembly average planar (x-y) power.

Duke Power Company currently uses two computer codes to calculate radial local factors, PDQØ7 and CASMO-2. PDQØ7 is a 1, 2, or 3 dimensional two neutron energy group diffusion theory code, whereas CASMO-2 is a 2-dimensional multigroup transport theory code, which utilizes transport probabilities in the solution of the transport equation. The 2-dimensional PDQØ7 code is the primary calculational tool used to model reactor cores (for additional information concerning the use of this code, refer to Section 3.4). Energy and burnup dependent Mixed Number Density (MND) cross sections used by PDQØ7 are developed in accordance with ARMP[14] procedures. CASMO-2 is used primarily to generate multigroup constants (i.e., control rod and burnable absorber cross sections), and as a benchmark code.

8.2 Comparison of PDQØ7 to CASMO-2 at Hot Full Power Condition

The predictive capability of PDQØ7 was assessed by performing a series of eighth assembly calculations using both PDQØ7 and CASMO-2. A typical Westinghouse 17x17, 3.2 w/o Uranium-235 optimized fuel assembly was modeled using these codes.

All simulations were performed at beginning of life (BOL), hot full power (HFP), no xenon conditions, for at this time severe pin power peaking is most prominent. Simulations were performed for a variety of burnable

absorber loadings and soluble boron concentrations. The enrichment, burnable absorber loadings, and boron concentration of each case investigated are representative of future McGuire and Catawba reloads. Table 8-1 contains a summary of the cases that were investigated.

Figures 8-1 through 8-10 contain 1/8 assembly pinwise power comparisons between PDQØ7 and CASMO-2. Results from these comparisons indicate that PDQØ7 conservatively overpredicts the maximum CASMO-2 pin power. This overprediction ranges from 0.86% to 2.26%. PDQØ7 also correctly identifies the location of the CASMO-2 maximum pin power. Comparisons between PDQØ7 and CASMO-2 maximum pin powers for each case are tabulated in Table 8-2.

The global predictive capability of PDQØ7 was assured by performing a statistical analysis over all pins in the problem and for pins with powers greater than or equal to 1.000. The average, and the average absolute differences along with respective standard deviations, are presented in Table 8-3 for all cases investigated.

8.3 Comparisons of PDQØ7 to Cold Criticals

The ability of PDQØ7 to predict pin powers at cold conditions was by performing a series of simulations based on the B&W uranium criticals. In all simulations, PDQØ7 conservatively and accurately predicted the maximum pin power. For additional specifics concerning the comparisons of PDQØ7 to the B&W uranium criticals, refer to Reference 3.

8.4 Conclusion

Comparisons between PDQØ7 and CASMO-2 at HFP conditions indicate that PDQØ7 conservatively predicts the maximum pin power within an assembly over a wide range of burnable absorber loadings and soluble boron concentrations. PDQØ7 comparisons to B&W cold criticals indicate that PDQØ7 also conservatively predicts maximum pin powers. This conservatism demonstrated by PDQØ7 can be directly attributed to the use of MND thermal

cross sections[3]. Therefore, in light of the conservatism that was demonstrated by PDQØ7 over a wide range of conditions, it is not necessary to apply an uncertainty factor to the PDQØ7 predicted radial local.

TABLE 8-1

Characteristics of 1/8th Assembly Simulations

CASE	ENRICHMENT W/O U-235	BURNABLE ABSORBER LOADING	BORON CONCENTRATION (PPMB)
1	3.2	0	0
2	3.2	0	950
3	3.2	4	0
4	3.2	4	950
5	3.2	12	0
6	3.2	12	950
7	3.2	16	0
8	3.2	16	950
9	3.2	20	0
10	3.2	20	950

TABLE 8-2

Peak Pin Power Comparison

CASE	PDQØ7 PEAK PIN POWER	CASMO PEAK PIN POWER	DIFFERENCE PDQØ7-CASMO	% DIFFERENCE (P-C)/C
1	1.053	1.042	0.011	1.056
2	1.051	1.039	0.012	1.155
3	1.055	1.046	0.009	0.860
4	1.053	1.043	0.010	0.959
5	1.152	1.131	0.021	1.857
6	1.137	1.119	0.018	1.609
7	1.188	1.163	0.025	2.150
8	1.170	1.149	0.021	1.828
9	1.178	1.152	0.026	2.257
10	1.164	1.140	0.024	2.105

TABLE 8-3

Statistical Summary of Percent Differences between PDQØ7 and CASMO-2
For Pins in Assembles with
Powers Greater Than or Equal to 1.000.

CASE	$\bar{D}$*	ABS ($\bar{D}$)	STANDARD DEVIATION ($\bar{D}$)	S.D [ABS ($\bar{D}$)]
1	0.4450	0.5566	0.5524	0.4339
2	0.4657	0.5554	0.5627	0.4697
3	0.2151	0.3470	0.4098	0.3010
4	0.2109	0.3595	0.4215	0.2987
5	0.8916	1.0620	0.8705	0.6396
6	0.7936	0.9548	0.7733	0.5503
7	0.9321	1.1509	1.0832	0.8311
8	0.8057	1.0241	0.9635	0.7107
9	0.7130	0.8202	0.8885	0.7851
10	0.6458	0.7530	0.8109	0.7069

Statistical Summary of Percent Differences between PDQØ7 and CASMO-2
For All Pins Within An Assembly

CASE	$\bar{D}$*	ABS ($\bar{D}$)	STANDARD DEVIATION ($\bar{D}$)	S.D [ABS ($\bar{D}$)]
1	0.0030	0.6395	0.7867	0.4463
2	0.0066	0.6572	0.8119	0.4648
3	-0.0255	0.4606	0.6328	0.4281
4	-0.0066	0.4520	0.6280	0.4298
5	0.0616	1.0682	1.2511	0.6310
6	0.0394	0.9801	1.1449	0.5713
7	0.0585	0.9416	1.2120	0.7499
8	0.0398	0.8436	1.0926	0.6819
9	0.0268	0.8776	1.1696	0.7604
10	0.0293	0.8059	1.0732	0.6972

* NOTE: $D = [(PDQØ7 - CASMO\text{-}2)/CASMO\text{-}2] * 100$

$$\bar{D} = \sum_{i=1}^{N} D_i/N$$

Figure 8-1

CASMO-2 AND PDQ-7
ROD POWER COMPARISON
BOL HFP NO XENON
3.2 W/O U-235 OPT 17x17 FA
CASE NUMBER 1

	PDQ-7	CASMO-2
PPMB	0	0
NUMBER BA	0	0
K-INFINITY	1.3486	1.3479
*MAX. ROD POWER	1.053	1.042

0.0 0.0								
1.020 1.024	1.002 1.009							
1.021 1.024	1.002 1.009	1.002 1.010						
0.0 0.0	1.024 1.025	1.026 1.027	0.0 0.0					
1.020 1.023	1.002 1.009	1.004 1.013	1.033 1.037	1.023 1.045				
1.018 1.021	1.000 1.007	1.002 1.011	1.033 1.038	1.042 * 1.053	0.0 0.0	CASMO-2 PDQ-7		
0.0 0.0	1.018 1.017	1.020 1.019	0.0 0.0	1.030 1.037	1.014 1.010	0.976 0.975		
1.008 1.006	0.990 0.993	0.990 0.994	1.011 1.006	0.986 0.989	0.970 0.964	0.959 0.947	0.955 0.940	
0.986 0.982	0.985 0.979	0.985 0.979	0.985 0.980	0.979 0.973	0.972 0.961	0.966 0.953	0.967 0.954	0.981 0.971

Figure 8-2

CASMO-2 AND PDQ-7
ROD POWER COMPARISON
BOL HFP NO XENON
3.2 W/O U-235 OPT 17x17 FA
CASE NUMBER 2

	PDQ-7	CASMO-2
PPMB	950	950
NUMBER BA	0	0
K-INFINITY	1.2122	1.2077
*MAX. ROD POWER	1.051	1.039

0.0 0.0								
1.017 1.021	1.000 1.007							
1.018 1.021	1.000 1.007	1.000 1.008						
0.0 0.0	1.021 1.022	1.023 1.024	0.0 0.0					
1.018 1.021	1.000 1.007	1.002 1.011	1.030 1.035	1.020 1.042				
1.016 1.020	0.999 1.006	1.001 1.010	1.030 1.035	1.039 * 1.051	0.0 0.0	CASMO-2 PDQ-7		
0.0 0.0	1.017 1.016	1.019 1.018	0.0 0.0	1.029 1.036	1.014 1.011	0.979 0.977		
1.007 1.006	0.990 0.993	0.990 0.994	1.011 1.007	0.988 0.991	0.973 0.966	0.963 0.950	0.960 0.945	
0.987 0.983	0.987 0.980	0.986 0.980	0.987 0.982	0.982 0.975	0.975 0.964	0.971 0.957	0.972 0.959	0.986 0.976

Figure 8-3

CASMO-2 AND PDQ-7
ROD POWER COMPARISON
BOL HFP NO XENON
3.2 W/O U-235 OPT 17x17 FA
CASE NUMBER 3

	PDQ-7	CASMO-2
PPMB	0	0
NUMBER BA	4	4
K-INFINITY	1.2978	1.2956
*MAX. ROD POWER	1.055	1.046

0.0 0.0								
1.011 1.013	0.988 0.991							
1.006 1.003	0.975 0.972	0.933 0.915						
0.0 0.0	0.989 0.977	0.893 0.890	0.0 0.0					
1.011 1.009	0.980 0.979	0.940 0.925	0.905 0.908	0.964 0.963				
1.022 1.027	0.998 1.006	0.989 0.992	1.011 1.008	1.032 1.040	0.0 0.0	CASMO-2 PDQ-7		
0.0 0.0	1.034 1.036	1.033 1.034	0.0 0.0	1.046 * 1.055	1.036 1.039	1.005 1.011		
1.033 1.037	1.014 1.024	1.015 1.023	1.037 1.036	1.014 1.022	1.000 1.000	0.992 0.987	0.990 0.983	
1.015 1.018	1.015 1.015	1.015 1.014	1.016 1.016	1.011 1.010	1.005 1.001	1.002 0.996	1.004 0.999	1.019 1.018

Figure 8-4

CASMO-2 AND PDQ-7
ROD POWER COMPARISON
BOL HFP NO XENON
3.2 W/O U-235 OPT 17x17 FA
CASE NUMBER 4

	PDQ-7	CASMO-2
PPMB	950	950
NUMBER BA	4	4
K-INFINITY	1.1757	1.1672
*MAX. ROD POWER	1.053	1.043

0.0 0.0								
1.012 1.014	0.990 0.993							
1.007 1.004	0.977 0.975	0.937 0.919						
0.0 0.0	0.991 0.980	0.898 0.896	0.0 0.0					
1.011 1.010	0.982 0.981	0.943 0.928	0.909 0.912	0.965 0.965				
1.021 1.026	0.998 1.006	0.989 0.993	1.010 1.009	1.030 1.039	0.0 0.0	CASMO-2 PDQ-7		
0.0 0.0	1.031 1.035	1.031 1.032	0.0 0.0	1.043 * 1.053	1.034 1.037	1.005 1.010		
1.031 1.035	1.013 1.022	1.013 1.021	1.035 1.034	1.013 1.020	1.000 0.999	0.992 0.987	0.991 0.983	
1.013 1.016	1.013 1.013	1.013 1.013	1.013 1.015	1.010 1.009	1.005 1.001	1.002 0.996	1.005 1.000	1.020 1.018

Figure 8-5

CASMO-2 AND PDQ-7
ROD POWER COMPARISON
BOL HFP NO XENON
3.2 W/O U-235 OPT 17x17 FA
CASE NUMBER 5

	PDQ-7	CASMO-2
PPMB	0	0
NUMBER BA	12	12
K-INFINITY	1.2073	1.2029
*MAX. ROD POWER	1.152	1.131

0.0 0.0								
1.131 * 1.152	1.108 1.132							
1.123 1.144	1.099 1.123	1.088 1.109						
0.0 0.0	1.109 1.123	1.093 1.102	0.0 0.0					
1.093 1.109	1.063 1.081	1.036 1.045	1.019 1.014	0.946 0.937				
1.076 1.085	1.038 1.047	0.980 0.970	0.905 0.906	0.864 0.855	0.0 0.0	CASMO-2 PDQ-7		
0.0 0.0	1.043 1.041	0.930 0.934	0.0 0.0	0.860 0.849	0.876 0.867	0.932 0.908		
1.055 1.062	1.020 1.028	0.967 0.956	0.907 0.906	0.930 0.910	0.950 0.934	0.973 0.959	0.996 0.989	
1.035 1.046	0.026 1.032	1.004 1.000	0.984 0.976	0.983 0.973	0.992 0.984	1.007 1.000	1.024 1.023	1.048 1.054

Figure 8-6

CASMO-2 AND PDQ-7
ROD POWER COMPARISON
BOL HFP NO XENON
3.2 W/O U-235 OPT 17x17 FA
CASE NUMBER 6

	PDQ-7	CASMO-2
PPMB	950	950
NUMBER BA	12	12
K-INFINITY	1.1010	1.0941
*MAX. ROD POWER	1.137	1.119

0.0 0.0								
1.119 * 1.137	1.097 1.118							
1.112 1.130	1.090 1.110	1.080 1.099						
0.0 0.0	1.100 1.112	1.086 1.094	0.0 0.0					
1.086 1.100	1.058 1.074	1.032 1.041	1.018 1.013	0.949 0.941				
1.070 1.079	1.035 1.044	0.981 0.970	0.909 0.911	0.871 0.864	0.0 0.0	CASMO-2 PDQ-7		
0.0 0.0	1.041 1.039	0.933 0.937	0.0 0.0	0.868 0.858	0.884 0.876	0.938 0.915		
1.052 1.059	1.019 1.027	0.969 0.958	0.912 0.912	936 0.917	0.956 0.940	0.977 0.964	0.999 0.992	
1.034 1.044	1.026 1.030	1.005 1.001	0.987 0.980	0.987 0.978	0.996 0.988	1.010 1.004	1.025 1.024	1.049 1.054

Figure 8-7

CASMO-2 AND PDQ-7
ROD POWER COMPARISON
BOL HFP NO XENON
3.2 W/O U-235 OPT 17x17 FA
CASE NUMBER 7

	PDQ-7	CASMO-2
PPMB	0	0
NUMBER BA	16	16
K-INFINITY	1.1629	1.1576
*MAX. ROD POWER	1.188	1.163

0.0 0.0								
1.163 * 1.188	1.138 1.166							
1.150 1.173	1.125 1.152	1.111 1.137						
0.0 0.0	1.123 1.138	1.110 1.124	0.0 0.0					
1.072 1.080	1.051 1.065	1.040 1.052	1.035 1.034	0.966 0.962				
0.950 0.952	0.975 0.962	0.966 0.953	0.915 0.918	0.885 0.879	0.0 0.0	CASMO-2 PDQ-7		
0.0 0.0	0.909 0.906	0.904 0.902	0.0 0.0	0.882 0.874	0.905 0.900	0.966 0.946		
0.922 0.919	0.949 0.934	0.948 0.933	0.916 0.918	0.955 0.937	0.983 0.971	1.010 1.001	1. [illegible] 1.0	
0.992 0.989	0.993 0.993	0.995 0.993	0.996 0.993	1.009 1.004	1.027 1.023	1.046 1.046	1.066 1.071	1.093 1.105

Figure 8-8

CASMO-2 AND PDQ-7
ROD POWER COMPARISON
BOL HFP NO XENON
3.2 W/O U-235 OPT 17x17 FA
CASE NUMBER 8

	PDQ-7	CASMO-2
PPMB	950	950
NUMBER BA	16	16
K-INFINITY	1.0655	1.0581
*MAX. ROD POWER	1.170	1.149

0.0 0.0								
1.149 * 1.170	1.126 1.130							
1.138 1.157	1.114 1.137	1.102 1.125						
0.0 0.0	1.113 1.127	1.102 1.115	0.0 0.0					
1.067 1.074	1.047 1.059	1.037 1.048	1.033 1.033	0.968 0.965				
0.952 0.953	0.976 0.963	0.968 0.955	0.919 0.923	0.890 0.886	0.0 0.0	CASMO-2 PDQ-7		
0.0 0.0	0.913 0.911	0.909 0.907	0.0 0.0	0.888 0.881	0.910 0.906	0.969 0.950		
0.927 0.925	0.953 0.939	0.953 0.938	0.921 0.923	0.959 0.943	0.986 0.974	1.011 1.002	1.035 1.033	
0.995 0.993	0.996 0.996	0.997 0.997	0.999 0.996	1.011 1.006	1.027 1.024	1.045 1.044	1.064 1.068	1.088 1.099

Figure 8-9

CASMO-2 AND PDQ-7
ROD POWER COMPARISON
BOL HFP NO XENON
3.2 W/O U-235 OPT 17x17 FA
CASE NUMBER 9

	PDQ-7	CASMO-2
PPMB	0	0
NUMBER BA	20	20
K-INFINITY	1.1206	1.1148
*MAX. ROD POWER	1.178	1.152

0.0 0.0								
1.152 * 1.178	1.121 1.148							
1.132 1.151	1.094 1.112	1.036 1.034						
0.0 0.0	1.084 1.087	0.967 0.977	0.0 0.0					
1.061 1.064	1.026 1.033	0.971 0.958	0.899 0.898	0.903 0.877				
0.952 0.956	0.972 0.959	0.951 0.931	0.891 0.887	0.873 0.865	0.0 0.0	CASMO-2 PDQ-7		
0.0 0.0	0.923 0.924	0.916 0.915	0.0 0.0	0.898 0.891	0.929 0.928	0.998 0.984		
0.948 0.950	0.976 0.964	0.975 0.962	0.943 0.948	0.985 0.971	1.017 1.010	1.048 1.046	1.077 1.084	
1.025 1.027	1.027 1.030	1.029 1.031	1.031 1.032	1.045 1.046	1.065 1.069	1.087 1.095	1.109 1.124	1.136 1.160

Figure 8-10

CASMO-2 AND PDQ-7
ROD POWER COMPARISON
BOL HFP NO XENON
3.2 W/O U-235 OPT 17x17 FA
CASE NUMBER 10

	PDQ-7	CASMO-2
PPMB	950	950
NUMBER BA	20	20
K-INFINITY	1.0315	1.0238
*MAX. ROD POWER	1.164	1.140

0.0 0.0								
1.140 * 1.164	1.112 1.136							
1.123 1.140	1.087 1.103	1.032 1.029						
0.0 0.0	1.078 1.082	0.967 0.977	0.0 0.0					
1.058 1.062	1.025 1.031	0.973 0.960	0.905 0.904	0.909 0.885				
0.954 0.958	0.974 0.962	0.954 0.936	0.897 0.894	0.880 0.873	0.0 0.0	CASMO-2 PDQ-7		
0.0 0.0	0.927 0.928	0.921 0.920	0.0 0.0	0.903 0.898	0.932 0.932	0.998 0.984		
0.951 0.953	0.978 0.967	0.978 0.966	0.946 0.951	0.986 0.973	1.016 1.010	1.045 1.043	1.072 1.077	
1.025 1.028	1.027 1.031	1.029 1.031	1.031 1.031	1.044 1.044	1.062 1.065	1.082 1.089	1.102 1.115	1.127 1.149

9. DEVELOPMENT OF CORE PHYSICS PARAMETERS

Upon completion of the Final Fuel Cycle Design, both PDQØ7 and EPRI-NODE depletions, boron concentrations and worths, power distributions, etc. have been generated primarily for HFP and some HZP conditions. The purpose of this stage of developing core physics parameters is to provide additional calculations to supplement those already performed. The results of these calculations are used for startup test predictions and core physics parameters throughout the cycle.

9.1 Startup Test Predictions

After each refueling, the reactor undergoes a startup test program aimed at verifying that the reactor core is correctly loaded and to verify reactor behavior is as predicted by the nuclear simulators which were used in generating the data used in the plant's safety analysis.

9.1.1 Critical Boron Concentrations and Boron Worths

EPRI-NODE and/or PDQØ7 may be used to calculate critical boron concentrations and boron worths at a variety of rod configurations, at HZP and HFP, as a function boron concentration, at different xenon concentrations, and at different times in the fuel cycle. EPRI-NODE is capable of critical boron searches and when critical boron concentrations are desired, it is usually run in this mode. An alternative method is to correct the input boron concentration to the critical boron concentration using a calculated boron worth and the calculated reactivity. PDQØ7 is usually run in this manner to determine critical boron concentrations.

Table 9-1 shows some of the critical boron calculations normally performed for startup physics tests. These calculations are performed after the sequential insertion of each control or shutdown bank and are sometimes referred to as boron endpoints.

Critical boron concentrations at HZP and HFP with all rods out are also calculated as a function of cycle burnup. Figure 9-1 illustrates the form in which these results are displayed. These curves are referred to as boron letdown curves.

The boron worths are usually calculated by running two identical cases except that the soluble boron concentration is different. The differential boron worth is calculated by subtracting the reactivities and dividing by the boron difference. Differential boron worths are usually quoted in PCM/PPMB. The inverse boron worth is the inverse of the differential boron worth and is usually quoted in PPMB/%Δρ.

Table 9-2 shows the soluble boron worths usually performed for startup physics tests. Similar to critical boron concentrations, these worths are calculated with sequential bank insertions.

Differential boron worth (or inverse boron worth) can also be calculated as a function of boron concentration and as a function of cycle burnup. Figures 9-2 and 9-3 show the form in which results of these types of calculations are displayed.

9.1.2 Xenon Worth and Defect

Xenon worth is calculated as a function of cycle burnup using either PDQØ7 or EPRI-NODE. The nominal HFP depletion cases with equilibrium xenon are used as input to a second set of cases where the xenon concentration is set to zero (or the xenon cross sections are set to zero). The difference in reactivities between the equilibrium xenon and no xenon cases equals the equilibrium xenon worth at HFP. The results are displayed in a format similar to Figure 9-4.

Xenon worth can also be presented as a function of power level. Worths presented in this manner are usually referred to as the equilibrium xenon reactivity defect and are quoted in either pcm or %Δρ. Figure 9-5 shows the results of a xenon defect calculation.

9.1.3 Rod Worths

9.1.3.1 Group Worths

The worth of the shutdown and control banks are calculated at BOC HZP for use in the zero power physics testing. The rod banks are sequentially inserted or withdrawn from the EPRI-NODE calculation assuming no control rod overlap. The bank worth is the difference in reactivity between the fully inserted case and the fully withdrawn case.

Integral rod worth curves are calculated at BOC HZP for control banks B, C and D. The rod banks are inserted both sequentially and with 50% overlap. Figure 9-6 shows the form in which these results are displayed.

Control bank worths with sequential insertion and integral rod worth curves with 50% overlap are calculated at HFP equilibrium xenon both at BOC and EOC.

9.1.3.2 Stuck Rod Worth

The maximum worth of a single control rod stuck out of the reactor core at HZP is calculated during the final fuel cycle design (Section 4.2.2.2). The worth of the stuck rod is used by the site engineers in the reactivity balance procedures to guarantee shutdown margin. If the stuck rod worth is to be measured during the startup test program, then a recalculation of the worth is performed simulating the test conditions. This worth would then be provided as a startup test prediction.

9.1.3.3 Dropped Rod Worth

The maximum worth of a single control rod dropped into the reactor core is calculated during the final fuel cycle design (Section 4.2.2.4). If this parameter is to be measured during the startup test program, then a recalculation of the worth is performed simulating the test conditions. This worth would then be provided as a startup test prediction.

9.1.3.4 Ejected Rod Worth

The maximum ejected control rod worth is calculated during the final fuel cycle design (Section 4.2.2.3). If this parameter is to be measured during the startup test program, then a recalculation of the worth is performed simulating the test conditions. This worth would then be provided as a startup test prediction.

9.1.4 Reactivity Coefficients

9.1.4.1 HZP Coefficients

At HZP the isothermal temperature coefficient is measured by varying the average moderator temperature approximately 5°F, taking data once equilibrium is reached, then returning the temperature back to its original value, taking data and establishing equilibrium. The calculations used for predicting the isothermal temperature coefficient should be run at 557°F and 562°F using either EPRI-NODE or PDQØ7. The resulting reactivity change is then divided by the 5°F temperature change to yield the HZP isothermal temperature coefficient.

The Doppler or fuel temperature coefficient at HZP can be calculated by varying the fuel temperature while maintaining the moderator temperature constant at 557°F. The resulting reactivity change divided by the change in fuel temperature is the Doppler coefficient at HZP.

The predicted moderator coefficient is calculated by subtracting the Doppler coefficient from the isothermal coefficient. It is compared to the (inferred) measured moderator coefficient obtained by subtracting the predicted Doppler coefficient from the measured isothermal coefficient.

Alternately, the moderator temperature coefficient can also be explicitly calculated.

9.1.4.2 HFP Coefficients

Both a temperature coefficient of reactivity and a power Doppler coefficient of reactivity are calculated at HFP. The temperature coefficient is calculated by running one equilibrium HFP case at BOC (4EFPD EPRI-NODE or PDQØ7) and a second case which has lowered the moderator temperature 5°F. The difference in reactivity divided by the temperature change is the temperature coefficient. To calculate the power Doppler coefficient, a third case is performed where the power level is reduced to 95% FP. All other parameters are kept at the HFP equilibrium values. The difference in reactivity between the HFP and the 95% FP cases divided by 5% FP is the power Doppler coefficient.

9.1.5 Power Distribution

Power distributions, both assembly radial and total peaking factors, are measured at various power levels as identified in the test procedures for McGuire/Catawba reload startups. Calculations using EPRI-NODE are run at these power levels and nominal conditions to provide predicted power distributions for comparison.

9.1.6 Kinetics Parameters

Kinetics parameters are calculated using the methodology and codes as discussed in Section 4.3.3.8. These parameters include the six group β^i effective and λ^i, total β effective and ℓ^*, and reactivity versus positive and negative doubling times. These kinetics parameters are generated for both BOC HZP and BOC HFP conditions with ARO. A second set of delayed neutron data is generated at EOC.

9.2 Core Physics Report

The purpose of the core physics report is to document the predicted behavior of the reactor core as a function of burnup and power level. It is intended to be used for operator guidance and to aid the site engineer. Portions of the information included will reiterate data found in the nuclear design report and the startup test prediction report, however, much data not needed for these reports is useful to the operator and site engineers.

This report will include sufficient information to calculate reactivity balance throughout the cycle. Table 9-3 lists items typical of what will be calculated for this report. Any additional calculations will be performed using either EPRI-NODE or PDQØ7.

Table 9-1

CRITICAL BORON CONCENTRATIONS (PPMB)

HZP, NOXE, ØEFPD

ARO

Bank D in

Banks D + C in

Banks D + C + B in

Banks D + C + B + A in

Banks D + C + B + A + S_E in

Banks D + C + B + A + S_E + S_D in

Banks D + C + B + A + S_E + S_D + S_C in

Banks D + C + B + A + S_E + S_D + S_C + S_B in

Banks D + C + B + A + S_E + S_D + S_C + S_B + S_A in

HFP, NOXE, ØEFPD

ARO

HFP, EQXE, 4EFPD

ARO

Bank D in

HFP,EQXE,EOC

ARO

Table 9-2

BORON WORTH (PCM/PPMB)

HZP, NOXE, ØEFPD

ARO

Bank D in*

Banks D + C in

Banks D + C + B in

Banks D + C + B + A in

ARI

HFP, EQXE, 4 EFPD

ARO

HFP, EQXE, EOC

ARO

*Note: When bank worths are determined using interchange (swap) with a reference control bank, the boron worth with the reference bank only inserted is evaluated in place of sequential insertions.

Table 9-3

Core Physics Data

A. Critical Boron Concentrations
   1. ARO HFP versus Burnup
   2. ARO HZP versus Burnup

B. Shutdown Boron Concentrations required for shutdown with highest worth rod stuck out (NoXe)
   1. HZP versus Burnup
   2. 500°F, 200°F and 68°F versus Burnup

C. Differential Boron Worth HFP, HZP versus Burnup

D. Power Distributions from the Cycle Depletion

E. Rod Worths BOC, EOC, HFP and HZP

F. Xenon Worth versus Power Level

G. Xenon Worth versus Burnup

H. Reactivity Coefficients versus Temperature, Power Level and Burnup

FIGURE 9-1
BORON LETDOWN CURVE
HFP, ARO

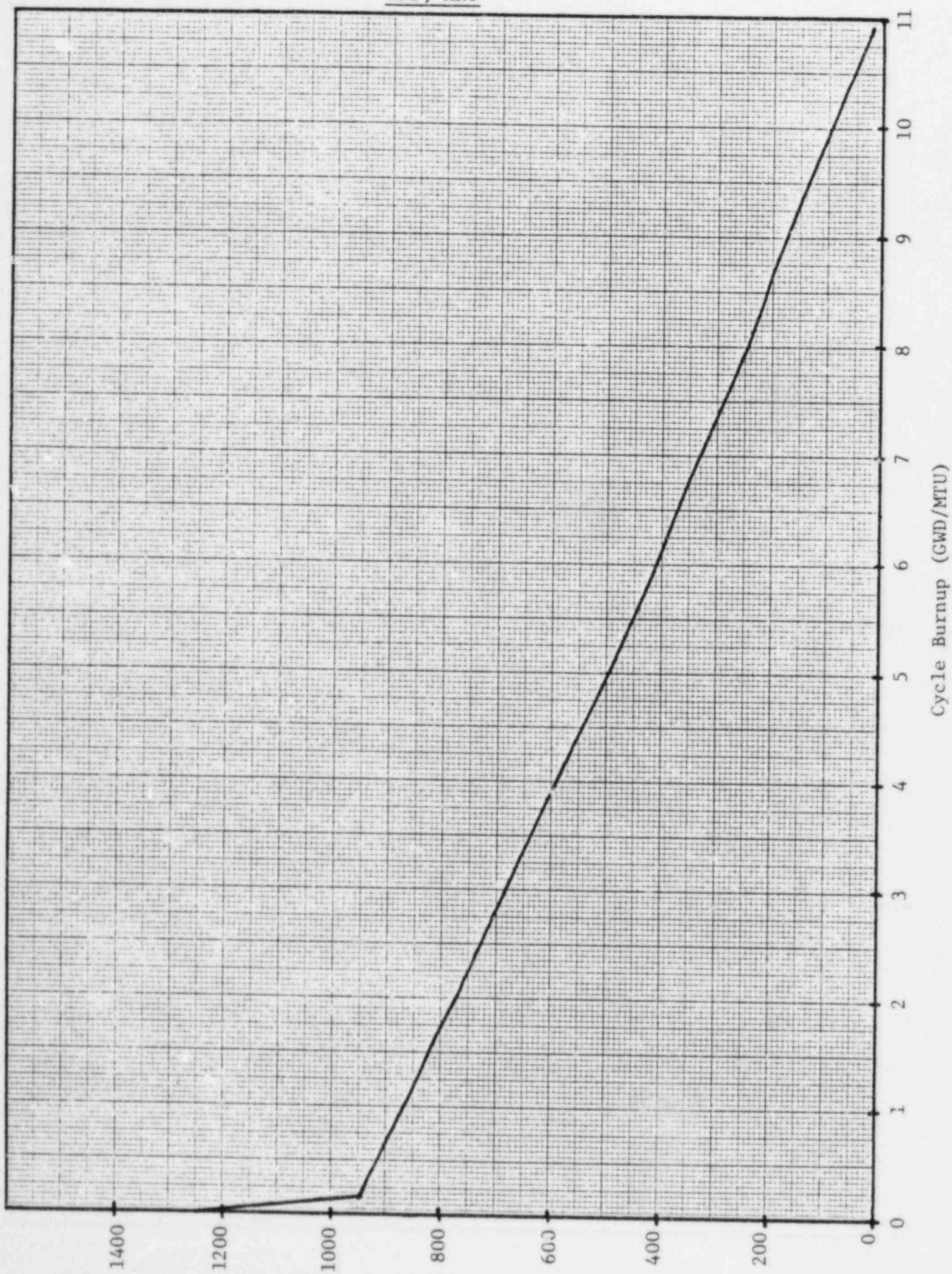

FIGURE 9-2

DIFFERENTIAL BORON WORTH

HZP, BOL

FIGURE 9-3

INVERSE BORON WORTH

HFP, ARO

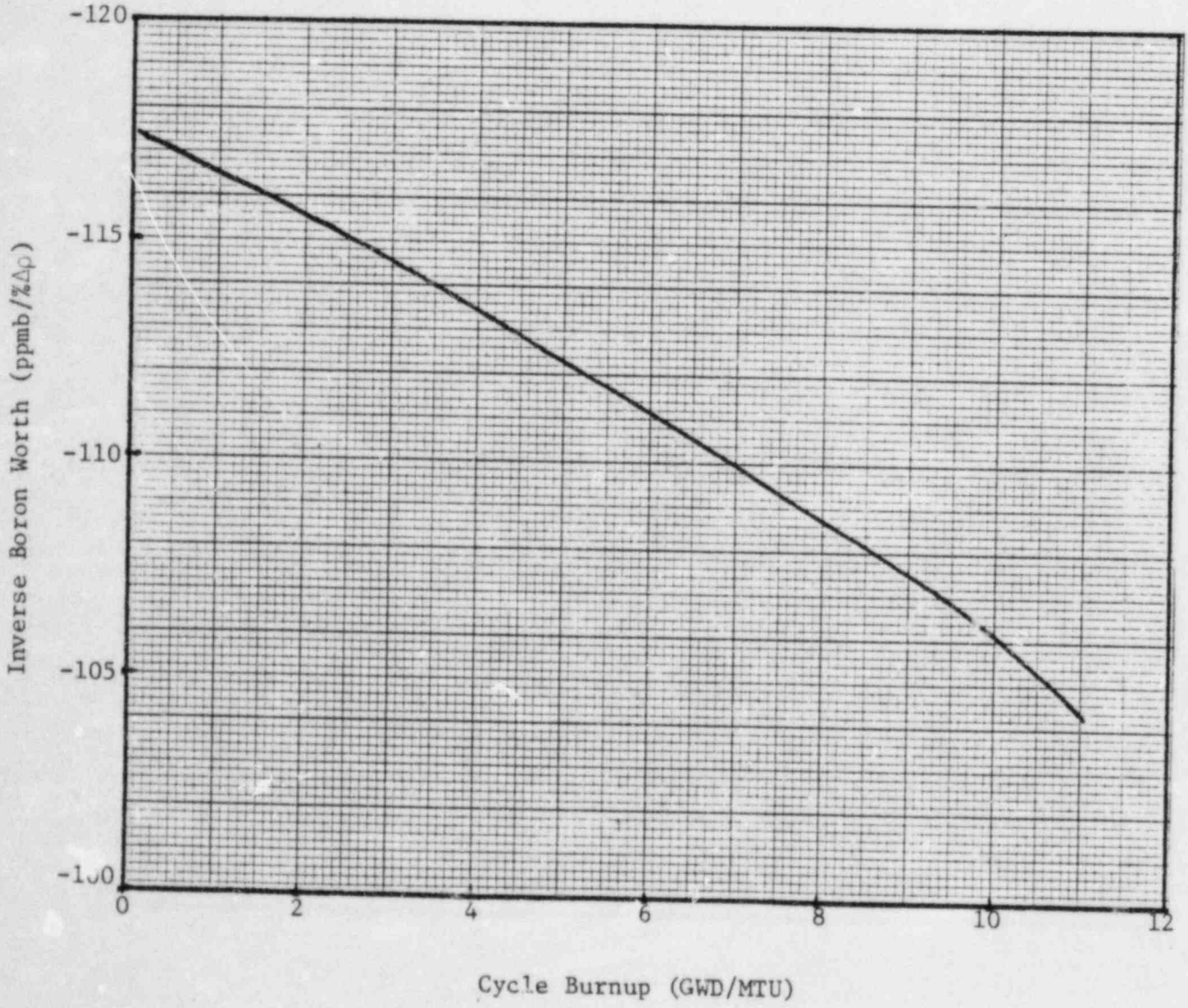

FIGURE 9-4

EQUILIBRIUM XENON WORTH

HFP

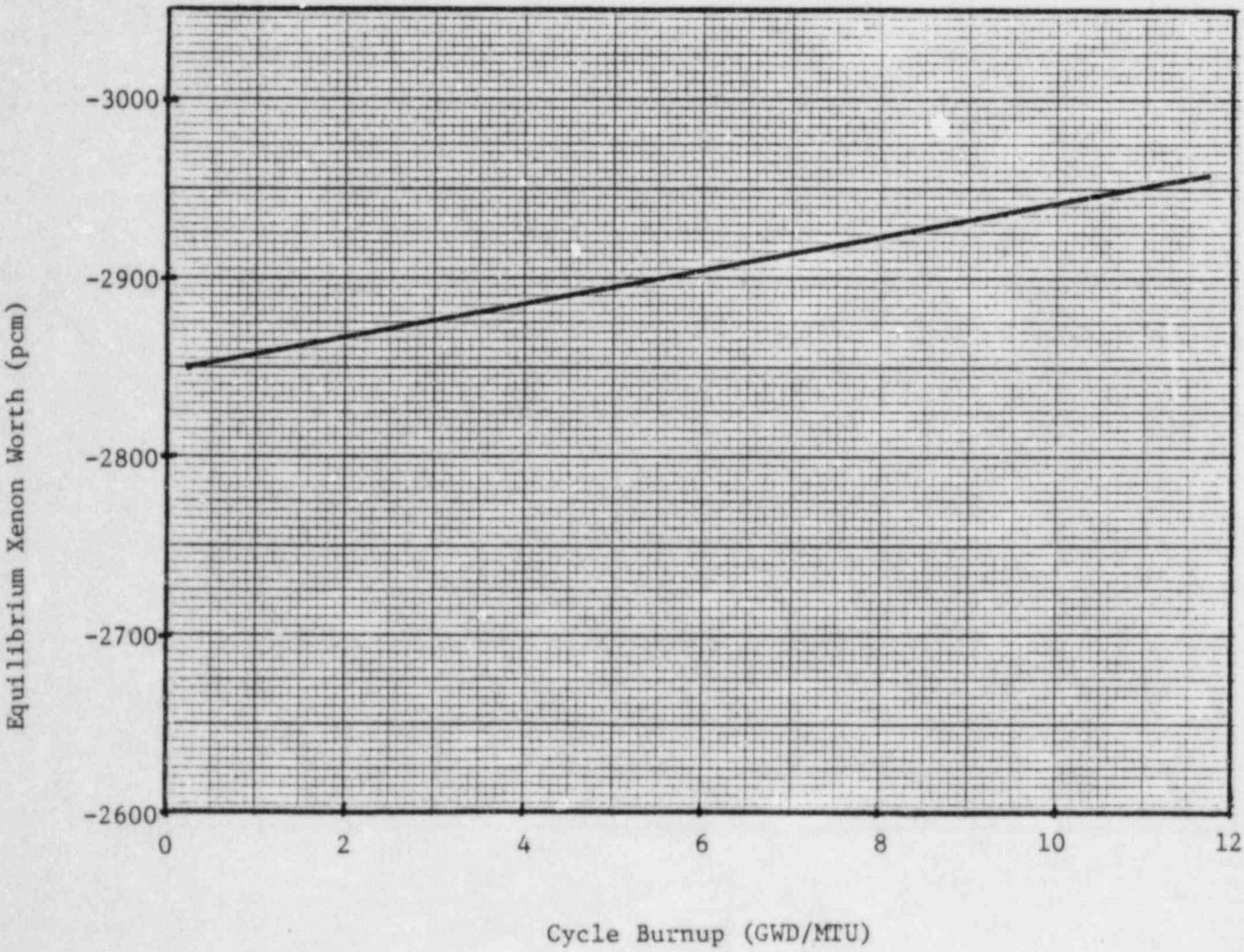

FIGURE 9-5

XENON REACTIVITY DEFECT

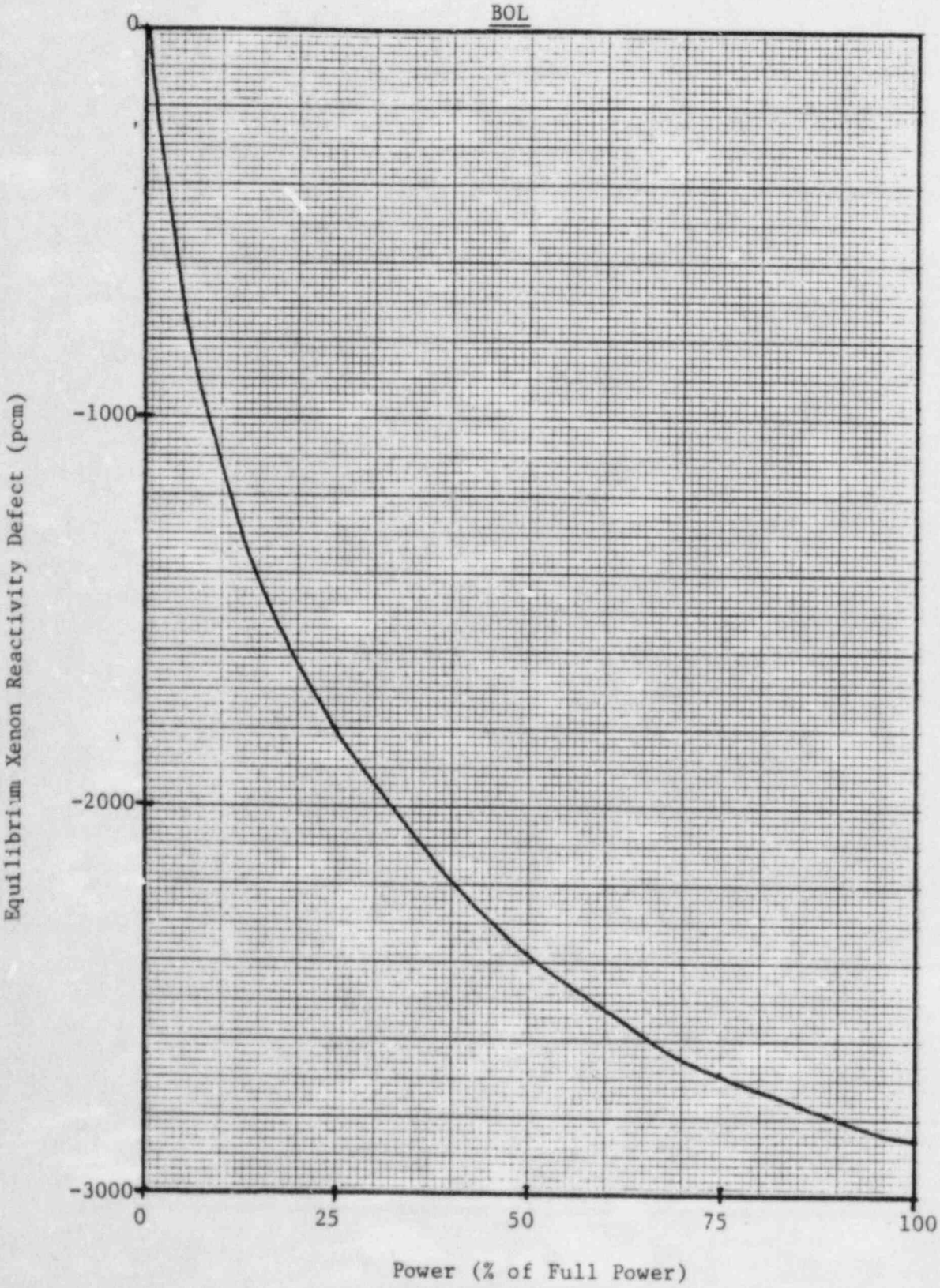

FIGURE 9-6

INTEGRAL ROD WORTH

HZP, BOL

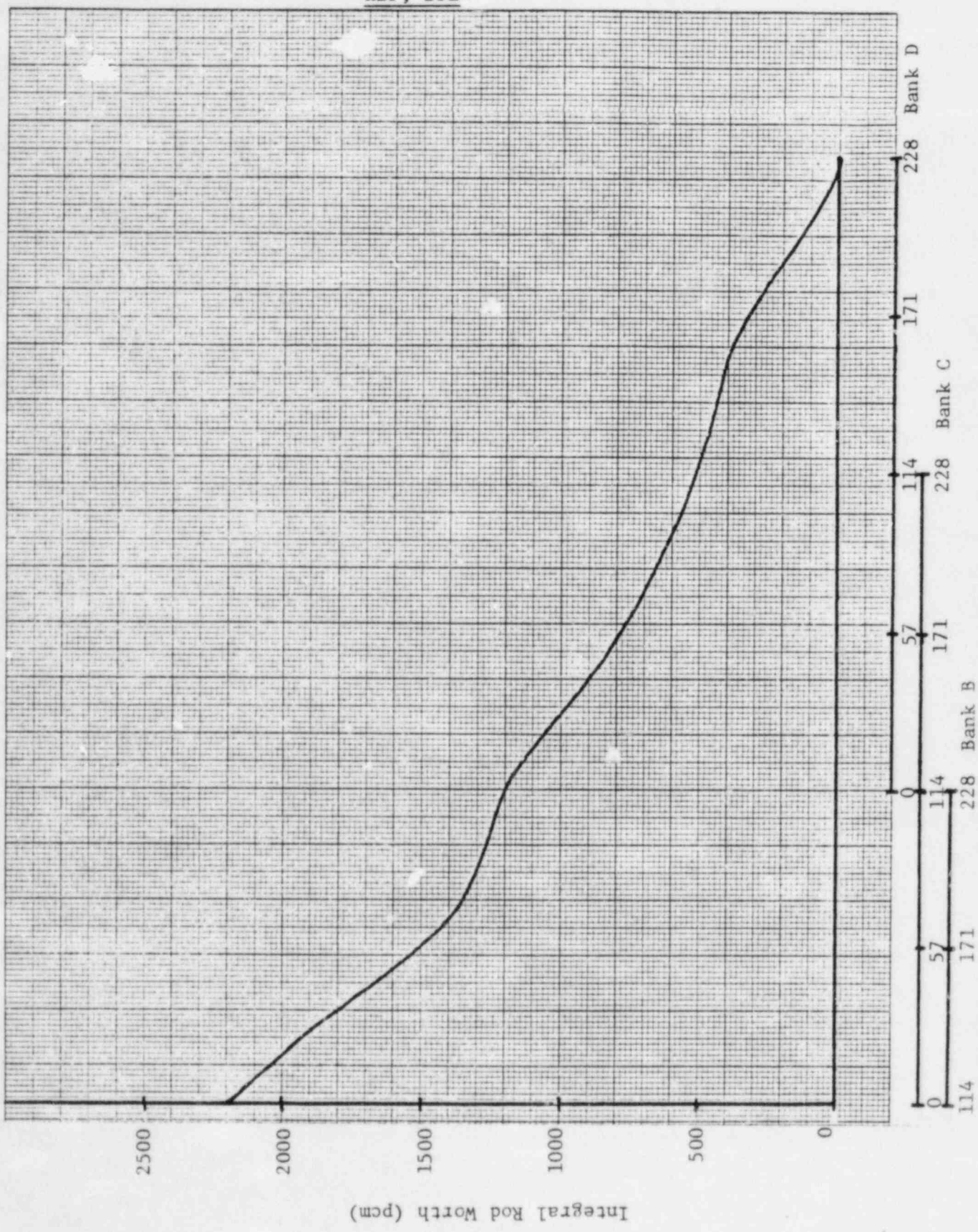

10.0 Physics Tests Comparisons

10.1 Introduction

This section presents measurement and calculational techniques and comparisons of calculated and measured results for some key core physics parameters. The physics parameters include hot zero power (HZP) and hot full power (HFP) critical boron concentrations, HZP control rod worths and ejected rod worths, and HZP isothermal temperature coefficients.

The measured data is from the McGuire Nuclear Station, Unit 1 Cycles 1 and 1A, and Unit 2, Cycle 1. (Broken hold down springs on some Burnable Poison rods were found during an outage on McGuire Unit 1 at 191.5 EFPD. During this outage, 94 of 96 Burnable Poison Rod Assemblies were removed from the core. Cycle 1A is the continuation of Cycle 1 but without the Burnable Poison Rods.) The measurment techniques discussed are those currently used at the station. The HZP measurments were taken at beginning-of-cycle (BOC) during the Zero Power Physics Testing. The HFP boron concentration measurements were taken at various time steps throughout the cycles. All calculations were performed with EPRI-NODE-P.

The comparisons of calculated and measured results present the means of the differences between the measured and calculated data and the corresponding standard deviations. The mean and standard deviation are defined as follows:

$$\text{Mean} = \bar{x} = \frac{\Sigma x_i}{n}$$

$$\text{Standard Deviation} = S = \sqrt{\frac{\Sigma (\bar{x} - x_i)^2}{n - 1}}$$

where: x_i = value for the i^{th} observation

n = number of observations.

10.2 Critical Boron Concentrations

10.2.1 Measurement Technique

Critical boron concentrations are measured at HZP and HFP by an acid-base titration of a reactor coolant system sample.

The measurement uncertainty for critical boron concentrations is due to (1) error in the titration method and (2) error due to differences between the sample concentration and the core average concentration. Based on conservative estimates of these errors, the total uncertainty associated with the critical boron concentration measurements is less than 20 ppmb.

10.2.2 Calculational Technique

Critical boron concentrations are calculated at HZP and HFP using EPRI-NODE-P in the boron search mode. Since the search does not yield an exactly critical value, fixed boron runs using EPRI-NODE-P are also made to calculate a boron worth, which is then used to correct the calculated boron concentration to exactly critical.

10.2.3 Comparison of Calculated and Measured Results

10.2.3.1 Hot Zero Power Comparison

The calculated and measured critical boron concentrations at HZP and BOC for McGuire Unit 1, Cycles 1 and 1A, and Unit 2, Cycle 1 are compared in Table 10-1. Each entry corresponds to a different control rod position. The mean of the differences for these three cycles was found to be -7 ppmb with a standard deviation of 16 ppmb.

10.2.3.2 Hot Full Power Comparison

The calculated and measured critical boron concentrations at HFP for McGuire Unit 1, Cycles 1 and 1A, are compared in Table 10-2. The mean of the differences for these cycles is -41 ppmb with a standard deviation of 11 ppmb.

The data displayed in Table 10-2 can be visualized better by examining plots of soluble boron concentration as a function of burnup. These boron letdown curves are shown in Figures 10-1 and 10-2.

10.2.4 Summary

The comparison between EPRI-NODE-P and measured critical boron concentrations at HZP and HFP indicate EPRI-NODE-P can adequately predict soluble boron concentrations.

10.3 Control Rod Worth

10.3.1 Measurement Techniques

Individual control rod bank worths are measured by the boron swap technique. This technique involves a continuous decrease in boron concentration together with an insertion of the control rods in small, discrete steps. The change in reactivity due to each insertion is determined from reactivity computer readings before and after the insertion. The worth of each rod bank is the sum of all the reactivity changes for that bank. Measured bank worths in ppmB can be determined independent of the reactivity computer by using the measured boron endpoints.

10.3.2 Calculational Techniques

Individual and total controlling rod bank worths in terms of reactivity are calculated by making two EPRI-NODE-P runs. The first is a boron search run with the rod bank(s) out. The boron concentration found in this run is then used in a fixed boron run with the rod bank(s) in. The difference in reactivity between these two runs with constant boron concentration is the rod bank(s) worth.

Bank worths were also calculated using the calculated Boron endpoints. These bank worths are in terms of ppmB.

10.3.3 Comparison of Calculated and Measured Results

A comparison of calculated and measured control rod worths in terms of reactivity is shown in Table 10-3. This table compares the worths of control banks: D, C, B, and A and shutdown banks: E, D, and C at HZP

and BOC for McGuire Unit 1, Cycles 1 and 1A, and McGuire Unit 2, Cycle 1. A comparison of calculated and measured control rod worths in terms of ppmB is shown in Table 10-4. This table also compares the worths of control banks: D, C, B, and A and shutdown banks: E, D, and C at HZP and BOC for McGuire Unit 1, Cycles 1 and 1A, and McGuire Unit 2 Cycle 1. Table 10-5 is a comparison of PDQØ7 calculated and measured control rod worths.

PDQØ7 calculated bank worths agree well to measured with an average difference of 2.7% and a standard deviation of 3.3%. EPRI-NODE-P calculated bank worths similarly agreed well with an average difference of -4.5% and a standard deviation of 5.1%. Rod worths calculated using boron endpoints also agreed well, with an average difference of -2.2% and a standard deviation of 7.9%.

10.3.4 Summary

The comparisons between the calculated and measured control rod worths at HZP indicate that EPRI-NODE-P can adequately predict control rod worths. Tables 10-3 and 10-4 indicate consistent agreement using either reactivity or boron endpoint measurement techniques.

10.4 Ejected Rod Worths

Ejected rod worth is defined here as the measured worth of the worst case ejected rod No error adjustments have been included.

10.4.1 Measurement Technique

Ejected rod worths are measured by boron swap. The boron swap method is similar to the method used to measure control rod worth. It involves maintaining criticality by varying the boron concentration to compensate for the ejection of the worst case rod. The control rod positions are held constant. As was done for control rod worth, the ejected rod worth is determined from the reactivity computer.

10.4.2 Calculational Techniques

Ejected rod worths are calculated using EPRI-NODE-P to simulate boron swap. A boron search run is first performed to determine the critical boron concentration at the rod group position. The boron concentration

as calculated in the EPRI-NODE-P run should be corrected for exact criticality. Using this corrected boron concentration and a constant rod group position, the reactivity is determined with the worst case rod first in and then out. The ejected rod worth is the difference in reactivity between the worst case rod in and out.

10.4.3 Comparison of Calculated and Measured Results

A comparison of calculated and measured ejected rod worth for McGuire Unit 1, Cycle 1, is given in Table 10-6.

10.5 Isothermal Temperature Coefficients

The isothermal temperature coefficient is defined as the change in reactivity per unit change in moderator temperature at hot zero power, i.e.,

$$\alpha_T = \frac{\Delta\rho}{\Delta T}$$

10.5.1 Measurement Techniques

The isothermal temperature coefficient is measured by executing an average moderator temperature ramp to +5°F and then a ramp down to the initial equilibrium critical conditions. During each change, reactivity is measured on the reactivity computer and other pertinent data is measured. After each change, steady state conditions are established. The isothermal temperature coefficient is determined as the change in reactivity between plateaus divided by the change in temperature. Since two different temperature ramps are executed, two coefficients can be determined. The reported isothermal temperature coefficient is an average of these two coefficients.

10.5.2 Calculational Technique

The isothermal temperature coefficient at HZP is calculated using EPRI-NODE-P. Two cases with the same boron concentration and rod positions but different moderator temperatures are run. The isothermal temperature coefficient is the difference in reactivity between the two cases divided by the difference in the moderator temperatures.

10.5.3 Comparison of Calculated and Measured Results

A comparison of calculated and measured isothermal temperature coefficients at HZP and BOC for McGuire Unit 1, Cycles 1 and 1A, and Unit 2, Cycle 1 is presented in Table 10-7. The mean of all the differences was found to be 1.38 pcm/°F with a standard deviation of 1.87 pcm/°F.

10.5.4 Summary

The comparison between calculated and measured isothermal temperature coefficients indicates that EPRI-NODE-P is a good predictor of isothermal temperature coefficients.

Table 10-1
MCGUIRE
CRITICAL BORON CONCENTRATIONS AT HOT ZERO POWER, BOC

Unit	Cycle	Critical Boron Conc. PPM Calculated	Measured	Difference
1	1	1301	1310	-9
		1242	1248	-6
		1123	1128	-5
		1033	1029	4
		972	967	5
		888	891	-3
		822	819	3
		728	723	5
1	1A	1269	1310	-41
		1200	1242	-42
		1090	1125	-35
2	1	1280	1295	-15
		1221	1217	4
		1101	1097	4
		1002	997	5
		944	938	6
		861	860	1
		788	791	-3
		691	694	-3
Mean		----	----	-6.6
Standard Deviation		----	----	15.7

Difference = Calculated - Measured

Table 10-2
MCGUIRE 1 CYCLES 1-1A
HOT FULL POWER CRITICAL BORON CONCENTRATIONS

Unit	EFPD	Critical Boron Conc. PPM Calculated	Measured	Difference PPM
1	24.6	860	880	-20
	34.4	846	865	-19
	39.2	838	864	-26
	49.2	823	862	-39
	82.2	761	801	-40
	90.4	745	790	-45
	99.0	729	771	-42
	101.2	724	762	-38
	126.0	667	724	-57
	154.4	600	650	-50
	180.7	531	591	-60
1A	203.7	782	831	-49
	217.5	713	751	-38
	227.8	673	719	-46
	232.9	653	696	-43
	238.5	631	677	-46
	255.2	566	615	-49
	279.8	473	511	-38
	300.6	395	434	-39
	330.8	281	318	-37
Mean		----	----	-41.1
Standard Deviation		----	----	10.5

Table 10-3
MCGUIRE
CONTROL ROD WORTHS AT HOT ZERO POWER, BOC

Unit/Cycle	Bank	Rod Worth (PCM) Calculated	Measured	Difference (PCM)	Difference (%)
1/1	CD	606	669	-63	-9.4
	CC	1217	1250	-33	-2.6
	CB	925	996	-71	-7.1
	CA	654	695	-41	-5.9
	SE	884	840	44	5.2
	SD	668	755	-87	-11.5
	SC	961	1011	-50	-4.9
1/1A	CD	685	712	-27	-3.8
	CC	1100	1038	62	6.0
2/1	CD	604	664	-60	-9.0
	CC	1224	1283	-59	-4.6
	CB	1004	1105	-101	-9.1
	CA	618	678	-60	-8.8
	SE	862	853	9	1.1
	SD	738	771	-33	-4.3
	SC	992	1026	-31	-3.0
Mean		----	----	-37.6	-4.5
Standard Deviation		----	----	43.8	5.1

Difference (pcm) = Calculated-Measured

$$\text{Difference (\%)} = \frac{\text{Calculated-Measured}}{\text{Measured}} \times 100$$

Table 10-4
MCGUIRE
CONTROL ROD WORTHS AT HOT ZERO POWER, BOC
USING BORON ENDPOINTS

Unit/Cycle	Bank	Rod Worth (PPM) Calculated	Measured	Difference (PPM)	Difference (%)
1/1	CD	59	62	-3	-4.8
	CC	119	120	-1	-0.8
	CB	90	99	-9	-9.1
	CA	61	62	-1	-1.6
	SE	84	76	8	10.5
	SD	66	72	-6	-8.3
	SC	94	96	-2	-2.1
1/1A	CD	69	68	1	1.5
	CC	110	117	-7	-6.0
2/1	CD	59	78	-19	-24.4
	CC	120	120	0	0.0
	CB	99	100	-1	-1.0
	CA	58	59	-1	-1.7
	SE	83	78	5	6.4
	SD	73	69	4	5.8
	SC	97	97	0	0.0
Mean		----	----	-2.0	-2.2
Standard Deviation		----	----	6.3	7.9

Table 10-5
MCGUIRE
PDQØ7 CALCULATED ROD WORTHS VS MEASURED ROD WORTHS AT HZP, BOC

Unit/Cycle	Bank	Rod Worth (PCM) Calculated	Measured	Difference (PCM)	Difference (%)
1/1	D	644	669	-25	-3.7
	C	1214	1250	-36	-2.9
	B	962	996	-34	-3.4
1/1A	D	667	712	-45	-6.3
	C	1088	1038	50	4.8
2/1	D	637	664	-27	-4.1
	C	1261	1283	-22	-1.7
	B	1090	1105	-15	-1.4
	A	638	678	-40	-5.9
Mean		----	----	-22	-2.7
Standard Deviation		----	----	28	3.3

$$\text{Difference (pcm)} = \text{Calculated-Measured}$$

$$\text{Difference (\%)} = \frac{\text{Calculated-Measured}}{\text{Measured}} \times 100$$

Table 10-6
MCGUIRE 1 CYCLE 1
EJECTED ROD WORTHS

Cycle	Location	Worth (PCM) Calculated	Measured	Difference (pcm)
1	D-12	406	432	-26

Table 10-7
MCGUIRE
ISOTHERMAL TEMPERATURE COEFFICIENTS AT HOT ZERO POWER, BOC

Unit/Cycle	Control Rod Configuration	Temp. Coeff., (pcm/°F) Calculated	Measured	Difference (pcm/°F)
1/1	ARO	-1.03	-0.57	-0.46
	Din	-2.09	-2.02	-0.07
	C & D in	-6.03	-5.86	-0.17
	B,C & D in	-6.08	-6.83	0.75
	A,B,C,& D in	-9.37	-9.72	0.35
1/1A	ARO	-4.51	-1.13	-3.38
	Din	-5.86	-1.98	-3.88
	C & D in	-9.76	-4.83	-4.93
2/1	ARO	-2.34	-1.41	-0.93
	Din	-3.54	-2.73	-0.81
	C & D in	-7.70	-6.07	-1.63
Mean	---	---	---	-1.38
Standard Deviation	---	---	---	1.87

Difference = Calculated-Measured

FIGURE 10-1

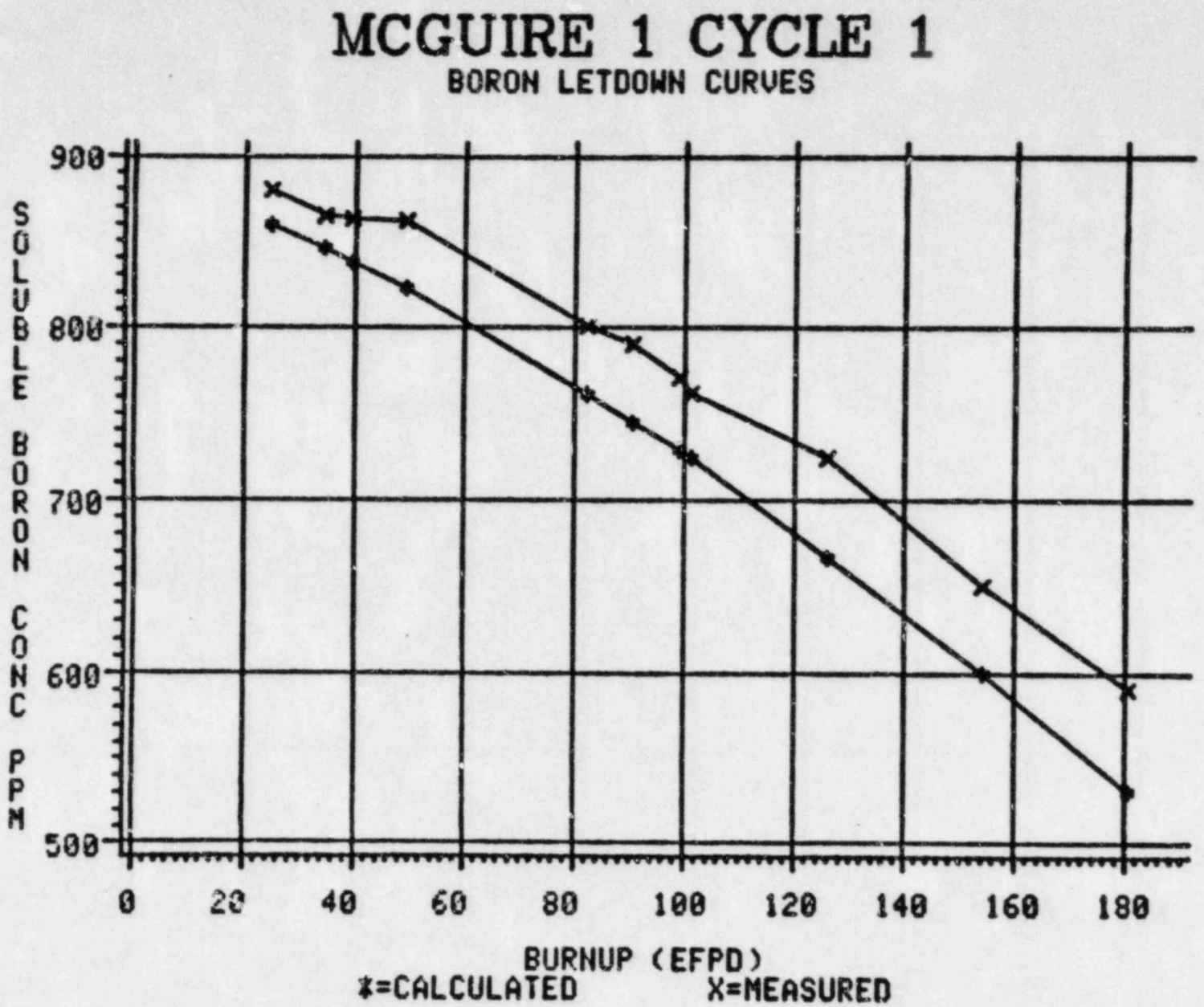
MCGUIRE 1 CYCLE 1
BORON LETDOWN CURVES
SOLUBLE BORON CONC PPM
900
800
700
600
500
0
20
40
60
80
100
120
140
160
180
BURNUP (EFPD)
*=CALCULATED
X=MEASURED

FIGURE 10-2

MCGUIRE 1 CYCLE 1-A

BORON LETDOWN CURVES

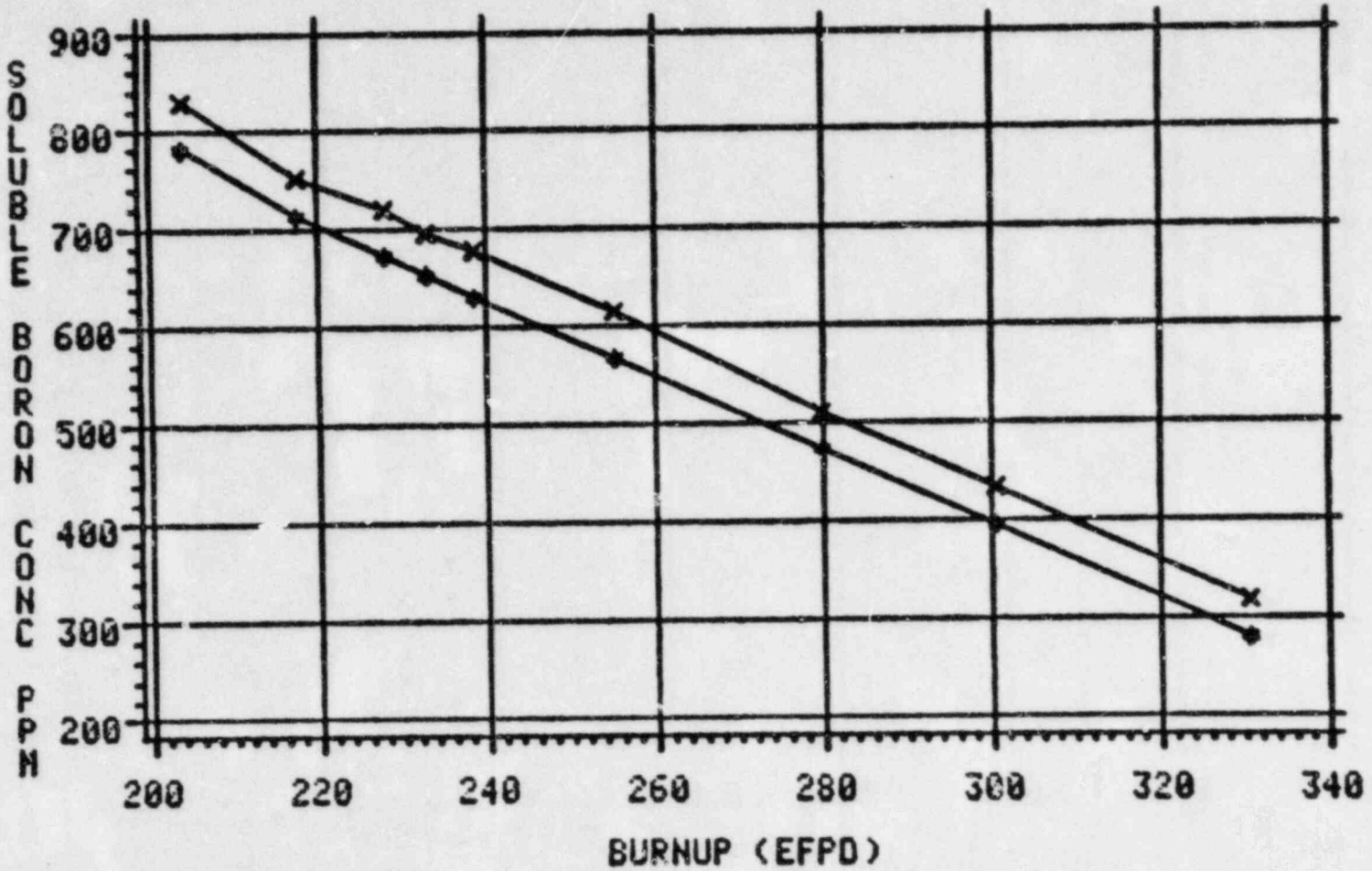

11.0 POWER DISTRIBUTION COMPARISONS

INTRODUCTION AND SUMMARY

11.1.1 Introduction

The current nuclear code employed by Duke Power Company for three dimensional assembly power calculations is EPRI-NODE-P. This code has been benchmarked against McGuire Unit 1 Cycle 1 and part of Cycle 1A. It has also been benchmarked against TVA's Sequoyah Unit 1 Cycle 1.

This work encompassed: derivation of measured power distributions for the above cycles, simulations of the above cycles using EPRI-NODE-P, development of fitting procedures for the calculated assembly peak axial powers, and development of a statistical basis for estimating the calculational accuracy of EPRI-NODE-P.

11.1.2 Summary

A data base consisting of McGuire Unit 1 Cycle 1 and part of Cycle 1A, and TVA's Sequoyah Unit 1 Cycle 1, measured and EPRI-NODE-P calculated fuel assembly powers was assembled. Calculated and measured powers were statistically combined to derive 95/95 Observed Nuclear Reliability Factors (ONRF) for EPRI-NODE-P. ONRF's were calculated for both assembly radial powers and assembly peak axial powers. The assembly radial power is defined as the ratio of assembly average power to core average power. The assembly peak axial power is defined as the maximum assembly x-y planar average power along the fuel assembly length relative to the core average power. F_Q is then the product of the assembly radial local and peak average power (see equation 6-1).

ORNFs of 1.03 for the radial powers and 1.06 for the peak axial powers were determined.

11.2 MEASURED DATA

11.2.1 Measured Assembly Power Data

The measured power data base comprises assembly power data from McGuire Unit 1, Cycle 1 and part of Cycle 1A, and TVA's Sequoyah Unit 1, Cycle 1. All measured assembly power data are directly traceable to signals from the incore detector system.

11.2.2 Measurement System Description

The incore detector systems at McGuire and Sequoyah consist of 6 movable miniature fission chamber neutron detectors. The detectors are inserted into the bottom of the reactor vessel and driven up through the core to the top. They are then slowly withdrawn through the core. Incore flux maps are obtained by taking voltage signal readings from the detectors as they are withdrawn through the core. This data is then stored on the plant computer.

The detectors travel inside thimbles that are located in the Instrument Guide Tube of the fuel assemblies. There are 58 instrumented assemblies out of a total of 193 fuel assemblies. There are 61 voltage signals recorded axially along each of instrumented fuel assemblies. The instrumented fuel assemblies are shown on Figure 11-1.

The detectors are inter-calibrated by inserting each detector into one reference (calibration) fuel assembly. After each flux map the detector signals are processed by Shanstrom Nuclear Associates Code for Operating Reactor Evaluation (SNA-CORE)[23]. SNA-CORE uses the 58 x 61 array of signals to calculate peaking factors, (radial powers and assembly peak axial powers) for each of the 193 assemblies. The 193 radial powers and assembly peak axial powers are then averaged into eighth core or quarter core, depending on the cycle. These peaking factors then make up the measured data base. All power measurements were taken at approximately equilibrium xenon conditions. Tables 11-1, 11-2, and 11-3 show the selected reactor state points.

11.3. EPRI-NODE-P POWER DISTRIBUTION COMPARISONS

11.3.1 EPRI-NODE-P Model

The primary three-dimensional nuclear code employed at Duke Power is EPRI-NODE-P. This code is used for all maneuvering analyses, core follow, and physics test data where three-dimensional core power distributions are required. In this section, comparisons of measured and EPRI-NODE-P calculated values will be shown for both radial powers and assembly peak axial powers. Comparisons were performed on a total of 37 reactor state points covering McGuire Unit 1, Cycle 1 and part of 1A, and Sequoyah Unit 1, Cycle 1.

McGuire Unit 1, Cycle 1 and Sequoyah Unit 1, Cycle 1 were modeled using eighth core symmetry. McGuire Unit 1, Cycle 1A was modeled using quarter core symmetry. Each fuel assembly was modeled with one radial and 12 equidistant axial nodes. The active stack height was set at 144 inches. Control rods could be positioned continuously in this model. Simulations of the McGuire and Sequoyah cores were performed using methods described in Section 3.5 and 5.2.

11.3.2 Fuel Cycle Simulations

Using the EPRI-NODE-P model described in section 11.3.1, McGuire Unit 1, Cycles 1 and part of 1A, and TVA's Sequoyah Unit 1, Cycle 1 were depleted using thermal and hydraulic feedbacks. The depletions were performed in a core follow mode, utilizing critical boron searches at each exposure step.

McGuire Unit 1, Cycle 1 operated until 191.5 EFPD. Control and shutdown bank locations are shown on Figure 11-2. The core loading pattern is shown on Figure 11-3. During this time the unit was operated mostly at the 50% and 75% power plateaus because of power limitations imposed by steam generator flow impingement problems.

The EPRI-NODE-P radial powers were normalized to PDQØ7 depletion at 25 EFPD for McGuire Unit 1, Cycle 1. There were 25 state points for this cycle. These are shown on Table 11-1. Figures 11-6 to 11-30 show

comparisons of calculated and measured radial powers. Figure 11-31 to 11-55 show comparisons of calculated and measured assembly peak axial powers.

The data used for McGuire Unit 1, Cycle 1A was through 250 EFPD. Control and shutdown bank locations are the same as those for McGuire Unit 1, Cycle 1. The core loading pattern for cycle 1A was the same as the loading pattern for Cycle 1 except all but 2 burnable poison rods were removed. The two that remained were in core locations H-3 and H-13. The unit was operated mostly at 100% power during this time after the steam generator flow impingement problem was corrected.

The EPRI-NODE-P radial powers were normalized to PDQØ7 depletion at 257 EFPD for McGuire Unit 1, Cycle 1A. There were 5 state points for the part of this cycle that was used. These are shown on Table 11-2. Figures 11-56 to 11-60 show comparison of calculated and measured radial powers. Figures 11-61 to 11-65 show comparisons of calculated and measured assembly peak axial powers.

TVA's Sequoyah Unit 1, Cycle 1 operated until the end of cycle which lasted 390 EFPD. Control and shutdown bank locations are shown on Figure 11-4. The core loading pattern is shown on Figure 11-5.

The EPRI-NODE-P radial powers were normalized to PDQØ7 depletion at 25 EFPD for Sequoyah Unit 1, Cycle 1. There were 7 state points for this cycle. These are shown on Table 11-3. Figures 11-66 to 11-72 show comparison of calculated and measured radial powers. Figures 11-73 to 11-79 show comparison of calculated and measured assembly peak axial powers.

11.3.3 Radial Power Methodology

The radial powers are radial peaking factors. Therefore, the radial peaking factors from SNA-CORE are compared directly to the normalized radial powers (P(I,J)) from EPRI-NODE-P.

11.3.4 Assembly Peak Axial Power Methodology

The assembly peak axial powers are peaking factors. There are 61 assembly axial powers for each fuel assembly calculated by SNA-CORE. Of these 61 assembly axial powers, the maximum is chosen for the "measured" assembly peak axial power. The EPRI-NODE-P model calculated 12 nodal axial powers per assembly. The assembly peak axial power could not be compared directly to the maximum nodal power.

Therefore, the nodal axial powers were curve fit using the following equation:

$$P(z) = \sum_{n=1}^{3} A_n \text{ Sin } (n\pi z) + B_n \text{ Cos } (n\pi z)$$

Where: A_n, B_n = Fourier series coefficients
z = normalized vertical axis variable
n = Fourier sequence number

The 12 level node powers were fit, yielding 61 assembly axial powers for each assembly at each state point. The assembly peak axial power was then selected from the 61 calculated assembly axial powers and the 12 nodal powers.

11.3.5 Conclusions

EPRI-NODE-P yielded consistently good power distributions when compared to measured power distributions. This conclusion applies for both radial and assembly peak axial power comparisons. Although the conclusions in this section are qualitative, quantitative statistical results of these comparisons will be shown in Section 11.5.

11.4 PDQØ7 - POWER DISTRIBUTION COMPARISONS

Radial power distributions from the PDQØ7 depletions of McGuire Unit 1, Cycle 1, Cycle 1A, and Sequoyah Unit 1, Cycle 1 were compared to measured radial power distributions from SNA-CORE at various burnups. The PDQØ7 model employed a 2-dimensional geometry with two neutron energy groups. (For additional information concerning the use of this code, refer to Section 3.4). All power distributions from PDQØ7

were performed at hot full power all rods out. Table 11-4 compares the state points of the measured data to that of PDQØ7. Figures 11-80 to 11-86 show the comparisons of the radial powers.

11.5. STATISTICAL ANALYSIS

11.5.1 Observed Nuclear Reliability Factor Derivation

This section will address quantitatively statistics arising from Section 11.3. Normal distribution theory will be used in deriving calculational uncertainties.

In deriving the calculational uncertainty for EPRI-NODE-P, the algebraic difference between a calculated and a measured value forms a normally distributed (refer to Section 11.5.2) random variable.

The difference variable is defined:

$$D_i = C_i - M_i \qquad (11\text{-}1)$$

where: D is the i^{th} difference; $1 \leq i \leq N$
C is the i^{th} calculated value (radial or assembly peak axial power)
M is the i^{th} measured value (radial or assembly peak axial power)

The mean of the difference as defined in equation 11-2 is:

$$\bar{D} = \bar{C} - \bar{M} \qquad (11\text{-}2)$$

where:

$$\bar{C} = \left(\sum_{i=1}^{n} C_i\right) \div n \qquad (11\text{-}2a)$$

$$\bar{M} = \left(\sum_{i=1}^{n} M_i\right) \div n \qquad (11\text{-}2b)$$

$$\bar{D} = \left(\sum_{i=1}^{n} D_i\right) \div n \qquad (11\text{-}2c)$$

n = number of observations in sample

Now a one sided upper bound factor is derived by employing One Sided Upper Tolerance Limit (OSUTL) methodology. For a normal random variable X with a sample mean X and standard deviation S, the OSUTL of X is defined by:

$$OSUTL(X) = \bar{X} + K \times S \qquad (11\text{-}3)$$

where: $$\bar{X} = \left(\sum_{i=1}^{n} X_i\right) \div n \qquad (11\text{-}4)$$

$$S = \left[\left(\sum_{i=1}^{n} (X_i - \bar{X})^2\right) \div (n-1)\right]^{\frac{1}{2}} \qquad (11\text{-}5)$$

In equation 11-3, K is the one-sided tolerance factor. Equation 11-3 is formulated such that a predetermined proportion of the population (P) is below the OSUTL with a confidence factor (α)[26]. K is explicitly dependent on n, P, and α.

Following industry practice, P = 95% and α = 95%.

The OSUTL is given for D by:

$$OSUTL(D) = \bar{D} + K \times S(D) \qquad (11\text{-}6)$$

C is a deterministic variable and does not have an OSUTL per se, but a reasonable upper limit to C can be defined by:

$$UL(C) = \bar{M} + OSUTL(D) \qquad (11\text{-}7)$$

$$UL(C) = M + \bar{D} + \bar{K} \times S(D) \qquad (11\text{-}7a)$$

If one substitutes equations 11-2 into equation 11-7 you obtain the following:

$$UL(C) = \bar{M} + \bar{C} - \bar{M} + K \times S(D) \qquad (11\text{-}8)$$

$$\text{or} \quad UL(C) = \bar{C} + K \times S(D) \qquad (11\text{-}8a)$$

From equation (11-8a), it is more obvious that the upper limit is a function of the calculated parameter. Also, it is obvious that the standard deviation being associated with the calculated limit is that of the difference distribution. This means that any error in the measurement of the radial or assembly peak axial power as well as any calculational error will be included in the UL(C) parameter.

While equation 11-7a and 11-8a are valid, the definition of $\bar{D} = \bar{C} - \bar{M}$ (equation 11-2) leads to UL(C) being smaller if the measured parameter is underpredicted. The conservative solution to this is to subtract $\bar{D}$ in equation 11-7a instead of adding it. This would yield the following equation:

$$UL(C) = \bar{M} - \bar{D} + K \times S(D) \qquad (11\text{-}9)$$

Finally, the Observed Nuclear Reliability Factor (ONRF) is defined as the quotient of UL(C) from equation 11-9 and the mean of the measurements:

$$ONRF = \frac{UL(C)}{\bar{M}} \qquad (11\text{-}10) \text{ or,}$$

$$ONRF = \frac{\bar{M} - \bar{D} + K \times S(D)}{\bar{M}} \qquad (11\text{-}11)$$

The ONRF from equation 11-11 will be used as a multiplicative factor applied to EPRI-NODE-P calculated powers such that:

$$ONRF \times C \geq M \qquad (11\text{-}12)$$

for 95% of the population and with a confidence factor of 95%. Separate ONRF's are derived for radial and assembly peak axial powers.

This procedure was employed in Reference 3 to statistically evaluate ORNFs for EPRI-NODE-P as part of the Oconee Reload Design Methodology.

11.5.2 Normality Test Results

In analyzing the normality of the difference distributions, C,M data were grouped into the following categories:

1) reactor cycle: McGuire 1, Cycle 1; McGuire 1, Cycle 1A; Sequoyah 1, Cycle 1
2) grouped cycles: All reactor cycles combined
3) type: radial powers or assembly peak axial powers

The difference distributions were analyzed for normality using the D' test from ANSI N15.15 - 1974.[27] Using the engineering judgement that only peaking factors greater than the core average are the area of concern, pairs of C,M where both are ≥ 1.0 will be treated. Table 11-5 displays the normality test results. The level of significance was chosen to be .05. Therefore, the D' statistic must be between the .025 and .975 percentage point D' values for normality. Here, 3 out of 4 assembly radial power distributions were normal and 4 assembly peak axial power distributions were normal. The remainder of the difference distributions yielded D' statistics that were close to the critical values and were therefore classified as nearly normal.

11.5.3 Observed Nuclear Reliability Factors (ONRF) for EPRI-NODE-P

In this subsection the statistical treatment developed in Section 11.5.1 will be utilized to develop ONRF's ($F^R_{\Delta H}$ and F^R_Q) for McGuire Unit 1, Cycle 1 and part of Cycle 1A, and TVA's Sequoyah Unit 1, Cycle 1, combined.

All pairs of C, M ≥ 1.0 from all 37 state points of McGuire Unit 1,

Cycle 1 and part of Cycle 1A, and Sequoyah Unit 1, Cycle 1, were obtained. The procedure was applied to radial powers and repeated for assembly peak axial powers. The variables shown in equation 11-11 were then derived and the ONRF's calculated.

As an example, for radial ORNF ($F^R_{\Delta H}$):

$$\bar{M} = 1.131$$
$$\bar{D} = 0.002$$
$$S(D) = 0.020$$
$$N = 846$$
$$K = 1.7343 \ (N = 846, \ 95\%/95\%)$$

Therefore, the ONRF would be:

$$ONRF = \frac{1.131 - 0.002 + (1.7343 \times 0.020)}{1.131} \qquad (11\text{-}13)$$

$$ONRF = 1.029 \qquad (11\text{-}13a)$$

Table 11-6 shows the calculated ORNF's and the data used to calculate them.

11.5.4 Quantitative Comparisons of EPRI-NODE-P to Measurement

By analyzing the variable D as defined in equation 11-1, the accuracy of EPRI-NODE-P can be assessed. Four important statistical properties of D are discussed.

$\bar{D}$ is the mean of the differences between EPRI-NODE-P and measured assembly powers. For McGuire Unit 1, Cycle 1 and part of 1A, and Sequoyah Unit 1, Cycle 1 $\bar{D}$ is 0.002 for radial powers and -0.031 for assembly peak axial powers. The above means were derived from all pairs of C, M $\geq$ 1.0 from all 37 state points. Subsequent statistics are also derived from this consideration.

S(D), the standard deviation of the differences, indicates the spread of the values of D about $\bar{D}$. For the above cycles, S(D) for radial powers is 0.020. S(D) for assembly peak axial powers is 0.028.

The mean of the absolute differences $\overline{ABS(D)}$ and its standard deviation can be combined to give limits on this variable. 95% confidence limits on the means were given by:

$$\overline{ABS(D)}_{U,L} = \overline{ABS(D)} \pm \frac{t(.05,n) \times S\,(ABS(D))}{\sqrt{n}} \qquad (11\text{-}14)$$

Equation 11-14 yields

$$\overline{ABS(D)}_{U,L} = 0.018 \pm 0.001$$

for radial powers for C, M pairs $\geq$ 1.0 for all 37 state points and:

$$\overline{ABS(D)}_{U,L} = 0.036 \pm 0.001$$

for assembly peak axial powers for all C, M pairs $\geq$ 1.0 for all 37 state points.

Tables 11-7 and 11-8 present summary D statistics for radial and assembly peak axial powers, respectively, where C,M $\geq$ 1.0 for all pairs considered.

11.5.5 Relative Percent Differences

The relative percent difference between EPRI-NODE-P calculated values and measured values will be defined:

$$\% \text{ Diff} = \frac{C - M}{M} \times 100 \qquad (11\text{-}15)$$

This section will address relative percent differences derived from:

a) the sample mean
b) the mean of the absolute value

Since negative percent differences represent calculational nonconservatisms, the minimum values will be more important. Relative percent differences for all C,M $\geq$ 1.0 will be discussed.

Combining data for McGuire Unit 1, Cycle 1, and part of Cycle 1A, and Sequoyah Unit 1, Cycle 1, the following results were obtained.

The average percent difference was 0.167 and the absolute 1.555 for radial powers. Also, the average percent difference was -2.195 and the absolute 2.392 for assembly peak axial powers.

Table 11-9 shows summary data for percent differences derived from calculated and measured radial powers. Values are presented by cycle and for all cycles combined. Table 11-10 is similar to Table 11-9 and provides data for assembly peak axial power percent differences.

11.5.6 Conclusions

A statistical analysis of EPRI-NODE-P calculated and plant measured power distributions has been performed. The resulting ONRF's for all C, M pairs $\geq$ 1.0 for all 37 state points are:

Radial ONRF ($F^R_{\Delta H}$)	Assembly Peak Axial ONRF (F^R_Q)
1.03	1.06

These values while based upon calculations and measurements performed on McGuire Unit 1, Cycles 1 and part of 1A, and Sequoyah Unit 1, Cycle 1 are applicable to all McGuire and Catawba units for the following reasons:

1. McGuire, Catawba, and Sequoyah have identical incore detector systems.

2. All units are manufactured by the same vendor and use similar fuel.

3. Calculations for all units were performed using the same calculational methods and procedures. Similarly, all calculations performed for McGuire and Catawba will use the same calculational methods and procedures.

As an additional verification of the conservatism in the 1.03 radial and 1.06 assembly peak axial ONRF's, all calculated maximum radial powers were multiplied by 1.03 and compared to measured. Similarly all calculated assembly peak axial powers were multiplied by 1.06 and compared to measured. 29 out of 843 (3.4%) radial powers exceeded the 1.03 x maximum calculated radial power. 43 out of 1038 (4.1%) assembly peak axial powers exceeded the 1.06 x maximum calculated assembly peak axial power. Therefore, the 1.03 radial factor was satisfactory for the entire population. The 1.06 assembly peak axial factor was also satisfactory for the entire population.

Table 11-1

MCGUIRE UNIT 1 CYCLE 1 STATE POINTS

Point #	EFPD	Power (%)	Control Bank D Position (Steps)	Axial Offset (Meas/Calc)(%)
1	1.28	30	213	-4.67/-4.78
2	5.27	30	170	-10.68/-9.20
3	7.70	48	200	-7.59/-6.83
4	11.42	48	164	-11.90/-11.07
5	37.10	50	186	-8.76/-7.70
6	41.59	50	201	-5.56/-6.30
7	48.75	50	201	-6.27/-6.01
8	59.37	50	201	-5.06/-5.83
9	75.38	50	198	-6.10/-5.86
10	80.46	75	213	-8.57/-6.94
11	91.54	75	213	-7.41/-6.75
12	104.47	50	215	-4.07/-3.58
13	112.05	50	215	-1.57/-3.43
14	115.69	75	217	-5.61/-6.52
15	118.71	50	180	-8.60/-7.50
16	122.15	75	215	-5.58/-6.36
17	130.59	75	215	-7.58/-6.17
18	135.44	75	215	-5.77/-5.99
19	139.82	50	180	-8.43/-6.82
20	141.52	50	215	-0.54/-2.52
21	146.01	75	215	-4.80/-5.86
22	150.19	50	215	-0.70/-2.32
23	162.76	50	215	-4.80/-2.33
24	173.34	50	215	-0.29/-2.27
25	185.58	50	215	-0.45/-2.24

Table 11-2

MCGUIRE UNIT 1 CYCLE 1A STATE POINTS

Point #	EFPD	Power (%)	Control Bank D Position (Steps)	Axial Offset (Meas/Calc)(%)
1	198.66	90	217	0.73/-0.93
2	217.53	100	209	1.35/-5.05
3	223.35	100	211	-3.51/-4.92
4	236.23	100	211	-3.44/-4.89
5	249.75	100	221	-2.51/-3.77

Table 11-3

SEQUOYAH UNIT 1 CYCLE 1 STATE POINTS

Point #	EFPD	Power (%)	Control Bank D Position (Steps)	Axial Offset (Meas/Calc)(%)
1	71.82	100	200	-7.31/-9.01
2	101.62	100	218	-4.36/-6.19
3	133.29	100	216	-3.95/-5.60
4	166.04	100	210	-2.68/-5.51
5	231.70	100	216	-1.36/-3.77
6	290.04	100	216	-1.51/-3.40
7	378.92	100	222	-1.43/-2.86

Table 11-4

MCGUIRE UNIT 1 CYCLES 1 AND 1A AND SEQUOYAH UNIT 1 CYCLE 1
STATE POINTS FOR PDQ07 CALCULATED AND MEASURED DATA

			PDQ07 Calculated			Measured		
Point #	Unit	Cycle	Burnup	Control Bank D Position (Steps)	Power (%)	Burnup	Control Bank D Position (Steps)	Power (%)
1	M1	1	52.2	228	100	48.8	201	50
2	M1	1	104.4	228	100	104.5	215	50
3	M1	1	156.7	228	100	150.2	215	50
4	M1	1A	208.9	228	100	198.7	217	90
5	S1	1	103.6	228	100	101.6	218	100
6	S1	1	155.5	228	100	133.3	210	100
7	S1	1	362.7	228	100	378.9	222	100

Table 11-5

DIFFERENCE DISTRIBUTION NORMALITY TESTS
FOR C,M $\geq$ 1.0 - 5% LEVEL OF SIGNIFICANCE

Assembly Radial Powers

Unit/Cycle	N	D'(P=.025)	D'	D'(P=.975)	Remarks
M1/C1	510	3215.0	3274.7	3275.0	Normal
M1/C1A	190	725.9	746.0	748.1	Normal
S1/C1	146	487.6	491.9	504.6	Normal
All Combined	846	6886.7	7000.9	6986.2	Nearly normal

Assembly Peak Axial Powers

Unit/Cycle	N	D'(P=.025)	D'	D'(P=.975)	Remarks
M1/C1	642	4546.4	4586.3	4621.7	Normal
M1/C1A	220	904.9	922.9	930.5	Normal
S1/C1	176	646.4	646.4	666.9	Normal
All Combined	1038	9345.5	9379.5	9489.8	Normal

Table 11-6

Calculated ORNFs and Associated Data

Assembly Radial Power ORNF ($F_{\Delta H}^{R}$)

$\bar{M}$ = 1.131

$\bar{D}$ = 0.002

S(D) = 0.020

N = 846

K = 1.7343 (N=846, 95%/95%)

ORNF ($F_{\Delta H}^{R}$) = 1.029

Assembly Peak Axial Power ORNF (F_{Q}^{R})

$\bar{M}$ = 1.375

$\bar{D}$ = -0.031

S(D) = 0.028

N = 1038

K = 1.7259 (N=1038, 95%/95%)

ORNF (F_{Q}^{R}) = 1.058

Table 11-7

DIFFERENCE MEANS AND STANDARD DEVIATIONS FOR ASSEMBLY RADIAL POWERS (C,M $\geq$1.0)

Unit/Cycle	N	$\bar{D}$	$S(\bar{D})$	$\overline{ABS(D)}$	$S(ABS(\bar{D})$
M1/C1	510	-0.001	0.019	0.017	0.008
M1/C1A	190	-0.001	0.025	0.023	0.010
S1/C1	146	0.013	0.012	0.014	0.010
All Combined	846	0.002	0.020	0.018	0.010

Table 11-8

DIFFERENCE MEANS AND STANDARD DEVIATIONS FOR ASSEMBLY PEAK AXIAL POWERS (C,M $\geq$1.0)

Unit/Cycle	N	$\bar{D}$	S($\bar{D}$)	ABS($\bar{D}$)	S(ABS($\bar{D}$))
M1/C1	642	-0.029	0.027	0.032	0.023
M1/C1A	220	-0.039	0.033	0.041	0.029
S1/C1	176	-0.028	0.026	0.031	0.023
All Combined	1038	-0.031	0.028	0.036	0.025

Table 11-9

PERCENT DIFFERENCE MEANS
(C,M $\geq$ 1.0) - ASSEMBLY RADIAL POWERS

Unit/Cycle	Mean % Difference	Mean Absolute % Difference
M1/C1	-0.058	1.452
M1/C1A	0.007	2.043
S1/C1	1.163	1.281
All Combined	0.167	1.555

Table 11-10

PERCENT DIFFERENCE MEANS
(C,M $\geq$ 1.0) - ASSEMBLY PEAK AXIAL POWERS

Unit/Cycle	Mean % Difference	Mean Absolute % Difference
M1/C1	-2.001	2.196
M1/C1A	-2.838	3.031
S1/C1	-2.099	2.310
All Combined	-2.195	2.392

Figure 11-1

Instrumented Fuel Assemblies
McGuire and Sequoyah

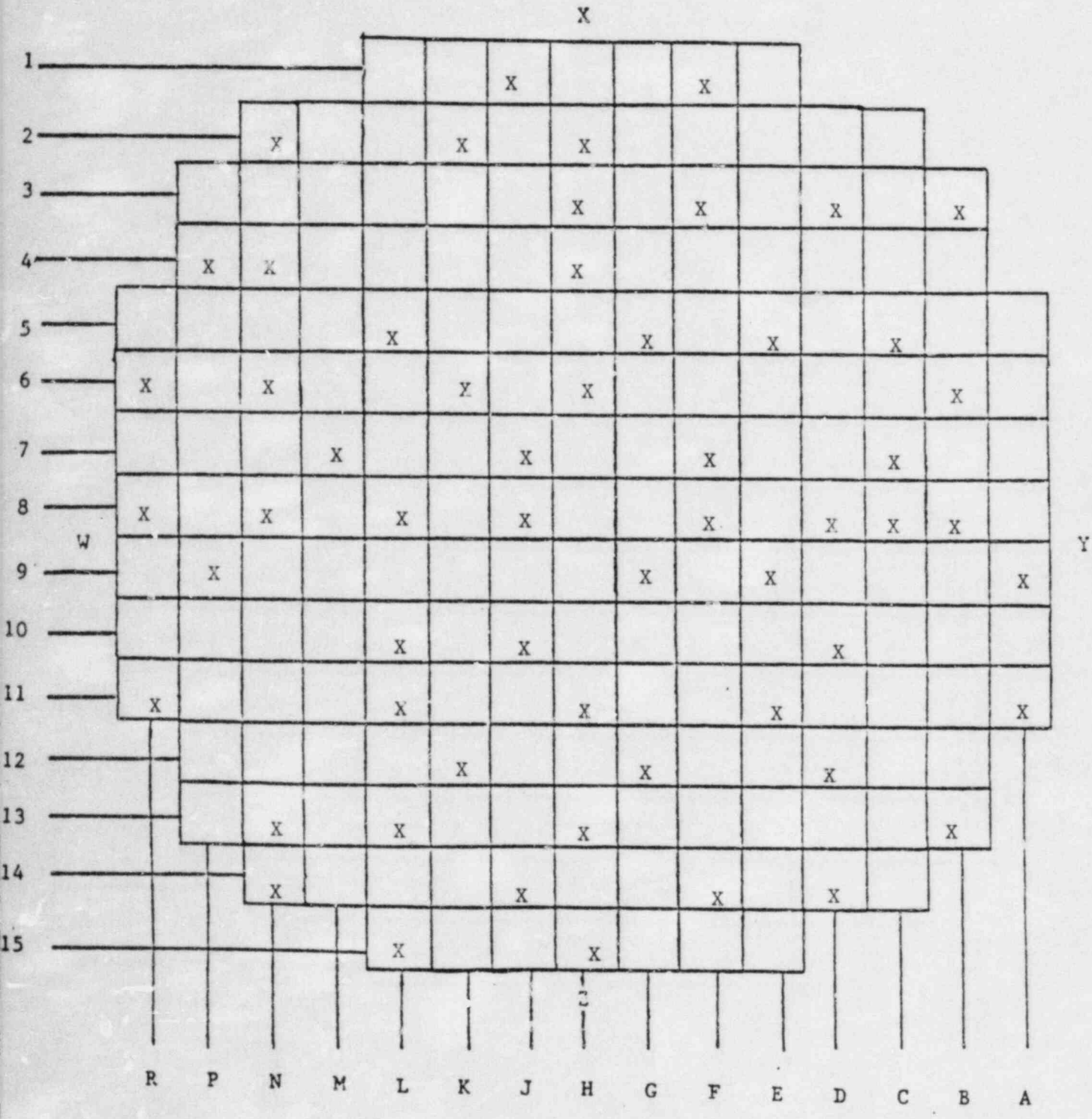

Figure 11-2

Control and Shutdown Bank Locations

McGuire 1 Cycle 1

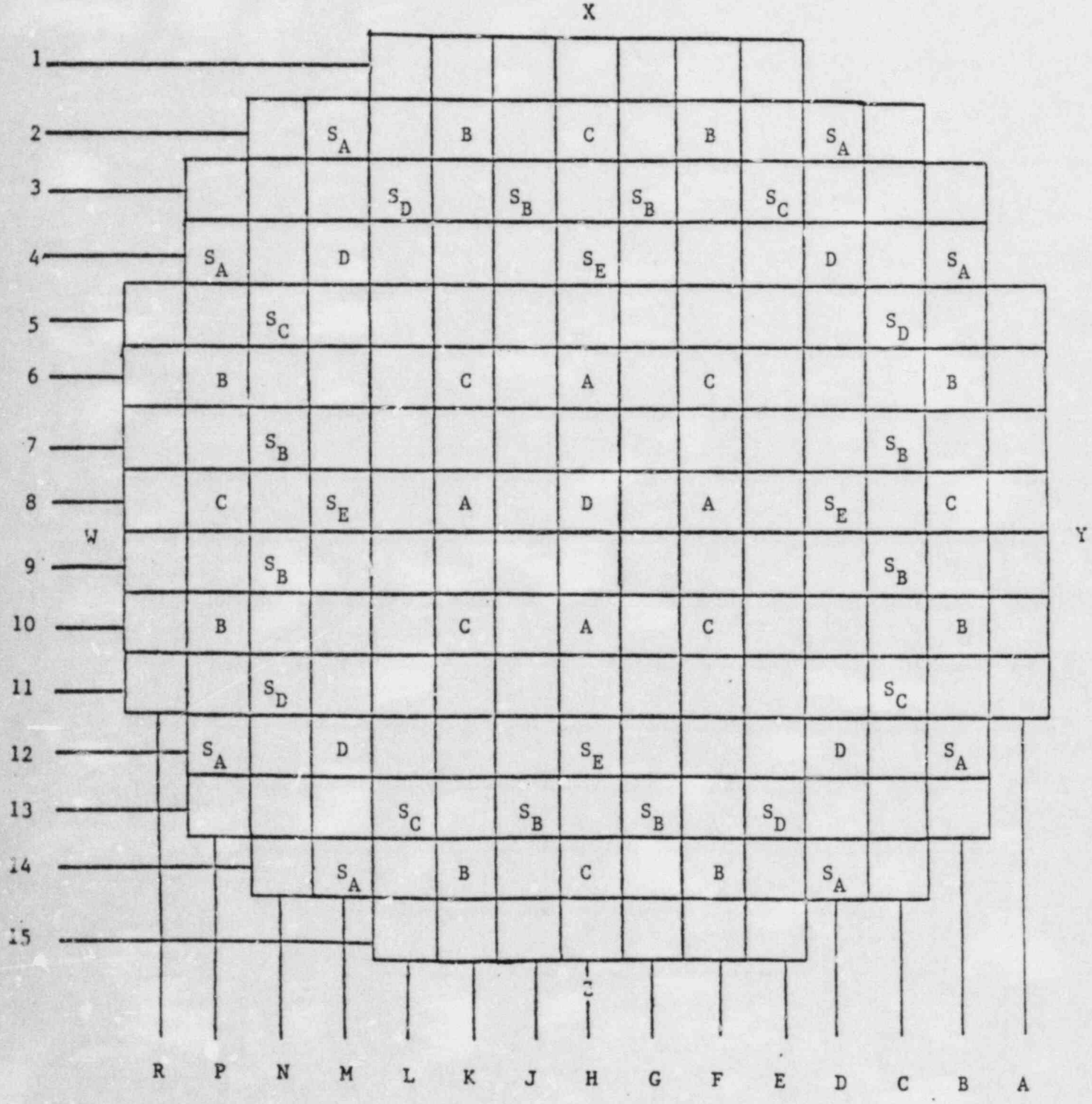

Figure 11-3

Core Loading Pattern
McGuire 1 Cycle 1

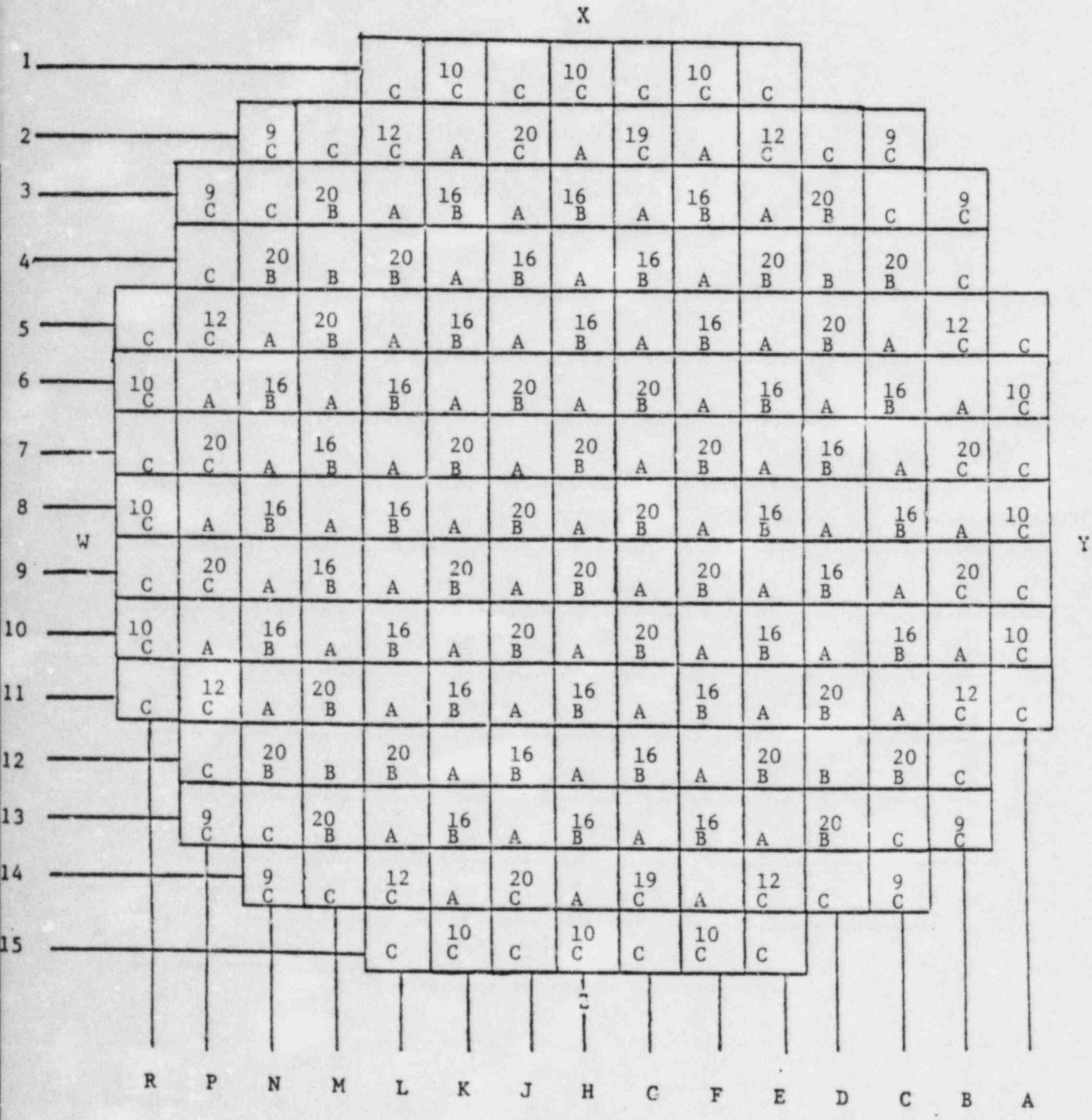

Figure 11-4

Control and Shutdown Bank Locations

Sequoyah 1 Cycle 1

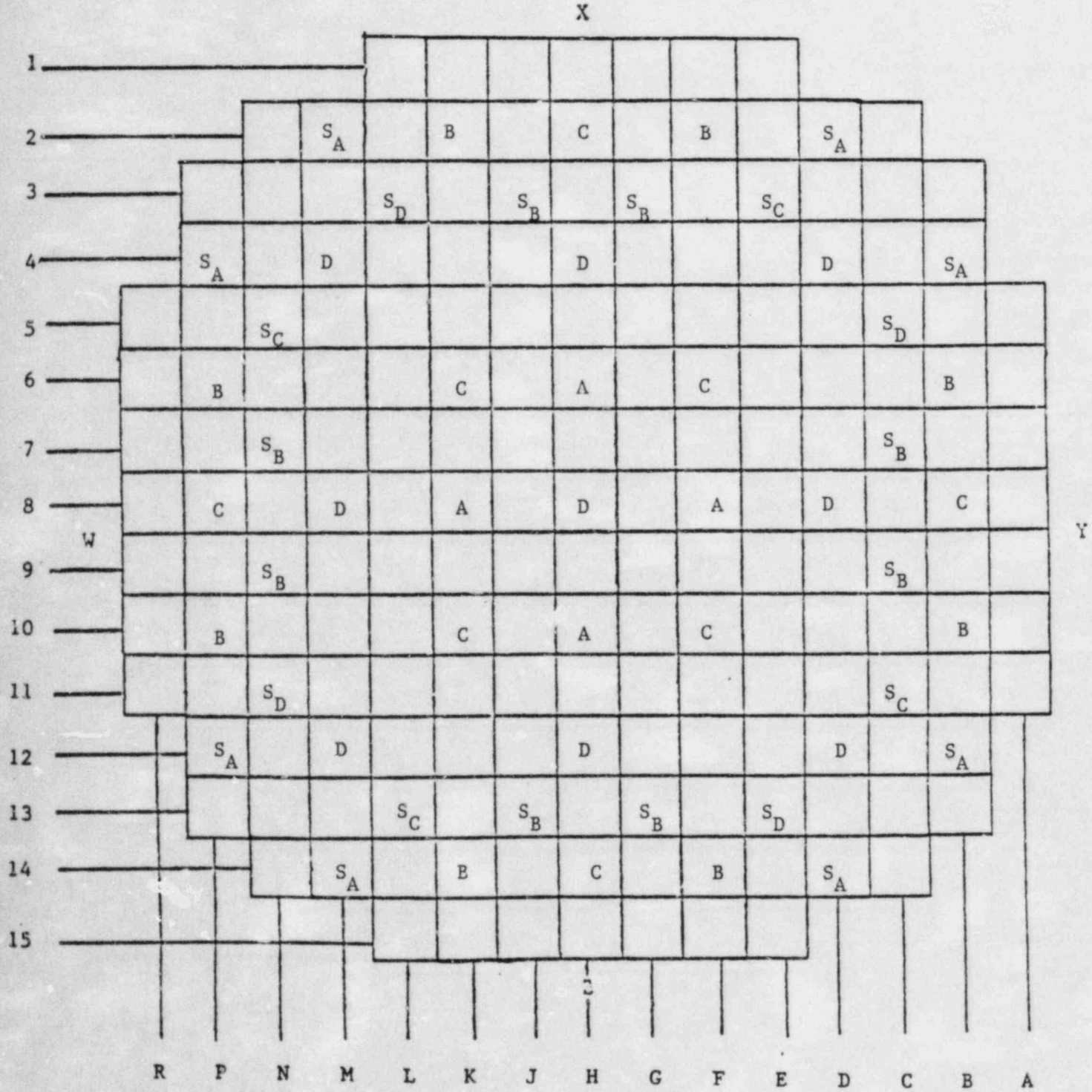

Figure 11-5

Core Loading Pattern
Sequoyah 1 Cycle 1

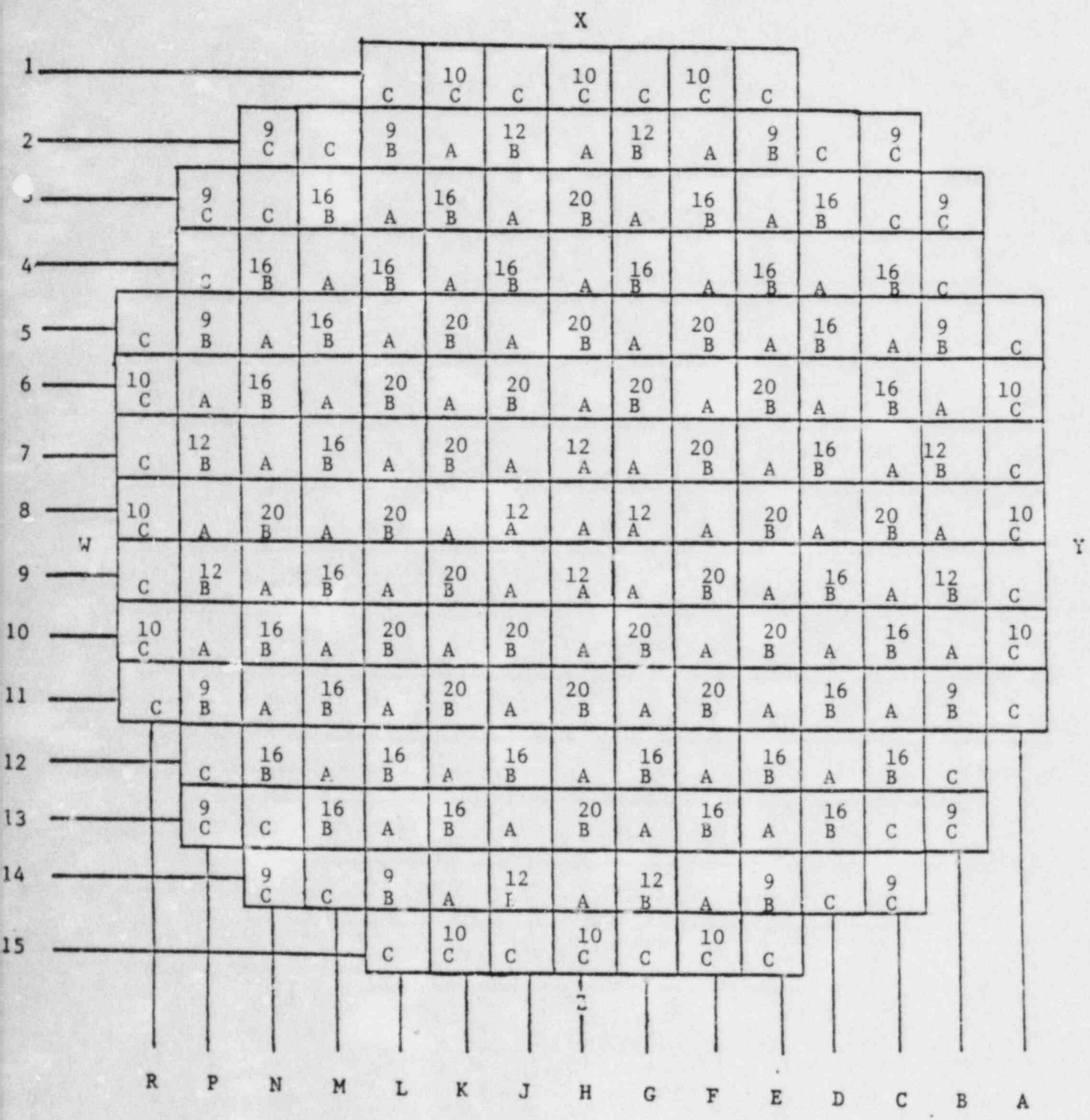

Figure 11-6

MCGUIRE-1 CY-1 ASSEMBLY RADIAL POWERS CALCULATED VS MEASURED

1.28 EFPD 30%FP CONTROL BANK D AT 213 STEPS WITHDRAWN

	H	G	F	E	D	C	B	A	
	1.03	.94	1.11	1.10	1.21	1.08	1.06	.73	
8	1.01	.96	1.10	1.12	1.20	1.09	1.05	.73	
		1.07	.99	1.18	1.11	1.17	1.01	.80	
	9	1.05	1.01	1.16	1.14	1.15	1.03	.79	
			1.15	1.10	1.19	1.06	1.04	.67	
		10	1.14	1.13	1.17	1.10	1.01	.68	
				1.18	1.04	1.12	1.02	.57	
			11	1.18	1.06	1.12	1.01	.58	
					1.27	.95	.87		
				12	1.24	.95	.87		
						1.06	.50		CALCULATED
					13	1.02	.49		MEASURED

Figure 11-7

MCGUIRE-1 CY-1 ASSEMBLY RADIAL POWERS CALCULATED VS MEASURED

5.27 EFPD 30%FP CONTROL BANK D AT 170 STEPS WITHDRAWN

	H	G	F	E	D	C	B	A	
8	.97	.93	1.12	1.12	1.23	1.10	1.07	.74	
	.97	.97	1.12	1.15	1.22	1.12	1.07	.74	
9		1.08	1.01	1.20	1.13	1.19	1.02	.81	
		1.06	1.03	1.18	1.16	1.17	1.05	.80	
10			1.17	1.11	1.19	1.07	1.04	.67	
			1.15	1.14	1.17	1.10	1.01	.68	
11				1.18	1.02	1.11	1.01	.57	
				1.17	1.04	1.09	.99	.57	
12					1.17	.92	.85		
					1.15	.91	.85		
13						1.03	.49	CALCULATED	
						.98	.48	MEASURED	

Figure 11-8

MCGUIRE-1 CY-1 ASSEMBLY RADIAL POWERS CALCULATED VS MEASURED

7.70 EFPD 48ZFP CONTROL BANK D AT 200 STEPS WITHDRAWN

	H	G	F	E	D	C	B	A	
8	1.05	.97	1.14	1.12	1.22	1.09	1.05	.72	
	1.05	1.00	1.14	1.15	1.22	1.10	1.03	.72	
9		1.10	1.02	1.21	1.13	1.18	1.00	.79	
		1.09	1.05	1.19	1.15	1.15	1.02	.78	
10			1.18	1.12	1.19	1.06	1.03	.66	
			1.15	1.14	1.17	1.09	1.00	.67	
11				1.19	1.04	1.11	1.00	.56	
				1.17	1.05	1.10	.99	.57	
12					1.23	.93	.84		
					1.22	.93	.85		
13						1.02	.48		CALCULATED
						1.00	.48		MEASURED

Figure 11-9

MCGUIRE-1 CY-1 ASSEMBLY RADIAL POWERS CALCULATED VS MEASURED

11.42 EFPD 48%FP CONTROL BANK D AT 164 STEPS WITHDRAWN

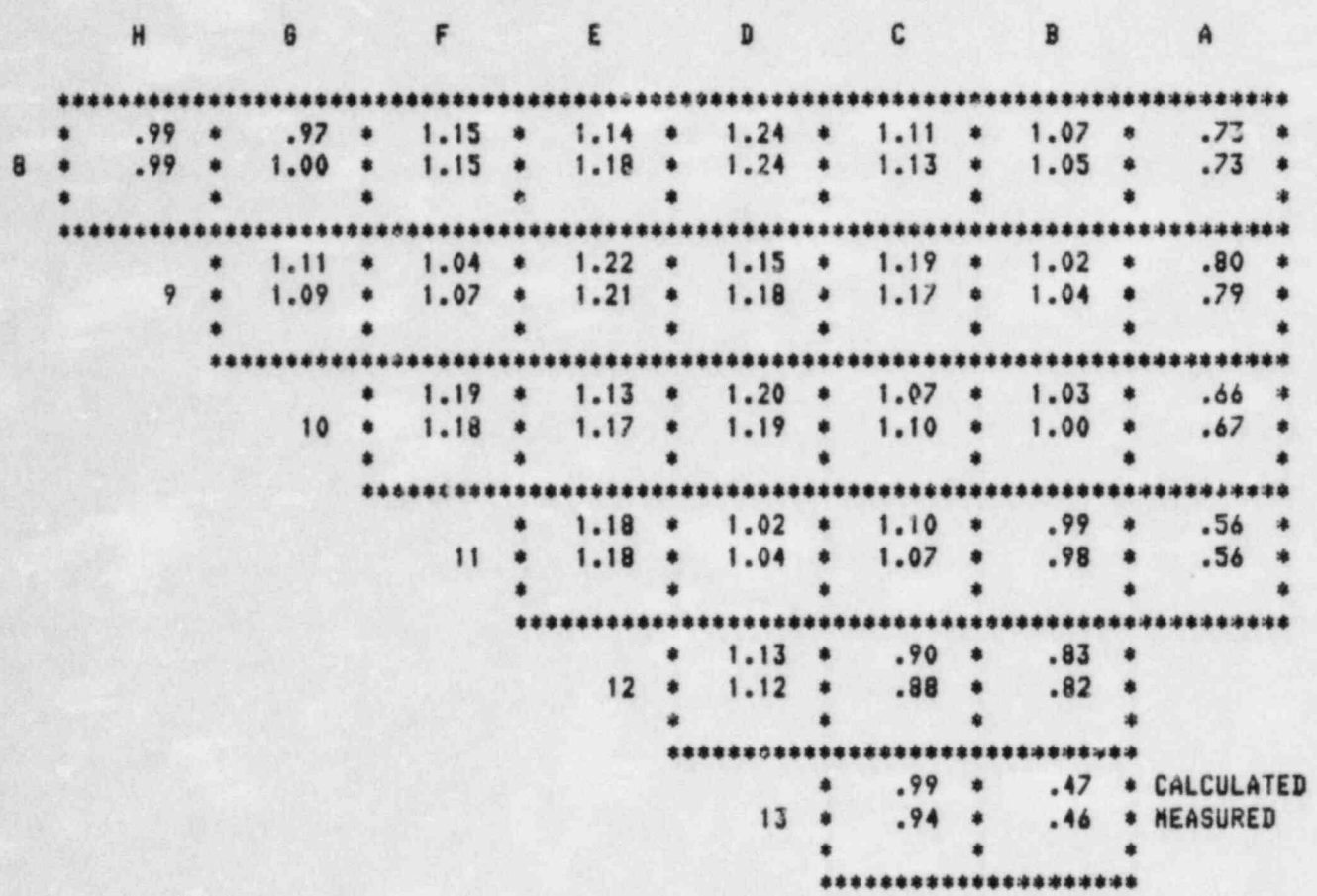

Figure 11-10

MCGUIRE-1 CY-1 ASSEMBLY RADIAL POWERS CALCULATED VS MEASURED

37.10 EFPD 50%FP CONTROL BANK D AT 186 STEPS WITHDRAWN

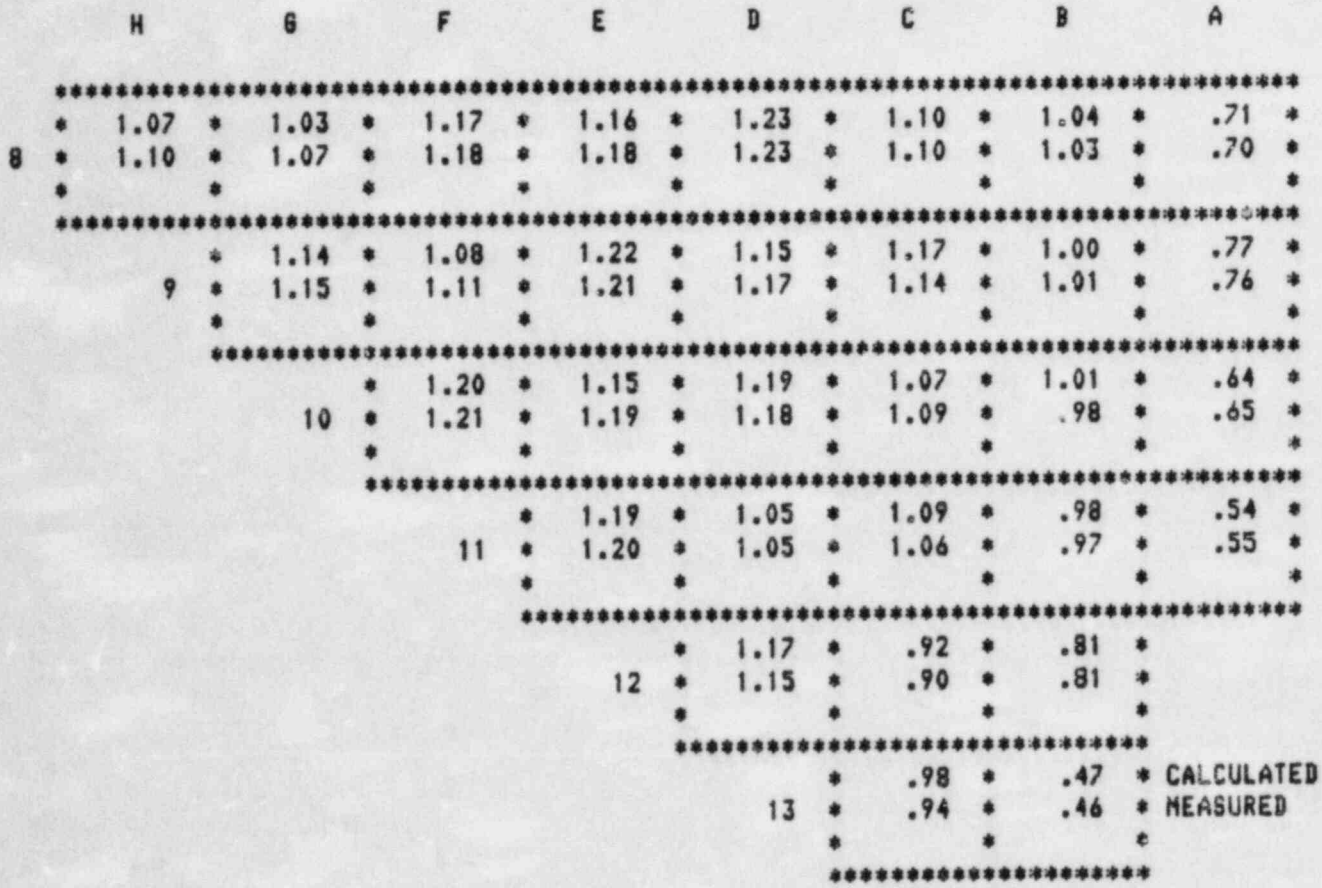

Figure 11-11

MCGUIRE-1 CY-1 ASSEMBLY RADIAL POWERS CALCULATED VS MEASURED

41.59 EFPD 50%FP CONTROL BANK D AT 201 STEPS WITHDRAWN

	H	G	F	E	D	C	B	A	
	1.10	1.04	1.18	1.16	1.22	1.10	1.03	.70	
8	1.10	1.08	1.18	1.21	1.22	1.11	1.01	.70	
		1.15	1.08	1.22	1.15	1.16	1.00	.76	
	9	1.15	1.12	1.21	1.18	1.14	1.01	.75	
		1.20	1.15	1.19	1.07	1.00	.64		
	10	1.19	1.19	1.18	1.09	.96	.64		
			1.19	1.06	1.09	.97	.54		
		11	1.19	1.08	1.07	.96	.54		
				1.20	.93	.81			
			12	1.18	.91	.80			
					.98	.47		CALCULATED	
				13	.94	.46		MEASURED	

Figure 11-12

MCGUIRE-1 CY-1 ASSEMBLY RADIAL POWERS CALCULATED VS MEASURED

48.75 EFPD 50%FP CONTROL BANK D AT 201 STEPS WITHDRAWN

	H	G	F	E	D	C	B	A	
		1.11	1.05	1.18	1.17	1.22	1.10	1.03	.70	
8		1.11	1.09	1.19	1.21	1.22	1.12	1.01	.70	
		1.15	1.09	1.22	1.15	1.16	1.00	.76		
	9	1.15	1.12	1.21	1.19	1.14	1.01	.75		
			1.20	1.19	1.19	1.07	1.00	.64		
		10	1.19	1.19	1.18	1.09	.96	.64		
				1.19	1.07	1.09	.97	.54		
			11	1.19	1.08	1.07	.95	.54		
					1.20	.93	.81			
				12	1.18	.91	.80			
						.98	.47		CALCULATED	
					13	.94	.46		MEASURED	

Figure 11-13

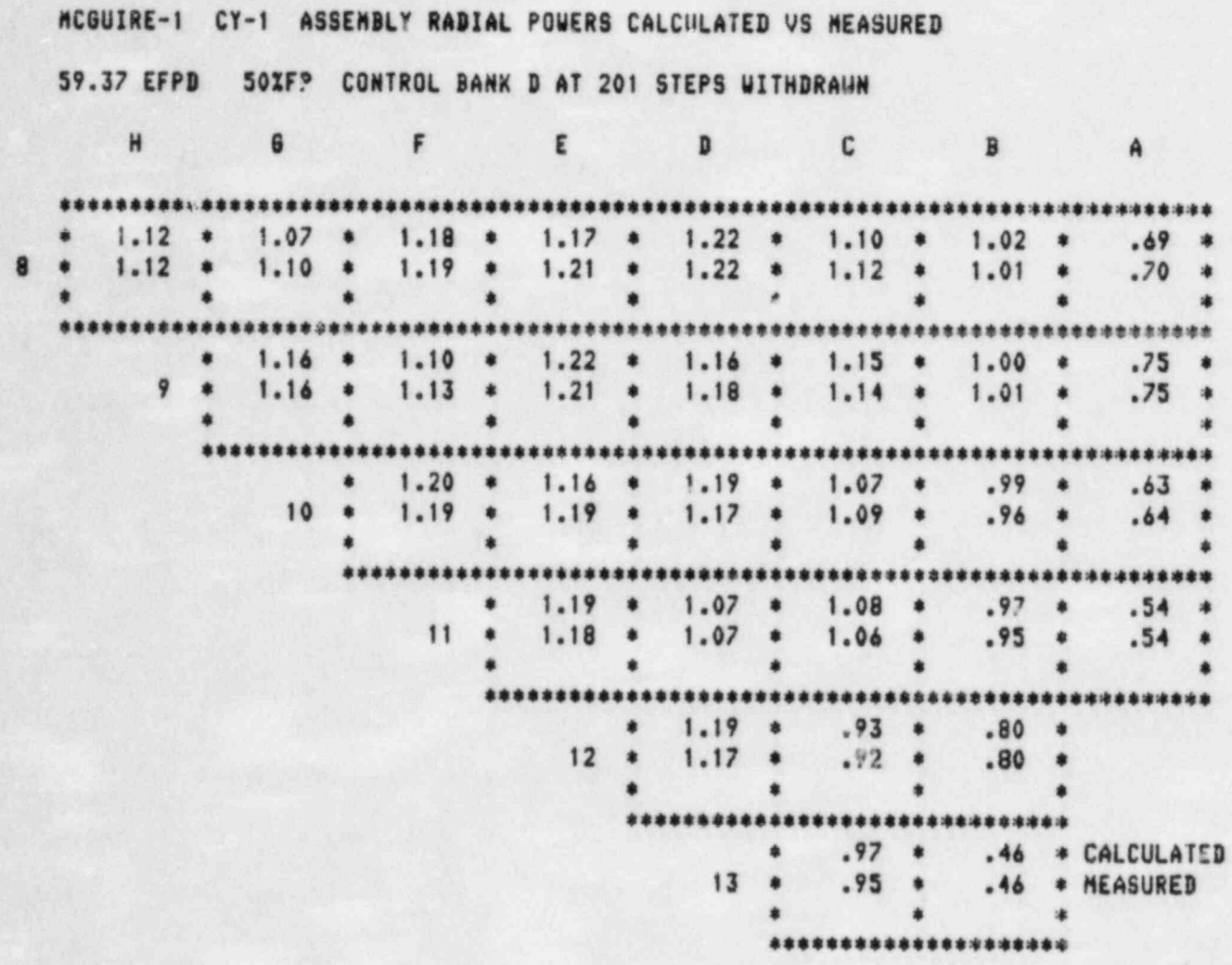
MCGUIRE-1 CY-1 ASSEMBLY RADIAL POWERS CALCULATED VS MEASURED
59.37 EFPD 50%FP CONTROL BANK D AT 201 STEPS WITHDRAWN
H G F E D C B A
8 1.12 1.07 1.18 1.17 1.22 1.10 1.02 .69
1.12 1.10 1.19 1.21 1.22 1.12 1.01 .70
9 1.16 1.10 1.22 1.16 1.15 1.00 .75
1.16 1.13 1.21 1.18 1.14 1.01 .75
10 1.20 1.16 1.19 1.07 .99 .63
1.19 1.19 1.17 1.09 .96 .64
11 1.19 1.07 1.08 .97 .54
1.18 1.07 1.06 .95 .54
12 1.19 .93 .80
1.17 .92 .80
.97 .46 CALCULATED
13 .95 .46 MEASURED

Figure 11-14

MCGUIRE-1 CY-1 ASSEMBLY RADIAL POWERS CALCULATED VS MEASURED

75.38 EFPD 50%FP CONTROL BANK D AT 198 STEPS WITHDRAWN

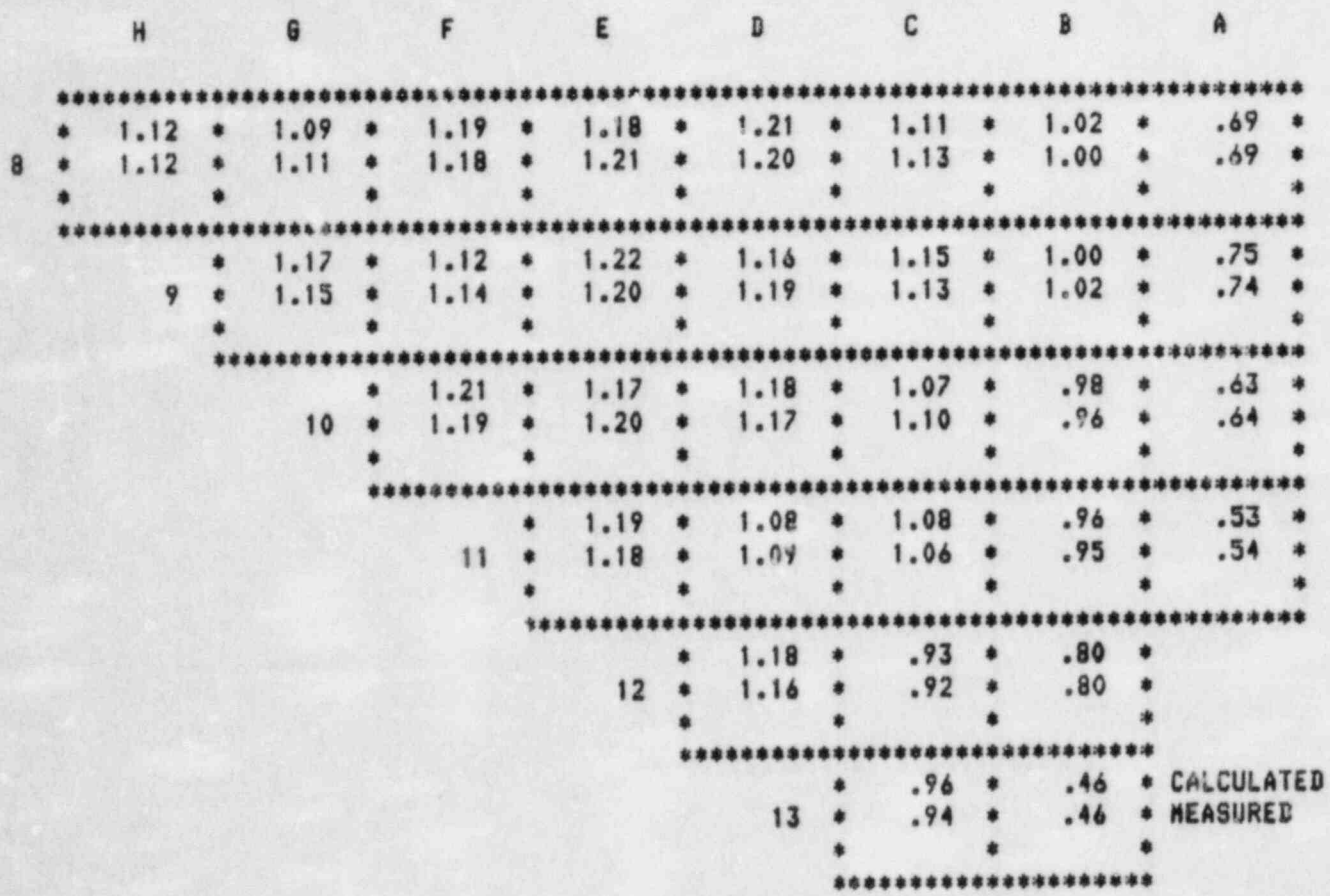

Figure 11-15

MCGUIRE-1 CY-1 ASSEMBLY RADIAL POWERS CALCULATED VS MEASURED

80.46 EFPD 75%FP CONTROL BANK D AT 213 STEPS WITHDRAWN

	H	G	F	E	D	C	B	A	
	1.17	1.11	1.20	1.19	1.21	1.10	1.01	.68	
8	1.16	1.14	1.20	1.22	1.20	1.11	1.00	.70	
		1.18	1.13	1.22	1.17	1.14	.99	.74	
	9	1.17	1.15	1.21	1.19	1.12	1.01	.74	
			1.21	1.18	1.18	1.07	.98	.63	
		10	1.19	1.19	1.17	1.09	.95	.64	
				1.19	1.09	1.07	.95	.53	
			11	1.18	1.09	1.05	.95	.53	
					1.19	.93	.79		
				12	1.17	.92	.80		
						.95	.46		CALCULATED
					13	.94	.46		MEASURED

Figure 11-16

MCGUIRE-1 CY-1 ASSEMBLY RADIAL POWERG CALCULATED VS MEASURED

91.54 EFPD 75%FP CONTROL BANK D AT 213 STEPS WITHDRAWN

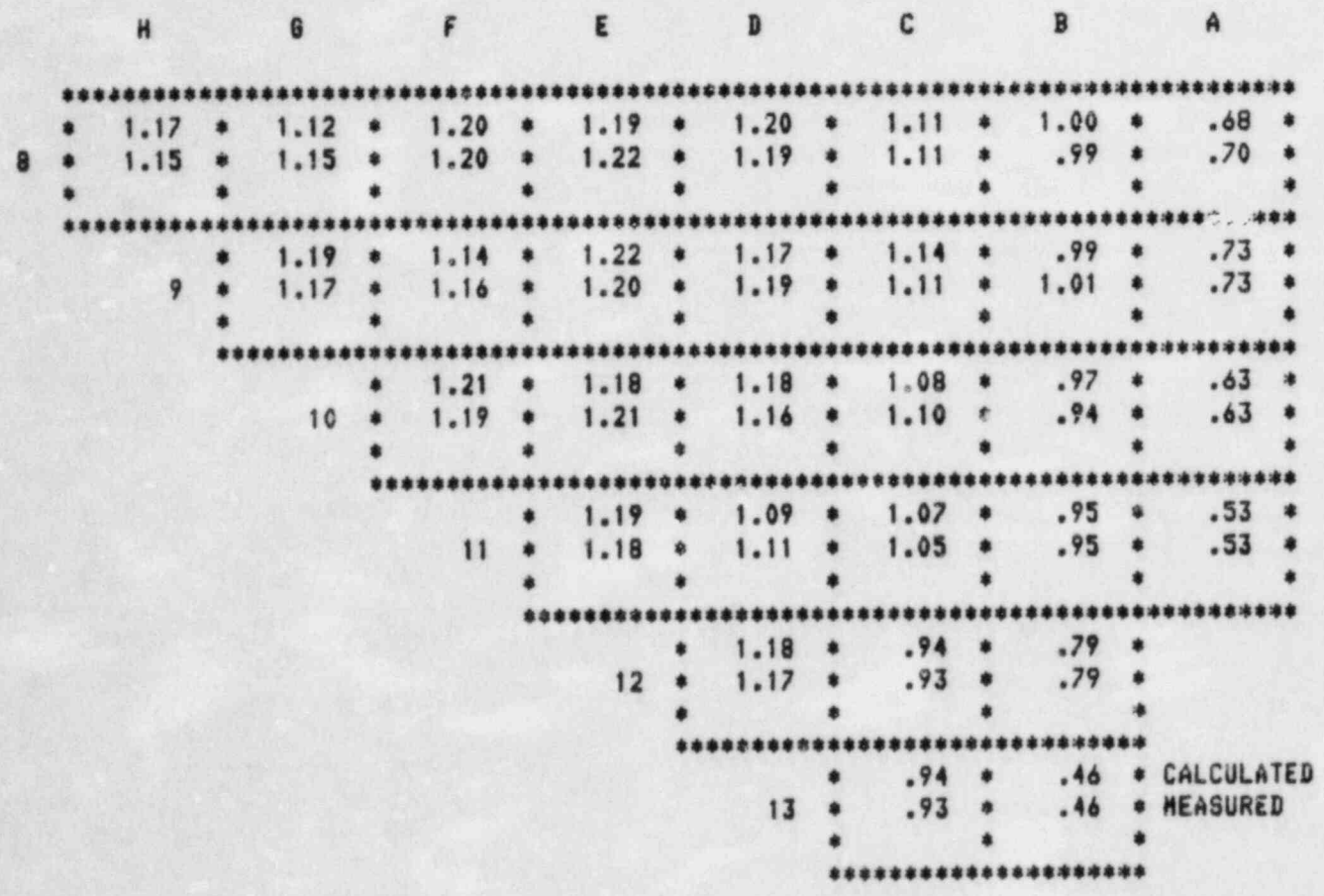

Figure 11-17

MCGUIRE-1 CY-1 ASSEMBLY RADIAL POWERS CALCULATED VS MEASURED

104.47 EFPD 50%FP CONTROL BANK D AT 215 STEPS WITHDRAWN

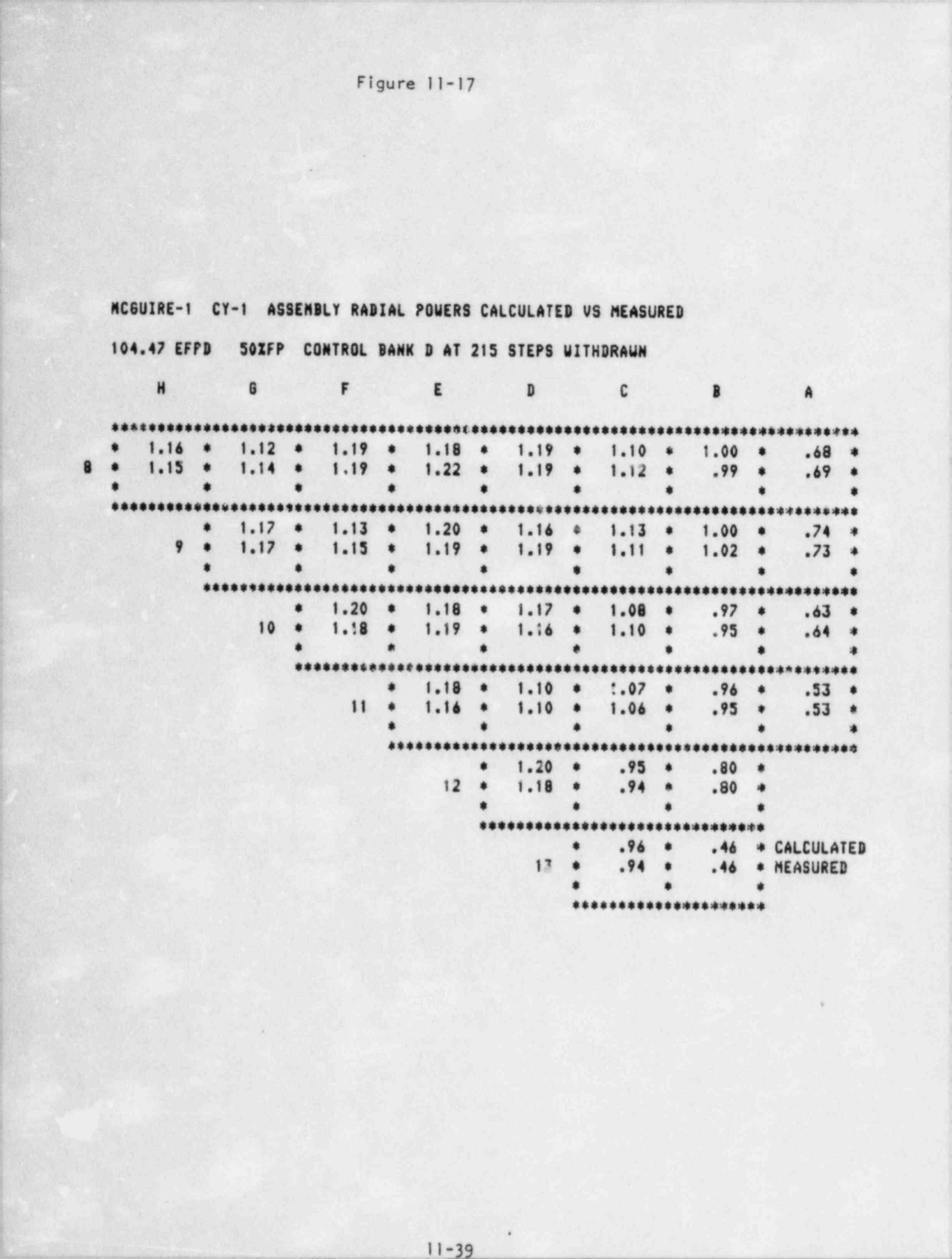

Figure 11-18

MCGUIRE-1 CY-1 ASSEMBLY RADIAL POWERS CALCULATED VS MEASURED

112.05 EFPD 50%FP CONTROL BANK D AT 215 STEPS WITHDRAWN

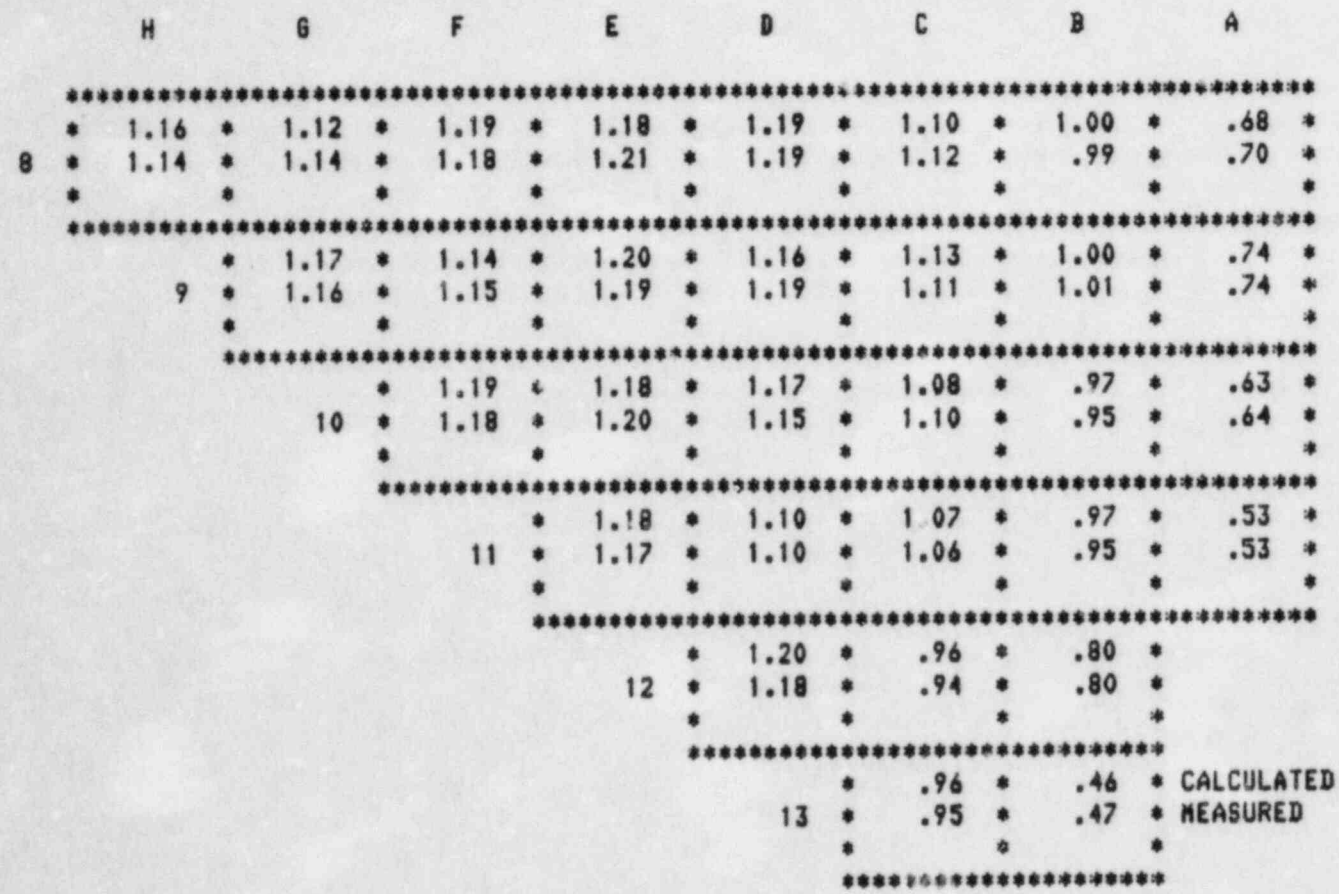

Figure 11-19

MCGUIRE-1 CY-1 ASSEMBLY RADIAL POWERS CALCULATED VS MEASURED

115.69 EFPD 75%FP CONTROL BANK D AT 217 STEPS WITHDRAWN

	H	G	F	E	D	C	B	A	
8	1.18 1.16	1.14 1.16	1.20 1.20	1.19 1.22	1.19 1.19	1.11 1.12	1.00 .99	.68 .69	
9		1.19 1.18	1.15 1.16	1.21 1.19	1.17 1.19	1.13 1.11	1.00 1.01	.73 .73	
10			1.20 1.19	1.18 1.20	1.17 1.15	1.08 1.10	.97 .95	.63 .64	
11				1.18 1.17	1.10 1.10	1.07 1.05	.95 .95	.53 .53	
12					1.18 1.17	.95 .94	.79 .80		
13						.94 .94	.46 .46		CALCULATED MEASURED

Figure 11-20

MCGUIRE-1 CY-1 ASSEMBLY RADIAL POWERS CALCULATED VS MEASURED

110.71 EFPD 50%FP CONTROL BANK D AT 180 STEPS WITHDRAWN

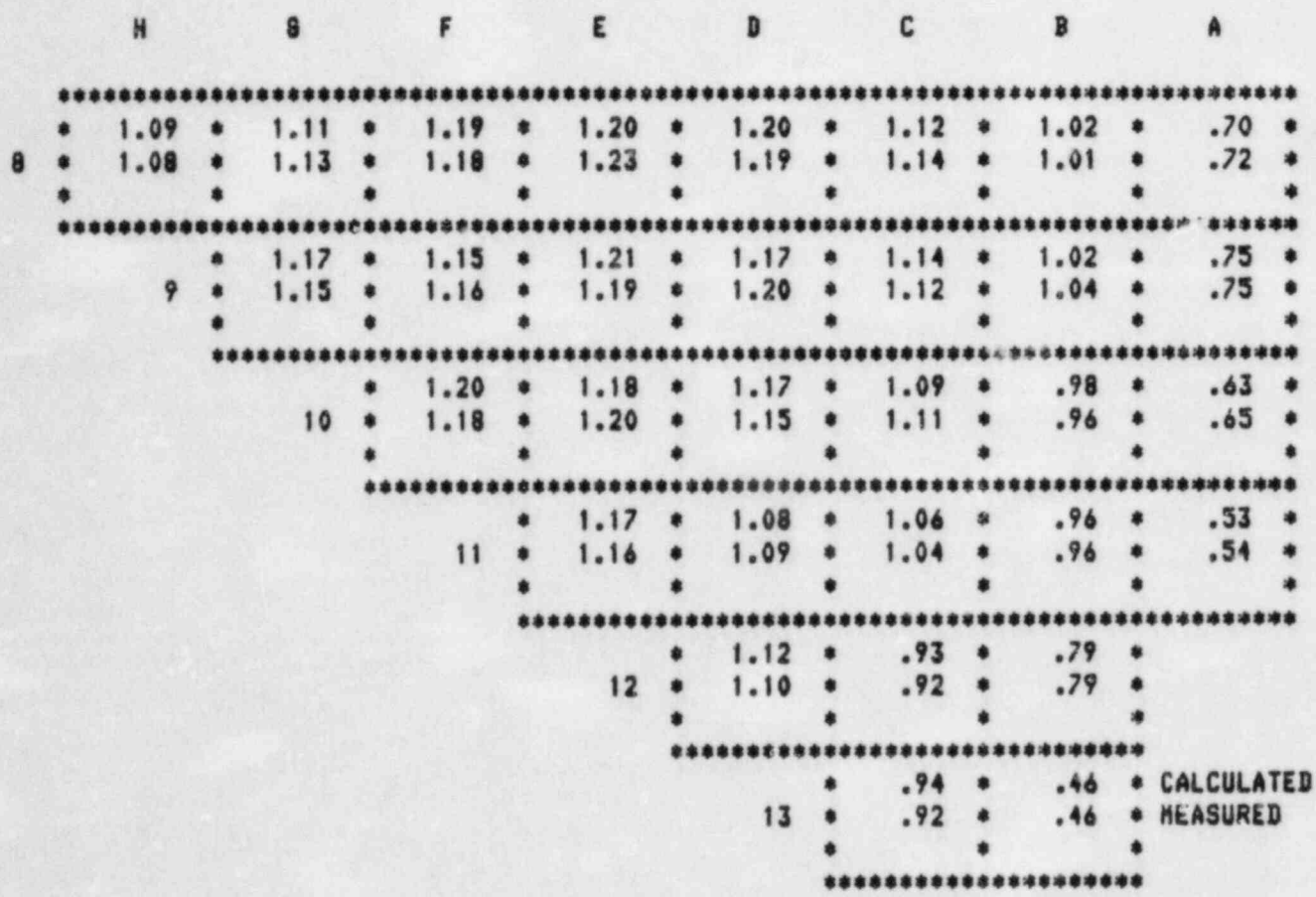

Figure 11-21

MCGUIRE-1 CY-1 ASSEMBLY RADIAL POWERS CALCULATED VS MEASURED

122.15 EFPD 75%FP CONTROL BANK D AT 215 STEPS WITHDRAWN

	H	G	F	E	D	C	B	A	
	1.17	1.14	1.20	1.19	1.19	1.11	1.00	.68	
8	1.15	1.16	1.19	1.22	1.18	1.12	.99	.70	
		1.19	1.15	1.20	1.17	1.13	1.00	.73	
	9	1.17	1.17	1.18	1.19	1.10	1.02	.73	
			1.20	1.18	1.17	1.08	.97	.63	
		10	1.18	1.21	1.15	1.10	.94	.64	
				1.18	1.10	1.07	.96	.53	
			11	1.17	1.11	1.05	.95	.53	
					1.18	.95	.79		
				12	1.17	.94	.79		
						.94	.46		CALCULATED
					13	.93	.47		MEASURED

FIGURE 11-22

MCGUIRE-1 CY-1 ASSEMBLY RADIAL POWERS CALCULATED VS MEASURED

130.59 EFPD 75%FP CONTROL BANK D AT 215 STEPS WITHDRAWN

	H	G	F	E	D	C	B	A	
8	1.17 1.16	1.15 1.16	1.19 1.18	1.19 1.22	1.18 1.17	1.11 1.13	1.00 .99	.68 .70	
9		1.19 1.17	1.15 1.17	1.20 1.18	1.17 1.18	1.12 1.10	1.00 1.01	.73 .73	
10			1.20 1.18	1.18 1.20	1.16 1.14	1.08 1.10	.97 .94	.63 .64	
11				1.17 1.17	1.11 1.11	1.07 1.05	.96 .95	.53 .53	
12					1.18 1.17	.96 .95	.79 80		
13						.94 .94	.46 .47		CALCULATED MEASURED

Figure 11-23

MCGUIRE-1 CY-1 ASSEMBLY RADIAL POWERS CALCULATED VS MEASURED

135.44 EFPD 75%FP CONTROL BANK D AT 215 STEPS WITHDRAWN

	H	G	F	E	D	C	B	A	
		1.17	1.15	1.19	1.19	1.18	1.11	1.00	.68	
8		1.16	1.17	1.19	1.22	1.17	1.12	.99	.70	
		1.18	1.16	1.20	1.17	1.12	1.00	.73		
	9	1.17	1.17	1.18	1.19	1.10	1.02	.73		
			1.19	1.18	1.16	1.08	.97	.63		
		10	1.18	1.20	1.15	1.10	.94	.64		
				1.17	1.11	1.07	.96	.53		
			11	1.16	1.11	1.05	.95	.53		
					1.18	.96	.79			
				12	1.17	.95	.80			
						.95	.46		CALCULATED	
					13	.94	.47		MEASURED	

Figure 11-24

MCGUIRE-1 CY-1 ASSEMBLY RADIAL POWERS CALCULATED VS MEASURED

139.82 EFPD 50ZFP CONTROL BANK D AT 180 STEPS WITHDRAWN

	H	G	F	E	D	C	B	A	
8	1.09 1.08	1.12 1.14	1.18 1.18	1.19 1.23	1.19 1.19	1.12 1.14	1.01 1.01	.70 .71	
9		1.17 1.15	1.15 1.17	1.20 1.19	1.17 1.20	1.13 1.12	1.03 1.04	.75 .75	
10			1.19 1.18	1.18 1.20	1.16 1.14	1.09 1.11	.98 .96	.64 .65	
11				1.16 1.15	1.09 1.09	1.06 1.04	.97 .95	.54 .54	
12					1.11 1.11	.94 .93	.79 .79		
13						.94 .92	.46 .46		CALCULATED MEASURED

Figure 11-25

MCGUIRE-1 CY-1 ASSEMBLY RADIAL POWERS CALCULATED VS MEASURED

141.52 EFPD 50%FP CONTROL BANK D AT 215 STEPS WITHDRAWN

	H	G	F	E	D	C	B	A	
	1.16	1.13	1.18	1.18	1.17	1.11	1.00	.69	
8	1.15	1.16	1.18	1.21	1.17	1.12	.99	.70	
		1.17	1.14	1.19	1.16	1.12	1.01	.74	
	9	1.16	1.16	1.17	1.18	1.10	1.02	.74	
			1.18	1.18	1.16	1.08	.97	.63	
		10	1.17	1.20	1.14	1.10	.95	.64	
				1.17	1.11	1.07	.97	.53	
			11	1.16	1.11	1.06	.96	.53	
					1.19	.97	.80		
				12	1.17	.96	.81		
						.96	.47	CALCULATED	
					13	.95	.47	MEASURED	

Figure 11-26

MCGUIRE-1 CY-1 ASSEMBLY RADIAL POWERS CALCULATED VS MEASURED

146.01 EFPD 75%FP CONTROL BANK D AT 215 STEPS WITHDRAWN

	H	G	F	E	D	C	B	A	
	1.17	1.15	1.19	1.19	1.17	1.11	1.00	.68	
8	1.16	1.18	1.18	1.22	1.17	1.12	.98	.70	
		1.18	1.16	1.15	1.16	1.12	1.01	.74	
	9	1.17	1.18	1.18	1.19	1.09	1.02	.73	
			1.19	1.18	1.16	1.09	.97	.63	
		10	1.17	1.21	1.14	1.10	.94	.64	
				1.17	1.11	1.07	.96	.53	
			11	1.16	1.12	1.04	.95	.53	
					1.18	.96	.79		
				12	1.16	.95	.79		
						.95	.46	CALCULATED	
					13	.93	.47	MEASURED	

Figure 11-27

MCGUIRE-1 CY-1 ASSEMBLY RADIAL POWERS CALCULATED VS MEASURED

150.19 EFPD 50%FP CONTROL BANK D AT 215 STEPS WITHDRAWN

	H	G	F	E	D	C	B	A	
	1.16	1.14	1.17	1.18	1.17	1.11	1.00	.69	
8	1.14	1.16	1.17	1.21	1.16	1.12	.99	.71	
	1.17	1.15	1.18	1.16	1.12	1.01	.74		
9	1.13	1.16	1.16	1.19	1.10	1.03	.74		
	1.18	1.17	1.15	1.09	.97	.63			
10	1.16	1.20	1.14	1.11	.95	.65			
	1.16	1.11	1.07	.97	.54				
11	1.16	1.12	1.05	.96	.54				
	1.19	.98	.80						
12	1.17	.97	.80						
	.97	.47	CALCULATED						
13	.95	.48	MEASURED						

Figure 11-28

MCGUIRE-1 CY-1 ASSEMBLY RADIAL POWERS CALCULATED VS MEASURED

162.76 EFPD 50%FP CONTROL BANK D AT 215 STEPS WITHDRAWN

	H	G	F	E	D	C	B	A	
8	1.15	1.14	1.17	1.18	1.16	1.11	1.00	.69	
	1.14	1.17	1,17	1.21	1.16	1.13	.99	.70	
9		1.16	1.15	1.17	1.16	1.11	1.02	.74	
		1.15	1.17	1.16	1.18	1.09	1.02	.74	
10			1.17	1.17	1.15	1.09	.97	.64	
			1.16	1.20	1.13	1.11	.94	.65	
11				1.16	1.12	1.07	.97	.54	
				1.15	1.12	1.05	.96	.54	
12					1.19	.98	.80		
					1.17	.97	.80		
13						.97	.47		CALCULATED
						.95	.48		MEASURED

Figure 11-29

MCGUIRE-1 CY-1 ASSEMBLY RADIAL POWERS CALCULATED VS MEASURED

173.34 EFPD 50%FP CONTROL BANK D AT 215 STEPS WITHDRAWN

	H	G	F	E	D	C	B	A	
					1.15	1.11	1.00	.69	
8	1.13	1.17	1.16	1.21	1.14	1.13	.99	.71	
		1.16	1.15	1.17	1.16	1.11	1.02	.74	
	9	1.14	1.17	1.15	1.18	1.09	1.03	.74	
			1.17	1.17	1.14	1.09	.97	.64	
		10	1.15	1.19	1.12	1.11	.94	.65	
				1.15	1.12	1.07	.98	.54	
			11	1.14	1.12	1.05	.96	.54	
					1.18	.99	.81		
				12	1.16	.98	.81		
						.97	.47		CALCULATED
					13	.95	.49		MEASURED

Figure 11-30

MCGUIRE-1 CY-1 ASSEMBLY RADIAL POWERS CALCULATED VS MEASURED

185.58 EFPD 50%FP CONTROL BANK D AT 215 STEPS WITHDRAWN

	H	G	F	E	D	C	B	A	
	1.15	1.14	1.16	1.17	1.15	1.11	1.00	.70	
8	1.13	1.16	1.15	1.20	1.14	1.12	.99	.72	
	1.16	1.15	1.16	1.15	1.11	1.03	.75		
9	1.14	1.16	1.14	1.18	1.09	1.04	.74		
	1.16	1.17	1.14	1.09	.97	.64			
10	1.14	1.19	1.12	1.11	.95	.66			
	1.15	1.12	1.07	.98	.54				
11	1.14	1.13	1.06	.97	.54				
	1.18	.99	.81						
12	1.17	.99	.81						
	.97	.48	CALCULATED						
13	.96	.49	MEASURED						

Figure 11-31

MCGUIRE-1 CY-1 ASSEMBLY PEAK AXIAL POWER - CALCULATED VS MEASURED

1.28 EFPD 30ZFP CONTROL BANK D AT 213 STEPS WITHDRAWN

	H	G	F	E	D	C	B	A	
	1.41	1.27	1.50	1.48	1.63	1.46	1.43	.99	
8	1.40	1.32	1.50	1.52	1.62	1.47	1.42	1.00	
	1.45	1.34	1.60	1.50	1.59	1.36	1.09		
9	1.43	1.38	1.57	1.54	1.55	1.40	1.08		
	1.56	1.49	1.61	1.43	1.41	.91			
10	1.55	1.54	1.59	1.49	1.37	.92			
	1.60	1.42	1.52	1.38	.77				
11	1.60	1.45	1.52	1.37	.78				
	1.74	1.29	1.18						
12	1.71	1.29	1.18						
	1.45	.68	CALCULATED						
13	1.39	.67	MEASURED						

Figure 11-32

MCGUIRE-1 CY-1 ASSEMBLY PEAK AXIAL POWER - CALCULATED VS MEASURED

5.27 EFPD 30%FP CONTROL BANK D AT 170 STEPS WITHDRAWN

	H	G	F	E	D	C	B	A	
	1.50	1.33	1.56	1.53	1.68	1.50	1.47	1.01	
8	1.48	1.40	1.58	1.61	1.71	1.55	1.47	1.03	
	1.50	1.39	1.65	1.55	1.63	1.40	1.11		
9	1.51	1.43	1.65	1.62	1.62	1.45	1.12		
	1.61	1.54	1.65	1.47	1.44	.93			
10	1.62	1.61	1.66	1.54	1.42	.95			
	1.65	1.46	1.56	1.41	.79				
11	1.67	1.50	1.57	1.40	.80				
	1.81	1.33	1.20						
12	1.76	1.33	1.21						
	1.47	.69	CALCULATED						
13	1.43	.69	MEASURED						

Figure 11-33

MCGUIRE-1 CY-1 ASSEMBLY PEAK AXIAL POWER - CALCULATED VS MEASURED

7.70 EFPD 48%FP CONTROL BANK B AT 200 STEPS WITHDRAWN

	H	G	F	E	D	C	B	A	
8	1.46	1.33	1.54	1.52	1.65	1.47	1.42	.97	
	1.47	1.38	1.56	1.58	1.66	1.50	1.40	.99	
9		1.49	1.38	1.63	1.52	1.58	1.35	1.06	
		1.50	1.43	1.62	1.58	1.57	1.39	1.07	
10			1.59	1.52	1.62	1.43	1.39	.89	
			1.58	1.57	1.61	1.49	1.36	.91	
11				1.61	1.42	1.51	1.35	.76	
				1.62	1.45	1.51	1.35	.77	
12					1.71	1.27	1.14		
					1.71	1.28	1.16		
13						1.39	.66		CALCULATED
						1.37	.66		MEASURED

Figure 11-34

MCGUIRE-1 CY-1 ASSEMBLY PEAK AXIAL POWER - CALCULATED VS MEASURED

11.42 EFPD 48%FP CONTROL BANK D AT 164 STEPS WITHDRAWN

	H	G	F	E	D	C	B	A	
	1.54	1.38	1.59	1.57	1.70	1.51	1.45	.99	
8	1.54	1.46	1.64	1.66	1.73	1.57	1.46	1.01	
		1.55	1.43	1.67	1.57	1.63	[illegible]	1.09	
	9	1.57	1.51	1.70	1.65	1.63	[illegible]	1.10	
			1.64	1.56	1.66	1.47	1.42	.91	
		10	1.67	1.65	1.68	1.55	1.41	.94	
				1.66	1.47	1.54	1.38	.77	
			11	1.69	1.52	1.56	1.39	.80	
					1.76	1.30	1.16		
				12	1.75	1.32	1.19		
						1.41	.67		CALCULATED
					13	1.40	.67		MEASURED

Figure 11-35

MCGUIRE-1 CY-1 ASSEMBLY PEAK AXIAL POWER - CALCULATED VS MEASURED

37.10 EFPD 50ZFP CONTROL BANK D AT 186 STEPS WITHDRAWN

	H	G	F	E	D	C	B	A	
		1.52	1.40	1.57	1.55	1.63	1.46	1.37	.93	
8		1.58	1.50	1.64	1.62	1.67	1.50	1.40	.95	
		1.53	1.44	1.62	1.53	1.54	1.33	1.01	
	9	1.61	1.53	1.66	1.60	1.56	1.38	1.03	
			1.60	1.54	1.59	1.43	1.33	.85	
		10	1.67	1.64	1.63	1.50	1.34	.89	
				1.59	1.43	1.46	1.30	.72	
			11	1.66	1.48	1.48	1.33	.75	
					1.65	1.25	1.09		
				12	1.66	1.26	1.13		
						1.32	.63	CALCULATED	
					13	1.32	.64	MEASURED	

Figure 11-36

MCGUIRE-1 CY-1 ASSEMBLY PEAK AXIAL POWER - CALCULATED VS MEASURED

41.59 EFPD 50ZFP CONTROL BANK D AT 201 STEPS WITHDRAWN

	H	G	F	E	D	C	B	A	
	1.50	1.37	1.55	1.53	1.60	1.44	1.35	.92	
8	1.55	1.49	1.61	1.64	1.65	1.51	1.37	.95	
		1.52	1.43	1.60	1.52	1.52	1.31	1.00	
	9	1.57	1.52	1.64	1.60	1.53	1.37	1.01	
			1.58	1.52	1.57	1.41	1.31	.84	
		10	1.62	1.61	1.60	1.48	1.30	.86	
				1.57	1.42	1.44	1.28	.71	
			11	1.62	1.48	1.45	1.29	.73	
					1.62	1.24	1.07		
				12	1.64	1.25	1.09		
						1.30	.62	CALCULATED	
					13	1.29	.62	MEASURED	

Figure 11-37

MCGUIRE-1 CY-1 ASSEMBLY PEAK AXIAL POWER - CALCULATED VS MEASURED

48.75 EFPD 50%FP CONTROL BANK D AT 201 STEPS WITHDRAWN

	H	G	F	E	D	C	B	A	
	1.50	1.40	1.54	1.53	1.58	1.44	1.33	.91	
8	1.56	1.50	1.62	1.64	1.64	1.51	1.36	.94	
	1.51	1.43	1.59	1.51	1.50	1.30	.99		
9	1.57	1.52	1.64	1.60	1.53	1.36	1.01		
	1.57	1.52	1.55	1.40	1.29	.83			
10	1.62	1.61	1.59	1.47	1.30	.86			
	1.56	1.41	1.42	1.27	.70				
11	1.61	1.47	1.44	1.28	.72				
	1.60	1.23	1.06						
12	1.63	1.25	1.09						
	1.28	.61	CALCULATED						
13	1.29	.62	MEASURED						

Figure 11-38

MCGUIRE-1 CY-1 ASSEMBLY PEAK AXIAL POWER - CALCULATED VS MEASURED

59.37 EFPD 50%FP CONTROL BANK D AT 201 STEPS WITHDRAWN

	H	G	F	E	D	C	B	A	
	1.49	1.41	1.53	1.52	1.56	1.43	1.31	.89	
8	1.54	1.47	1.59	1.60	1.61	1.48	1.33	.92	
	1.51	1.44	1.57	1.50	1.48	1.29	.97		
9	1.55	1.50	1.60	1.56	1.50	1.33	.99		
	1.55	1.51	1.53	1.39	1.27	.82			
10	1.58	1.57	1.55	1.44	1.27	.84			
	1.54	1.41	1.40	1.25	.69				
11	1.57	1.43	1.41	1.26	.71				
	1.58	1.22	1.04						
12	1.60	1.23	1.07						
	1.26	.60	CALCULATED						
13	1.27	.61	MEASURED						

Figure 11-39

MCGUIRE-1 CY-1 ASSEMBLY PEAK AXIAL POWER - CALCULATED VS MEASURED

75.38 EFPD 50%FP CONTROL BANK D AT 198 STEPS WITHDRAWN

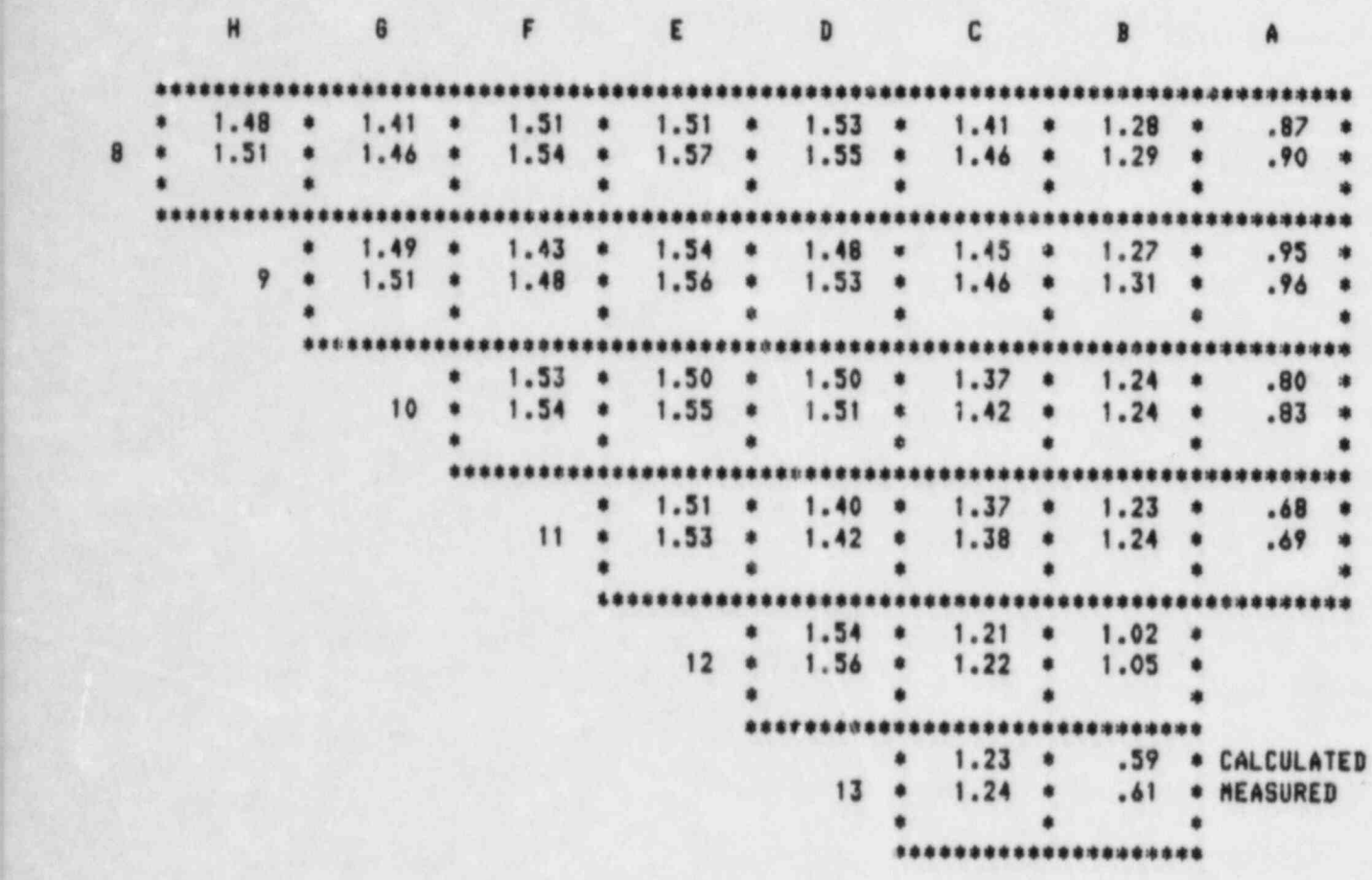

Figure 11-40

MCGUIRE-1 CY-1 ASSEMBLY PEAK AXIAL POWER - CALCULATED VS MEASURED

80.46 EFPD 75%FP CONTROL BANK D AT 213 STEPS WITHDRAWN

	H	G	F	E	D	C	B	A	
8	1.49 1.54	1.42 1.48	1.51 1.55	1.50 1.57	1.51 1.54	1.39 1.44	1.26 1.29	.86 .90	
9		1.49 1.53	1.43 1.48	1.52 1.56	1.47 1.53	1.43 1.45	1.25 1.30	.93 .96	
10			1.52 1.53	1.48 1.53	1.48 1.50	1.36 1.41	1.22 1.23	.79 .82	
11				1.49 1.51	1.38 1.40	1.35 1.36	1.21 1.22	.67 .68	
12					1.52 1.53	1.19 1.20	1.00 1.04		
13						1.20 1.22	.58 .60	CALCULATED MEASURED	

Figure 11-41

MCGUIRE-1 CY-1 ASSEMBLY PEAK AXIAL POWER - CALCULATED VS MEASURED

91.54 EFPD 75%FP CONTROL BANK D AT 213 STEPS WITHDRAWN

	H	G	F	E	D	C	B	A	
	1.47	1.41	1.49	1.48	1.48	1.38	1.25	.85	
8	1.50	1.47	1.52	1.56	1.50	1.41	1.26	.89	
	1.47	1.43	1.50	1.45	1.41	1.24	.92		
9	1.50	1.48	1.52	1.51	1.41	1.28	.93		
	1.50	1.47	1.46	1.34	1.21	.78			
10	1.51	1.53	1.47	1.39	1.20	.80			
	1.47	1.37	1.33	1.19	.66				
11	1.49	1.40	1.33	1.20	.67				
	1.50	1.19	.99						
12	1.50	1.19	1.01						
	1.19	.57	CALCULATED						
13	1.19	.59	MEASURED						

Figure 11-42

MCGUIRE-1 CY-1 ASSEMBLY PEAK AXIAL POWER - CALCULATED VS MEASURED

104.47 EFPD 50ZFP CONTROL BANK D AT 215 STEPS WITHDRAWN

	H	G	F	E	D	C	B	A	
		1.43	1.38	1.44	1.45	1.44	1.35	1.22	.84	
8		1.47	1.44	1.49	1.53	1.48	1.40	1.24	.86	
		1.43	1.39	1.45	1.42	1.37	1.23	.90	
	9	1.46	1.45	1.49	1.48	1.39	1.27	.92	
		1.45	1.44	1.41	1.32	1.18	.77	
	10	1.46	1.48	1.44	1.38	1.19	.79	
			1.43	1.36	1.31	1.18	.65	
		11	1.44	1.38	1.33	1.19	.66	
				1.47	1.18	.98		
			12	1.49	1.18	1.00		
					1.18	.57		CALCULATED
				13	1.18	.58		MEASURED

Figure 11-43

MCGUIRE-1 CY-1 ASSEMBLY PEAK AXIAL POWER - CALCULATED VS MEASURED

112.05 EFPD 50%FP CONTROL BANK D AT 215 STEPS WITHDRAWN

	H	G	F	E	D	C	B	A	
	1.41	1.38	1.43	1.43	1.42	1.34	1.20	.83	
8	1.44	1.42	1.47	1.51	1.46	1.39	1.23	.86	
	1.42	1.39	1.43	1.41	1.35	1.22	.90		
9	1.44	1.43	1.47	1.47	1.37	1.26	.91		
	1.43	1.42	1.40	1.31	1.17	.77			
10	1.46	1.48	1.43	1.36	1.18	.79			
	1.41	1.35	1.29	1.18	.65				
11	1.45	1.37	1.32	1.19	.66				
	1.46	1.18	.97						
12	1.48	1.18	1.00						
	1.17	.57	CALCULATED						
13	1.19	.59	MEASURED						

Figure 11-44

MCGUIRE-1 CY-1 ASSEMBLY PEAK AXIAL POWER - CALCULATED VS MEASURED

115.69 EFPD 75%FP CONTROL BANK D AT 217 STEPS WITHDRAWN

	H	G	F	E	D	C	B	A	
		1.45	1.40	1.45	1.45	1.44	1.35	1.21	.83	
8		1.47	1.44	1.48	1.50	1.46	1.38	1.22	.86	
		1.44	1.41	1.46	1.42	1.37	1.23	.90		
	9	1.46	1.44	1.47	1.46	1.37	1.25	.90		
		1.45	1.44	1.42	1.32	1.18	.77			
		10	1.46	1.47	1.42	1.35	1.17	.78		
			1.43	1.36	1.30	1.17	.65			
			11	1.43	1.35	1.30	1.17	.65		
				1.46	1.18	.97				
				12	1.47	1.17	.99			
					1.16	.56			CALCULATED
					13	1.17	.58		MEASURED

Figure 11-45

MCGUIRE-1 CY-1 ASSEMBLY PEAK AXIAL POWER - CALCULATED VS MEASURED

118.71 EFPD 50%FP CONTROL BANK D AT 180 STEPS WITHDRAWN

	H	G	F	E	D	C	B	A	
	1.46	1.41	1.46	1.46	1.45	1.37	1.23	.85	
8	1.48	1.47	1.50	1.54	1.48	1.43	1.26	.89	
	1.45	1.42	1.47	1.44	1.38	1.25	.92		
9	1.47	1.47	1.49	1.50	1.40	1.30	.94		
	1.46	1.45	1.43	1.34	1.20	.78			
10	1.48	1.52	1.45	1.40	1.20	.82			
	1.44	1.37	1.32	1.20	.66				
11	1.47	1.41	1.34	1.21	.68				
	1.49	1.20	.99						
12	1.51	1.22	1.02						
	1.20	.58	CALCULATED						
13	1.21	.60	MEASURED						

Figure 11-46

MCGUIRE-1 CY-1 ASSEMBLY PEAK AXIAL POWER - CALCULATED VS MEASURED

122.15 EFPD 75%FP CONTROL BANK D AT 215 STEPS WITHDRAWN

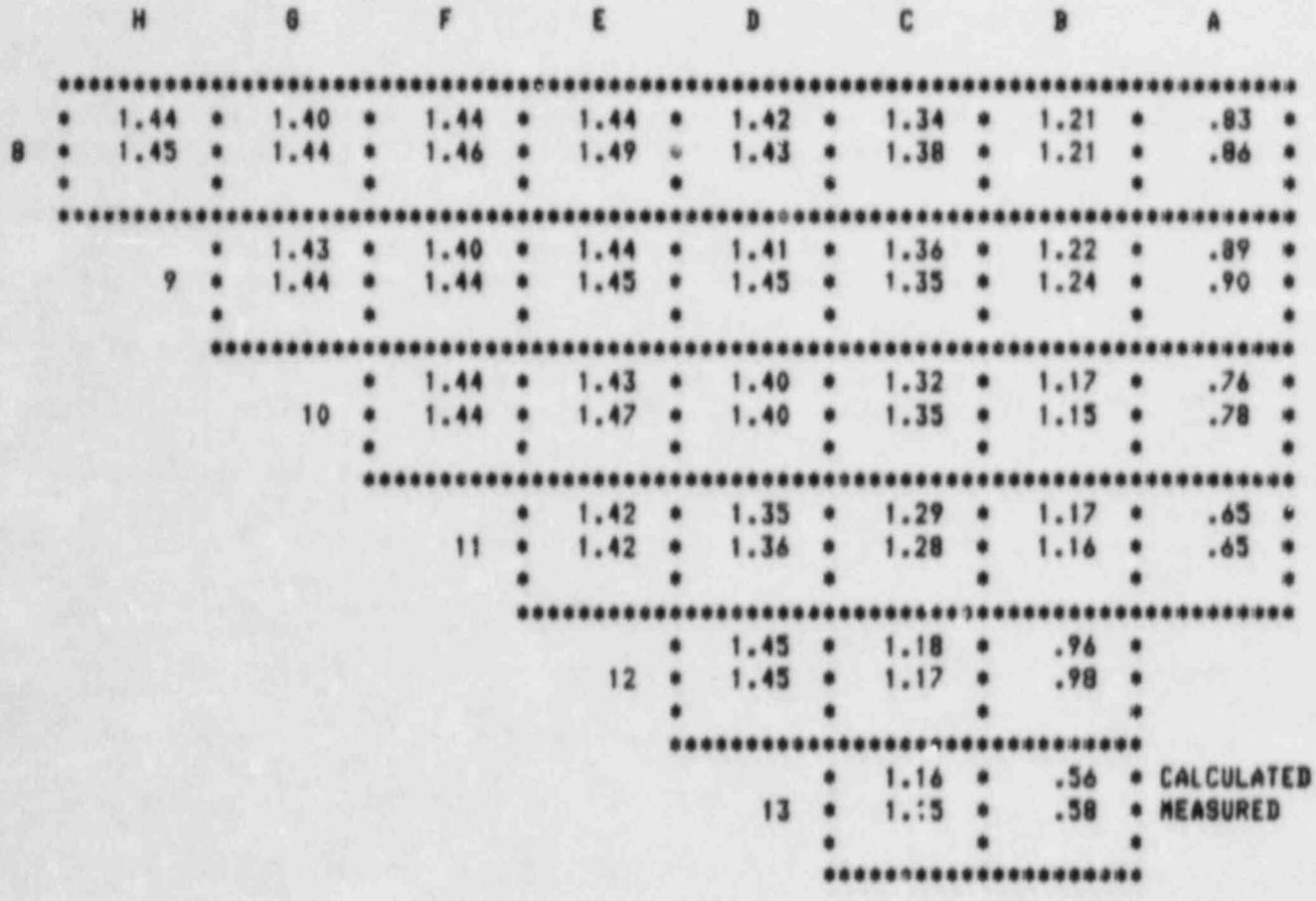

Figure 11-47

MCGUIRE-1 CY-1 ASSEMBLY PEAK AXIAL POWER - CALCULATED VS MEASURED

130.59 EFPD 75%FP CONTROL BANK D AT 215 STEPS WITHDRAWN

	H	G	F	E	D	C	B	A	
8	1.43	1.39	1.43	1.43	1.41	1.34	1.20	.83	
	1.45	1.43	1.44	1.49	1.42	1.38	1.22	.86	
9	1.42	1.39	1.43	1.40	1.34	1.22	.89		
	1.44	1.44	1.45	1.43	1.34	1.25	.90		
10	1.43	1.42	1.39	1.31	1.16	.76			
	1.45	1.47	1.39	1.35	1.16	.79			
11	1.41	1.35	1.29	1.16	.64				
	1.42	1.36	1.29	1.17	.66				
12	1.44	1.17	.96						
	1.46	1.18	.99						
13	1.15	.56	CALCULATED						
	1.17	.58	MEASURED						

Figure 11-48

MCGUIRE-1 CY-1 ASSEMBLY PEAK AXIAL POWER - CALCULATED VS MEASURED

135.44 EFPD 75%FP CONTROL BANK D AT 215 STEPS WITHDRAWN

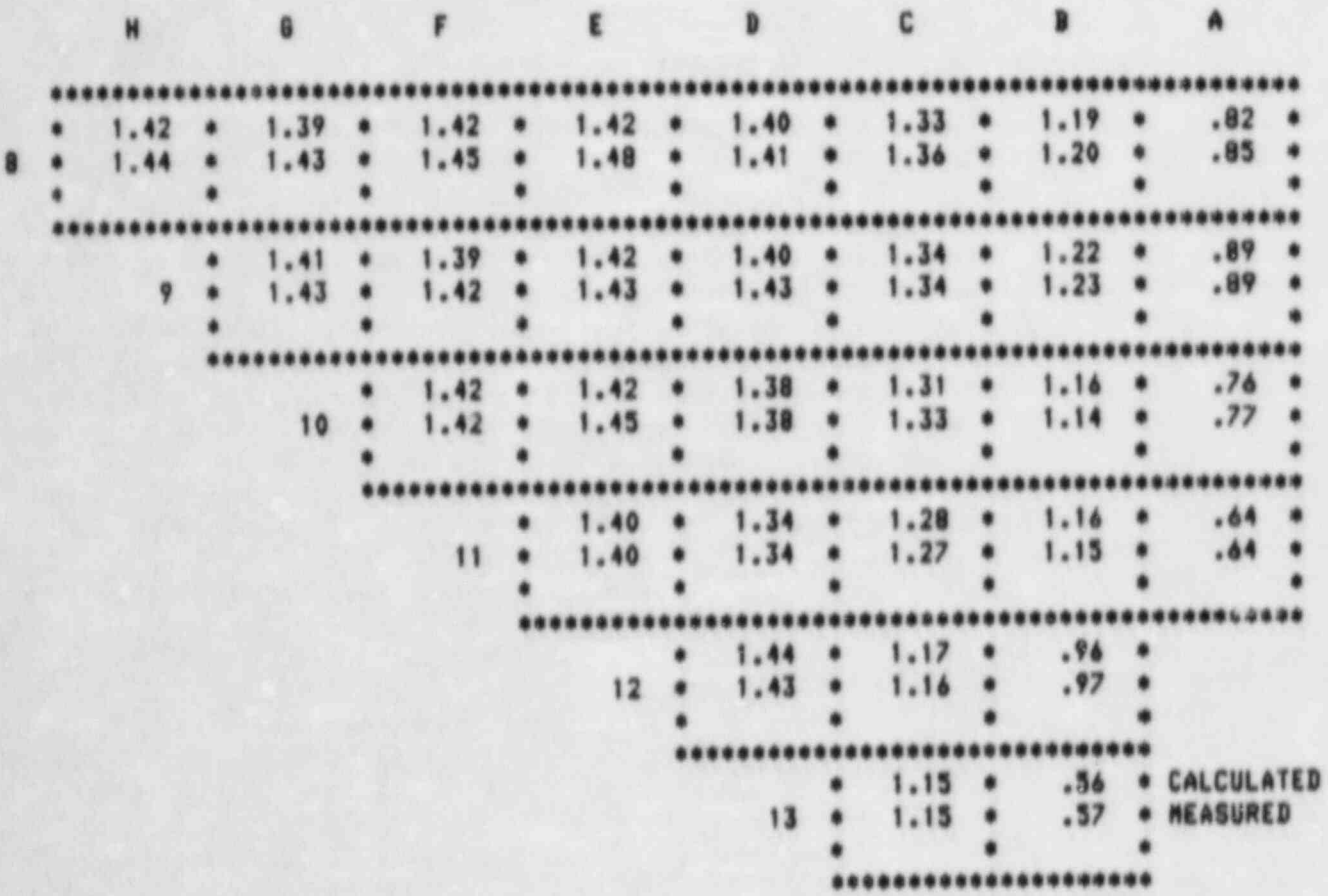

Figure 11-49

MCGUIRE-1 CY-1 ASSEMBLY PEAK AXIAL POWER - CALCULATED VS MEASURED

139.82 EFPD 50ZFP CONTROL BANK D AT 180 STEPS WITHDRAWN

	H	G	F	E	D	C	B	A	
		1.42	1.38	1.42	1.43	1.40	1.34	1.21	.84	
8		1.48	1.46	1.48	1.51	1.45	1.41	1.24	.88	
		1.41	1.39	1.42	1.41	1.35	1.24	.91		
	9	1.47	1.46	1.47	1.47	1.38	1.28	.92		
			1.42	1.42	1.39	1.32	1.17	.77		
		10	1.47	1.49	1.43	1.38	1.19	.80		
				1.40	1.35	1.29	1.19	.65		
		11	1.44	1.41	1.32	1.20	.67			
					1.45	1.19	.98			
				12	1.50	1.21	1.01			
						1.18	.57		CALCULATED	
					13	1.20	.60		MEASURED	

Figure 11-50

MCGUIRE-1 CY-1 ASSEMBLY PEAK AXIAL POWER - CALCULATED VS MEASURED

141.52 EFPD 50%FP CONTROL BANK D AT 215 STEPS WITHDRAWN

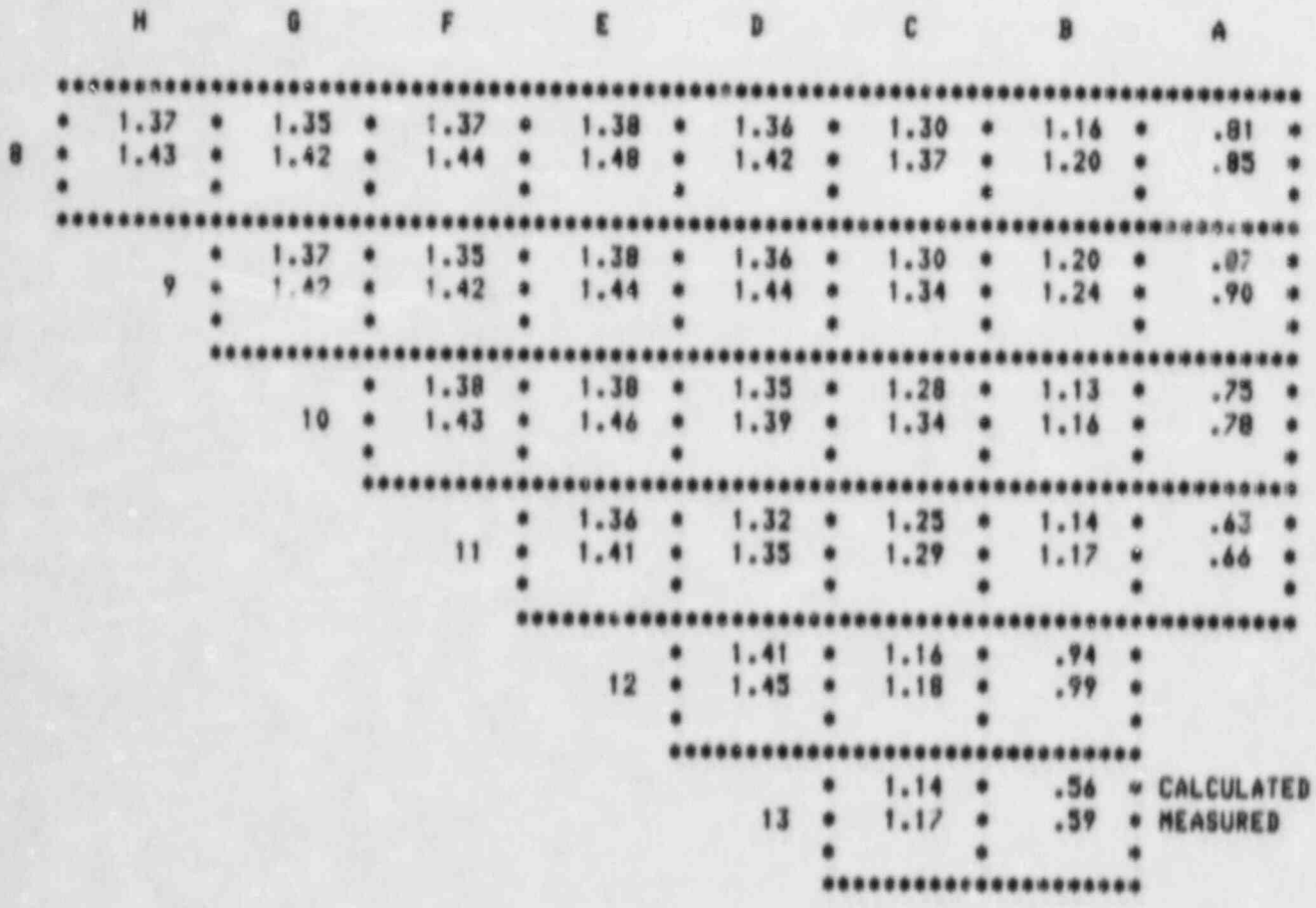

MCGUIRE-1 CY-1 ASSEMBLY PEAK AXIAL POWER - CALCULATED VS MEASURED

146.01 EFPD 75%FP CONTROL BANK B AT 215 STEPS WITHDRAWN

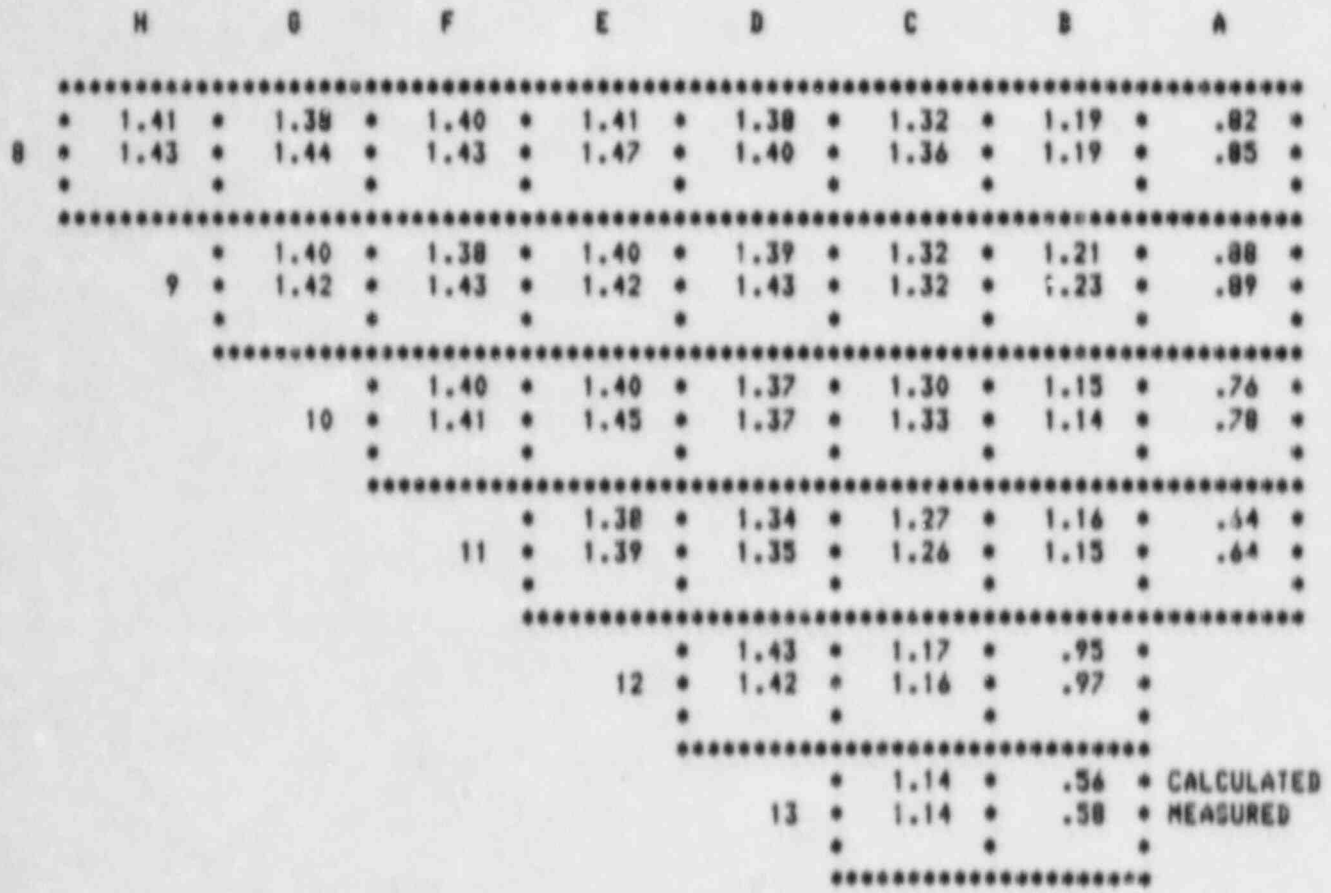

Figure 11-52

MCGUIRE-1 CY-1 ASSEMBLY PEAK AXIAL POWER - CALCULATED VS MEASURED

150.19 EFPD 50IFP CONTROL BANK D AT 215 STEPS WITHDRAWN

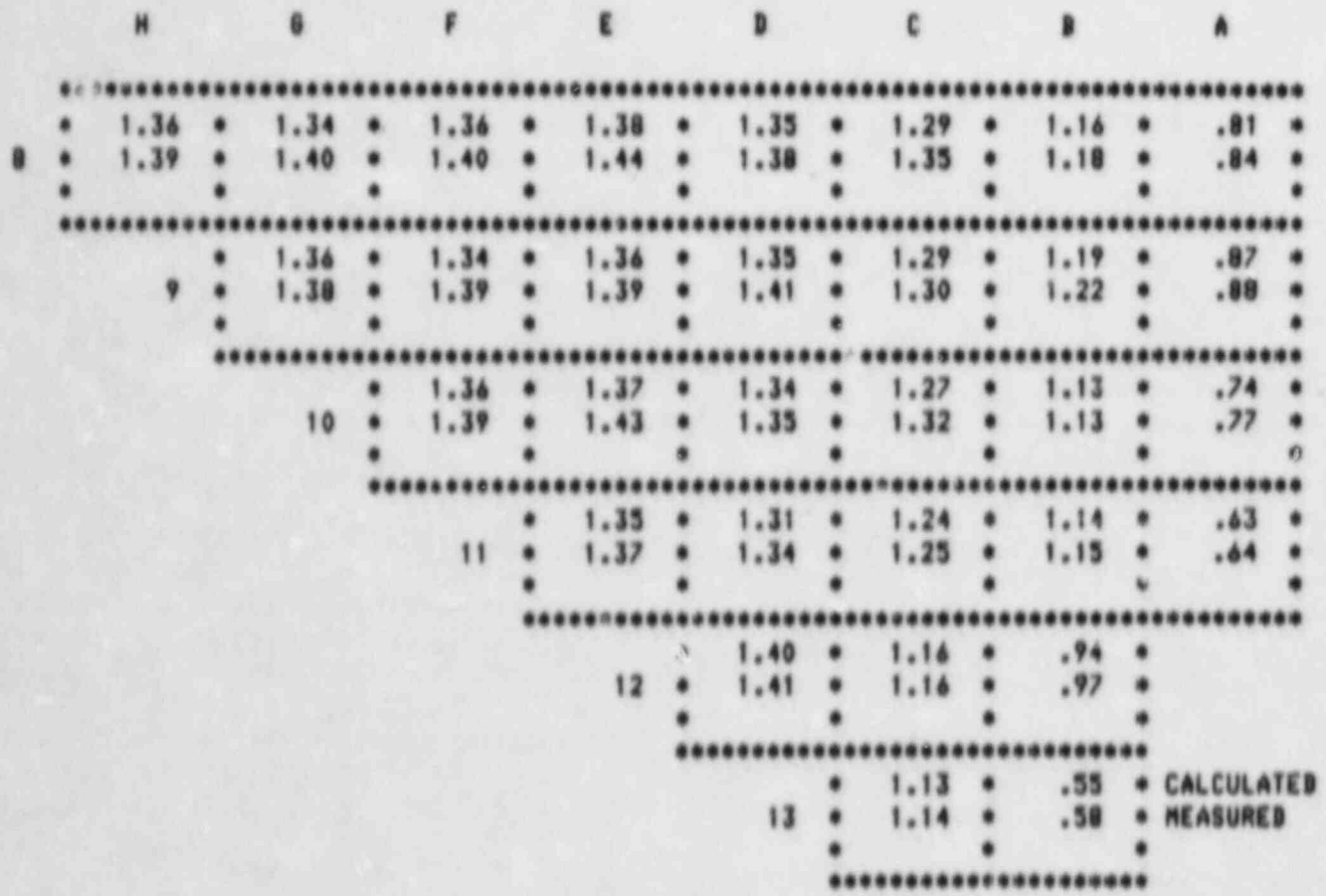

Figure 11-53

MCGUIRE-1 CY-1 ASSEMBLY PEAK AXIAL POWER - CALCULATED VS MEASURED

162.76 EFPD 50%FP CONTROL BANK D AT 215 STEPS WITHDRAWN

	H	G	F	E	D	C	B	A	
	1.35	1.33	1.35	1.36	1.33	1.28	1.15	.80	
8	1.39	1.39	1.39	1.43	1.36	1.33	1.17	.83	
	1.34	1.33	1.35	1.34	1.28	1.18	.86		
9	1.37	1.38	1.38	1.39	1.29	1.21	.87		
	1.35	1.36	1.32	1.26	1.12	.74			
10	1.37	1.42	1.34	1.31	1.12	.77			
	1.34	1.30	1.23	1.13	.63				
11	1.36	1.32	1.24	1.14	.64				
	1.38	1.15	.93						
12	1.40	1.15	.96						
	1.12	.55	CALCULATED						
13	1.14	.58	MEASURED						

Figure 11-54

MCGUIRE-1 CY-1 ASSEMBLY PEAK AXIAL POWER - CALCULATED VS MEASURED

173.34 EFPD 50%FP CONTROL BANK D AT 215 STEPS WITHDRAWN

	H	G	F	E	D	C	B	A	
	1.35	1.33	1.33	1.35	1.32	1.28	1.14	.80	
8	1.36	1.39	1.37	1.42	1.34	1.34	1.17	.84	
		1.33	1.33	1.33	1.33	1.27	1.18	.86	
	9	1.35	1.38	1.36	1.39	1.28	1.22	.88	
			1.34	1.35	1.31	1.26	1.11	.74	
		10	1.35	1.41	1.33	1.31	1.12	.77	
				1.32	1.30	1.23	1.13	.62	
			11	1.34	1.33	1.24	1.14	.64	
					1.38	1.15	.93		
				12	1.39	1.17	.96		
						1.12	.55		CALCULATED
					13	1.14	.58		MEASURED

Figure 11-55

MCGUIRE-1 CY=1 ASSEMBLY PEAK AXIAL POWER - CALCULATED VS MEASURED

185.58 EFPD 50%FP CONTROL BANK D AT 215 STEPS WITHDRAWN

	H	G	F	E	D	C	B	A
	1.34	1.32	1.32	1.34	1.30	1.27	1.13	.80
8	1.35	1.37	1.35	1.40	1.33	1.32	1.16	.84
	1.32	1.32	1.32	1.32	1.32	1.26	1.18	.86
9	1.34	1.36	1.34	1.38	1.27	1.21	.87	
	1.32	1.34	1.30	1.25	1.11	.74		
10	1.34	1.39	1.31	1.30	1.11	.77		
	1.31	1.30	1.22	1.13	.62			
11	1.33	1.32	1.24	1.14	.64			
	1.37	1.15	.93					
12	1.39	1.17	.96					
	1.12	.55	CALCULATED					
13	1.13	.58	MEASURED					

Figure 11-56

MCGUIRE-1 CY-1A ASSEMBLY RADIAL POWER CALCULATED VS MEASURED

198.66 EFPD 90%FP CONTROL BANK D AT 217 STEPS WITHDRAWN

	H	G	F	E	D	C	B	A
	1.12	1.20	1.11	1.16	1.07	1.13	1.00	.76
8	1.08	1.22	1.08	1.18	1.05	1.18	.99	.79
	1.20	1.12	1.19	1.09	1.15	1.07	1.14	.76
9	1.21	1.08	1.20	1.05	1.18	1.04	1.17	.76
	1.10	1.18	1.09	1.16	1.08	1.13	.96	.70
10	1.06	1.19	1.06	1.19	1.06	1.15	.93	.71
	1.13	1.07	1.15	1.10	1.19	1.06	1.02	.54
11	1.16	1.04	1.17	1.07	1.21	1.03	1.03	.54
	1.01	1.11	1.06	1.18	1.18	1.12	.82	
12	.99	1.13	1.04	1.20	1.16	1.13	.83	
	.96	1.00	1.09	1.04	1.11	1.01	.56	
13	.98	.98	1.13	1.02	1.11	1.01	.57	
	.92	1.07	.93	1.00	.81	.56		
14	.91	1.11	.90	1.00	.81	.57		
	.71	.72	.67	.53	CALCULATED			
15	.73	.72	.69	.52	MEASURED			

Figure 11-57

MCGUIRE-1 CY-1A ASSEMBLY RADIAL POWER CALCULATED VS MEASURED

217.53 EFPD 100%FP CONTROL BANK D AT 209 STEPS WITHDRAWN

	H	G	F	E	D	C	B	A
8	1.10 1.06	1.19 1.21	1.10 1.08	1.15 1.18	1.07 1.05	1.13 1.17	1.00 .99	.76 .79
9	1.19 1.20	1.11 1.07	1.18 1.19	1.08 1.05	1.15 1.17	1.07 1.04	1.13 1.17	.76 .77
10	1.09 1.06	1.17 1.18	1.09 1.05	1.16 1.17	1.08 1.05	1.12 1.15	.96 .94	.71 .72
11	1.13 1.16	1.07 1.04	1.15 1.17	1.09 1.07	1.17 1.19	1.05 1.02	1.02 1.03	.55 .55
12	1.02 1.00	1.11 1.13	1.06 1.04	1.17 1.19	1.15 1.13	1.10 1.11	.82 .83	
13	.98 .99	1.01 .98	1.10 1.13	1.04 1.02	1.10 1.10	1.00 1.00	.57 .58	
14	.94 .93	1.09 1.12	.94 .92	1.01 1.02	.82 .82	.56 .57		
15	.73 .76	.74 .74	.69 .71	.54 .54	CALCULATED MEASURED			

Figure 11-58

MCGUIRE-1 CY-1A ASSEMBLY RADIAL POWER CALCULATED VS MEASURED

223.35 EFPD 100%FP CONTROL BANK D AT 211 STEPS WITHDRAWN

	H	G	F	E	D	C	B	A
	1.09	1.18	1.10	1.15	1.07	1.13	1.00	.77
8	1.06	1.21	1.08	1.18	1.05	1.18	.99	.79
	1.18	1.11	1.17	1.08	1.14	1.07	1.13	.77
9	1.20	1.07	1.19	1.05	1.17	1.05	1.17	.77
	1.09	1.17	1.09	1.15	1.08	1.12	.96	.71
10	1.07	1.19	1.05	1.17	1.05	1.14	.93	.72
	1.13	1.07	1.14	1.09	1.17	1.05	1.02	.55
11	1.17	1.04	1.17	1.07	1.19	1.02	1.02	.55
	1.02	1.11	1.06	1.17	1.16	1.10	.82	
12	1.01	1.13	1.04	1.19	1.14	1.11	.82	
	.99	1.02	1.10	1.04	1.10	1.00	.57	
13	.99	.99	1.13	1.01	1.10	.99	.58	
	.95	1.09	.95	1.01	.82	.57		
14	.93	1.12	.92	1.02	.82	.57		
	.74	.74	.69	.54	CALCULATED			
15	.76	.74	.71	.54	MEASURED			

Figure 11- 59

MCGUIRE-1 CY-1A ASSEMBLY RADIAL POWER CALCULATED VS MEASURED

236.23 EFPD 100%FP CONTROL BANK D AT 211 STEPS WITHDRAWN

	H	G	F	E	D	C	B	A
	1.09	1.17	1.09	1.14	1.07	1.13	1.00	.77
8	1.06	1.21	1.08	1.17	1.05	1.17	.99	.80
	1.17	1.10	1.16	1.07	1.14	1.07	1.13	.77
9	1.20	1.07	1.18	1.05	1.16	1.04	1.17	.77
	1.08	1.16	1.08	1.15	1.07	1.12	.97	.71
10	1.06	1.18	1.05	1.17	1.05	1.14	.94	.73
	1.13	1.06	1.14	1.08	1.17	1.05	1.02	.55
11	1.16	1.04	1.16	1.06	1.18	1.02	1.02	.56
	1.03	1.11	1.06	1.16	1.15	1.10	.83	
12	1.01	1.13	1.04	1.18	1.13	1.10	.82	
	1.00	1.02	1.10	1.04	1.10	1.00	.57	
13	1.00	.99	1.13	1.01	1.10	.99	.58	
	.96	1.10	.95	1.01	.82	.57		
14	.94	1.12	.93	1.02	.82	.58		
	.75	.75	.70	.55	CALCULATED			
15	.77	.75	.72	.55	MEASURED			

Figure 11-60

MCGUIRE-1 CY-1A ASSEMBLY RADIAL POWER CALCULATED VS MEASURED

249.75 EFPD 100%FP CONTROL BANK D AT 221 STEPS WITHDRAWN

	H	G	F	E	D	C	B	A
	1.10	1.17	1.08	1.13	1.06	1.12	1.00	.77
8	1.07	1.20	1.06	1.15	1.05	1.16	.99	.80
	1.17	1.09	1.15	1.07	1.13	1.06	1.13	.77
9	1.19	1.06	1.17	1.05	1.17	1.04	1.15	.77
	1.08	1.15	1.07	1.14	1.07	1.12	.97	.72
10	1.06	1.17	1.05	1.17	1.05	1.14	.93	.72
	1.12	1.06	1.13	1.08	1.17	1.05	1.02	.56
11	1.17	1.04	1.15	1.05	1.18	1.03	1.03	.55
	1.03	1.11	1.06	1.17	1.17	1.10	.83	
12	1.03	1.14	1.02	1.17	1.14	1.11	.83	
	1.01	1.03	1.10	1.05	1.10	1.00	.58	
13	1.00	1.00	1.14	1.02	1.09	1.00	.59	
	.96	1.10	.96	1.02	.83	.58		
14	.95	1.13	.94	1.03	.81	.58		
	.76	.76	.71	.55	CALCULATED			
15	.78	.75	.73	.56	MEASURED			

Figure 11-6i

MCGUIRE-1 CY-1A ASSEMBLY PEAK AXIAL POWERS CALCULATED VS MEASURED

198.66 EFPD 90%FP CONTROL BANK D AT 217 STEPS WITHDRAWN

	H	G	F	E	D	C	B	A
	1.34	1.41	1.30	1.35	1.25	1.29	1.13	.86
8	1.34	1.51	1.33	1.44	1.27	1.41	1.19	.94
	1.41	1.32	1.38	1.27	1.33	1.23	1.30	.86
9	1.50	1.33	1.47	1.29	1.42	1.25	1.40	.91
	1.29	1.37	1.28	1.35	1.26	1.29	1.09	.79
10	1.31	1.46	1.30	1.45	1.29	1.39	1.11	.86
	1.32	1.25	1.34	1.28	1.37	1.21	1.17	.61
11	1.43	1.27	1.43	1.32	1.47	1.25	1.24	.65
	1.18	1.28	1.23	1.36	1.37	1.28	.94	
12	1.21	1.37	1.26	1.45	1.41	1.36	1.00	
	1.11	1.15	1.25	1.19	1.27	1.15	.64	
13	1.19	1.17	1.36	1.22	1.34	1.21	.69	
	1.04	1.22	1.05	1.14	.92	.64		
14	1.08	1.32	1.08	1.21	.98	.69		
	.81	.82	.76	.60	CALCULATED			
15	.87	.86	.83	.63	MEASURED			

Figure 11-62

MCGUIRE-1 CY-1A ASSEMBLY PEAK AXIAL POWERS CALCULATED VS MEASURED

217.53 EFPD 100%FP CONTROL BANK D AT 209 STEPS WITHDRAWN

	H	G	F	E	D	C	B	A
	1.33	1.43	1.30	1.37	1.26	1.34	1.18	.90
8	1.31	1.48	1.33	1.42	1.26	1.39	1.18	.94
	1.42	1.31	1.40	1.27	1.36	1.26	1.36	.90
9	1.47	1.31	1.44	1.27	1.40	1.24	1.38	.91
	1.29	1.39	1.28	1.37	1.27	1.33	1.13	.83
10	1.30	1.44	1.27	1.42	1.26	1.36	1.11	.86
	1.34	1.25	1.36	1.28	1.41	1.24	1.21	.64
11	1.41	1.26	1.41	1.29	1.44	1.21	1.22	.65
	1.19	1.31	1.25	1.40	1.41	1.32	.97	
12	1.21	1.36	1.25	1.43	1.36	1.31	.98	
	1.14	1.18	1.30	1.23	1.32	1.19	.67	
13	1.19	1.17	1.34	1.21	1.31	1.18	.68	
	1.10	1.29	1.10	1.19	.97	.67		
14	1.10	1.32	1.09	1.21	.97	.68		
	.86	.87	.81	.63	CALCULATED			
15	.90	.87	.84	.64	MEASURED			

Figure 11-63

MCGUIRE-1 CY-1A ASSEMBLY PEAK AXIAL POWER - CALCULATED VS MEASURED

223.35 EFPD 100%FP CONTROL BANK D AT 211 STEPS WITHDRAWN

	H	G	F	E	D	C	B	A
	1.32	1.41	1.29	1.36	1.25	1.33	1.17	.90
8	1.33	1.49	1.32	1.43	1.28	1.45	1.21	.97
	1.41	1.30	1.39	1.26	1.35	1.25	1.35	.90
9	1.48	1.31	1.45	1.28	1.43	1.28	1.42	.93
	1.28	1.38	1.27	1.36	1.26	1.33	1.13	.83
10	1.30	1.45	1.28	1.43	1.28	1.40	1.13	.87
	1.33	1.25	1.35	1.28	1.40	1.24	1.21	.64
11	1.42	1.27	1.42	1.30	1.47	1.25	1.23	.66
	1.19	1.31	1.24	1.39	1.40	1.32	.97	
12	1.21	1.36	1.26	1.45	1.43	1.36	.99	
	1.14	1.18	1.29	1.22	1.31	1.19	.67	
13	1.19	1.19	1.37	1.24	1.35	1.21	.69	
	1.10	1.29	1.10	1.19	.96	.66		
14	1.12	1.35	1.11	1.23	.98	.69		
	.87	.87	.81	.63	CALCULATED			
15	.91	.88	.85	.65	MEASURED			

Figure 11-64

MCGUIRE-1 CY-1A ASSEMBLY PEAK AXIAL POWER - CALCULATED VS MEASURED

236.23 EFPD 100%FP CONTROL BANK D AT 211 STEPS WITHDRAWN

	H	G	F	E	D	C	B	A
8	1.29 1.32	1.39 1.47	1.27 1.31	1.34 1.42	1.24 1.27	1.32 1.43	1.17 1.20	.90 .96
9	1.39 1.45	1.28 1.30	1.37 1.43	1.25 1.27	1.33 1.41	1.24 1.27	1.34 1.41	.90 .93
10	1.26 1.28	1.36 1.42	1.26 1.27	1.34 1.41	1.25 1.27	1.32 1.38	1.12 1.12	.83 .87
11	1.32 1.41	1.23 1.26	1.34 1.40	1.26 1.29	1.38 1.45	1.23 1.24	1.20 1.22	.64 .66
12	1.18 1.21	1.30 1.36	1.24 1.25	1.38 1.44	1.38 1.41	1.31 1.34	.97 .98	
13	1.15 1.19	1.18 1.19	1.29 1.36	1.22 1.23	1.30 1.34	1.18 1.20	.67 .69	
14	1.11 1.12	1.30 1.34	1.10 1.11	1.19 1.22	.96 .98	.67 .69		
15	.88 .91	.88 .89	.82 .86	.64 .65	CALCULATED MEASURED			

Figure 11-65

MCGUIRE-1 CY-1A ASSEMBLY PEAK AXIAL POWER - CALCULATED VS MEASURED

249.75 EFPD 100%FP CONTROL BANK D AT 221 STEPS WITHDRAWN

	H	G	F	E	D	C	B	A
8	1.26 1.26	1.35 1.40	1.24 1.24	1.31 1.36	1.21 1.25	1.29 1.38	1.15 1.18	.89 .95
9	1.35 1.41	1.25 1.26	1.33 1.39	1.22 1.24	1.30 1.39	1.22 1.23	1.32 1.37	.89 .91
10	1.23 1.25	1.33 1.39	1.23 1.25	1.31 1.38	1.22 1.25	1.29 1.35	1.11 1.09	.83 .85
11	1.29 1.39	1.21 1.24	1.31 1.36	1.23 1.24	1.35 1.41	1.20 1.22	1.18 1.20	.64 .65
12	1.17 1.22	1.28 1.34	1.21 1.20	1.35 1.38	1.35 1.37	1.28 1.32	[illegible]5 .97	
13	1.15 1.18	1.17 1.18	1.27 1.35	1.20 1.22	1.28 1.30	1.16 1.17	.66 .68	
14	1.10 1.12	1.29 1.34	1.09 1.12	1.18 1.22	.95 .96	.66 .67		
15	.88 .91	.88 .88	.82 .86	.64 .66	CALCULATED MEASURED			

Figure 11-66

SEQUOYAH-1 CY-1 ASSEMBLY RADIAL POWER CALCULATED VS MEASURED

71.82 EFPD 100(Z)FP CONTROL BANK D AT 200 STEPS WITHDRAWN

	H	G	F	E	D	C	B	A	
	1.14	1.09	1.19	1.12	1.16	1.05	1.01	.69	
8	1.12	1.05	1.17	1.11	1.15	1.05	1.01	.71	
	1.18	1.12	1.20	1.16	1.14	1.00	.75		
9	1.16	1.11	1.19	1.16	1.13	1.01	.77		
	1.20	1.13	1.19	1.09	.98	.64			
10	1.18	1.12	1.18	1.09	.98	.66			
	1.19	1.13	1.10	.93	.53				
11	1.18	1.13	1.08	.92	.56				
	1.10	.98	.82						
12	1.09	.99	.86						
	.98	.48	CALCULATED						
13	1.02	.51	MEASURED						

Figure 11-67

SEQUOYAH-1 CY-i ASSEMBLY RADIAL POWER CALCULATED VS MEASURED

101.62 EFPD 100(%)FP CONTROL BANK D AT 218 STEPS WITHDRAWN

	H	G	F	E	D	C	B	A	
	1.17	1.11	1.20	1.15	1.18	1.06	1.00	.69	
8	1.14	1.06	1.16	1.13	1.17	1.06	1.00	.71	
	1.19	1.15	1.21	1.17	1.13	1.00	.74		
9	1.16	1.12	1.18	1.16	1.12	1.01	.76		
	1.20	1.15	1.18	1.09	.97	.63			
10	1.18	1.13	1.17	1.09	.97	.65			
	1.19	1.14	1.08	.92	.53				
11	1.17	1.13	1.08	.91	.55				
	1.11	.99	.81						
12	1.11	1.00	.85						
	.97	.48	CALCULATED						
13	1.02	.51	MEASURED						

Figure 11-68

SEQUOYAH-1 CY-1 ASSEMBLY RADIAL POWER CALCULATED VS MEASURED

133.30 EFPD 100(%)FP CONTROL BANK D AT 216 STEPS WITHDRAWN

	H	G	F	E	D	C	B	A	
	1.17	1.13	1.20	1.17	1.18	1.08	.99	.68	
8	1.14	1.08	1.17	1.14	1.16	1.07	.99	.70	
	1.19	1.17	1.20	1.18	1.12	1.00	.73		
9	1.17	1.14	1.19	1.17	1.12	1.01	.76		
	1.21	1.16	1.17	1.09	.96	.63			
10	1.18	1.14	1.17	1.09	.96	.65			
	1.18	1.14	1.07	.91	.53				
11	1.16	1.13	1.06	.91	.55				
	1.09	.99	.80						
12	1.09	1.00	.84						
	.96	.47	CALCULATED						
13	1.01	.51	MEASURED						

Figure 11-69

SEQUOYAH-1 CY-1 ASSEMBLY RADIAL POWER CALCULATED VS MEASURED

166.04 EFPD 100(%)FP CONTROL BANK D AT 210 STEPS WITHDRAWN

	H	G	F	E	D	C	B	A	
	1.15	1.13	1.20	1.18	1.16	1.09	.99	.69	
8	1.13	1.09	1.17	1.15	1.14	1.08	.99	.71	
	1.19	1.18	1.20	1.18	1.12	1.00	.74		
9	1.16	1.15	1.19	1.17	1.11	1.01	.76		
	1.20	1.17	1.17	1.10	.96	.63			
10	1.18	1.15	1.16	1.09	.96	.66			
	1.18	1.14	1.06	.91	.53				
11	1.16	1.13	1.06	.91	.55				
	1.08	.99	.80						
12	1.08	1.00	.84						
	.96	.48	CALCULATED						
13	1.00	.51	MEASURED						

Figure 11-70

SEQUOYAH-1 CY-1 ASSEMBLY RADIAL POWER CALCULATED VS MEASURED

231.70 EFPD 100(%)FP CONTROL BANK D AT 216 STEPS WITHDRAWN

	H	G	F	E	D	C	B	A	
	1.12	1.11	1.17	1.18	1.15	1.10	.99	.71	
8	1.10	1.08	1.14	1.16	1.13	1.09	.99	.72	
	1.16	1.18	1.17	1.17	1.11	1.01	.75		
9	1.13	1.16	1.16	1.17	1.09	1.02	.76		
		1.18	1.18	1.15	1.10	.96	.65		
10		1.16	1.16	1.14	1.10	.96	.67		
			1.16	1.14	1.06	.92	.54		
11			1.14	1.14	1.05	.92	.56		
				1.08	1.01	.81			
12				1.07	1.02	.84			
					.96	.49			CALCULATED
13					1.00	.53			MEASURED

Figure 11-71

SEQUOYAH-1 CY-1 ASSEMBLY RADIAL POWER CALCULATED VS MEASURED

292.04 EFPD 100(%)FP CONTROL BANK D AT 216 STEPS WITHDRAWN

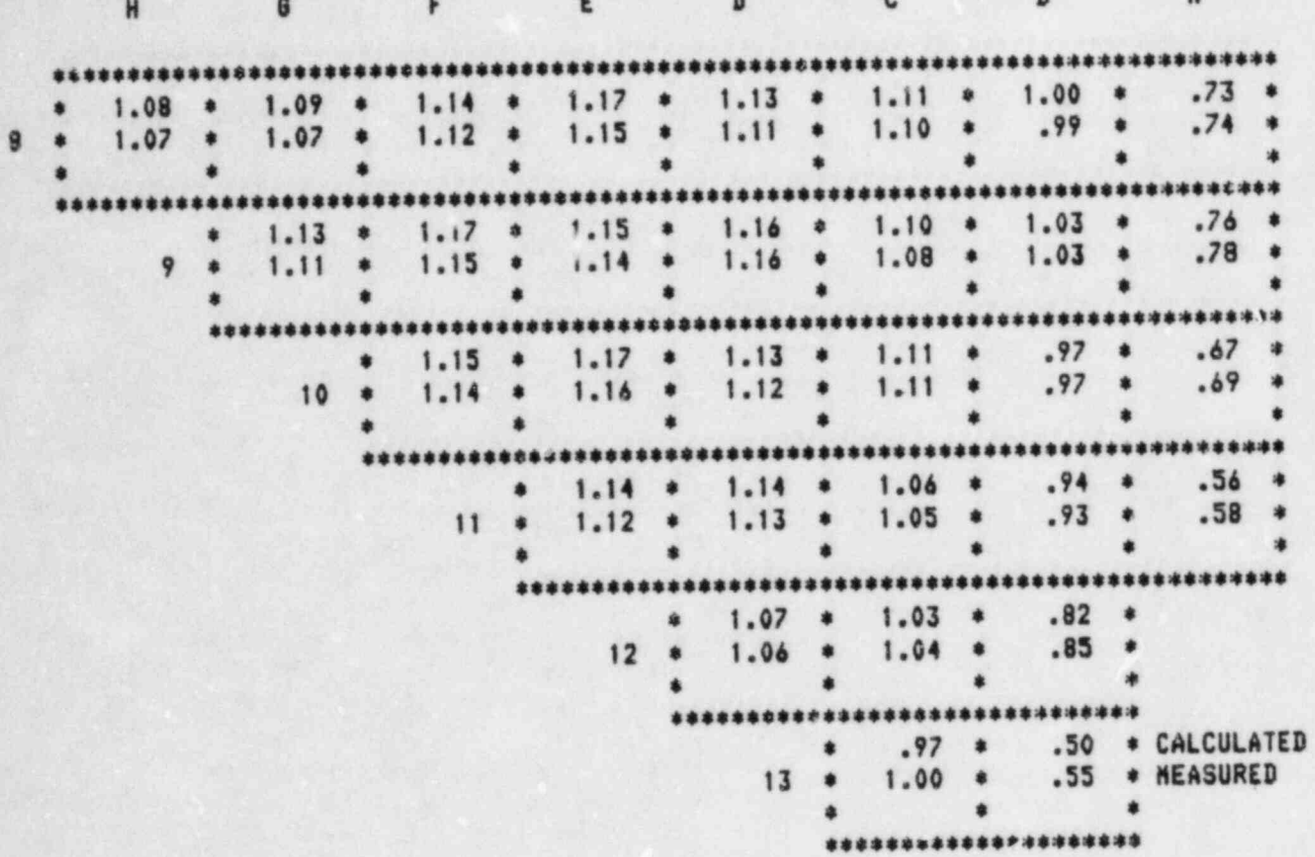

Figure 11-72

SEQUOYAH-1 CY-1 ASSEMBLY RADIAL POWER CALCULATED VS MEASURED

378.92 EFPD 100(%)FP CONTROL BANK D AT 222 STEPS WITHDRAWN

	H	G	F	E	D	C	B	A	
	1.06	1.06	1.10	1.14	1.11	1.12	1.01	.76	
8	1.02	1.04	1.08	1.14	1.09	1.10	1.00	.77	
	1.09	1.14	1.12	1.14	1.09	1.04	.79		
9	1.07	1.13	1.10	1.14	1.07	1.05	.80		
	1.12	1.14	1.11	1.11	.99	.71			
10	1.10	1.14	1.09	1.11	.98	.73			
	1.11	1.13	1.06	.96	.59				
11	1.09	1.13	1.05	.96	.60				
	1.08	1.05	.84						
12	1.06	1.06	.87						
	.98	.53	CALCULATED						
13	1.02	.58	MEASURED						

Figure 11-73

SEQUOYAH 1 CYCLE 1 ASSEMBLY PEAK AXIAL POWER - CALCULATED VS MEASURED

71.82 EFPD 100(%)FP CONTROL BANK D AT 200 STEPS WITHDRAWN

	H	G	F	E	D	C	B	A	
	1.48	1.40	1.51	1.45	1.51	1.35	1.26	.87	
8	1.55	1.42	1.57	1.50	1.60	1.42	1.33	.93	
	1.50	1.44	1.53	1.48	1.44	1.27	.94		
9	1.56	1.48	1.59	1.56	1.51	1.34	1.02		
	1.52	1.44	1.50	1.38	1.23	.80			
10	1.57	1.49	1.57	1.45	1.29	.86			
	1.51	1.44	1.38	1.17	.67				
11	1.57	1.51	1.43	1.21	.74				
	1.41	1.26	1.03						
12	1.50	1.32	1.13						
	1.25	.60	CALCULATED						
13	1.36	.67	MEASURED						

Figure 11-74

SEQUOYAH 1 CYCLE 1 ASSEMBLY PEAK AXIAL POWER - CALCULATED VS MEASURED

101.62 EFPD 100(%)FP CONTROL BANK D AT 218 STEPS WITHDRAWN

	H	G	F	E	D	C	B	A	
	1.44	1.37	1.46	1.41	1.45	1.30	1.20	.83	
8	1.46	1.35	1.48	1.44	1.50	1.36	1.26	.88	
	1.45	1.41	1.47	1.43	1.37	1.21	.89		
9	1.47	1.42	1.50	1.47	1.42	1.27	.96		
	1.47	1.41	1.43	1.32	1.16	.76			
10	1.48	1.42	1.48	1.37	1.22	.82			
	1.44	1.39	1.31	1.11	.64				
11	1.48	1.43	1.35	1.14	.69				
	1.35	1.21	.98						
12	1.40	1.25	1.06						
	1.18	.57	CALCULATED						
13	1.27	.64	MEASURED						

Figure 11-75

SEQUOYAH 1 CYCLE 1 ASSEMBLY PEAK AXIAL POWER - CALCULATED VS MEASURED

133.30 EFPD 100(%)FP CONTROL BANK D AT 216 STEPS WITHDRAWN

	H	G	F	E	D	C	B	A	
		1.40	1.35	1.43	1.40	1.41	1.29	1.17	.81	
8		1.42	1.33	1.44	1.41	1.45	1.33	1.21	.85	
		1.42	1.40	1.43	1.40	1.32	1.18	.87	
	9	1.43	1.40	1.46	1.44	1.37	1.23	.92	
			1.43	1.39	1.39	1.30	1.13	.74	
		10	1.44	1.39	1.42	1.33	1.17	.79	
				1.40	1.36	1.26	1.08	.62	
			11	1.42	1.38	1.29	1.10	.66	
					1.30	1.18	.95		
				12	1.34	1.22	1.03		
						1.14	.56	CALCULATED	
					13	1.23	.62	MEASURED	

Figure 11-76

SEQUOYAH 1 CYCLE 1 ASSEMBLY PEAK AXIAL POWER - CALCULATED VS MEASURED

166.04 EFPD 100(%)FP CONTROL BANK D AT 210 STEPS WITHDRAWN

	H	G	F	E	D	C	B	A
	1.37	1.33	1.40	1.39	1.38	1.28	1.15	.81
8	1.37	1.29	1.39	1.38	1.39	1.29	1.17	.84
		1.39	1.40	1.40	1.39	1.30	1.17	.86
	9	1.38	1.37	1.42	1.40	1.32	1.20	.90
			1.40	1.38	1.36	1.28	1.11	.74
		10	1.40	1.36	1.38	1.30	1.13	.78
				1.37	1.34	1.24	1.06	.62
			11	1.36	1.34	1.25	1.08	.66
					1.28	1.17	.93	
				12	1.30	1.19	1.00	
						1.12	.56	CALCULATED
					13	1.19	.61	MEASURED

Figure 11-77

SEQUOYAH 1 CYCLE 1 ASSEMBLY PEAK AXIAL POWER - CALCULATED VS MEASURED

231.70 EFPD 100(%)FP CONTROL BANK D AT 216 STEPS WITHDRAWN

	H	G	F	E	D	C	B	A	
	1.27	1.26	1.32	1.35	1.31	1.26	1.12	.80	
8	1.28	1.24	1.31	1.34	1.31	1.26	1.13	.83	
		1.31	1.35	1.33	1.34	1.25	1.15	.85	
	9	1.30	1.33	1.33	1.35	1.26	1.17	.88	
			1.33	1.34	1.29	1.26	1.08	.74	
		10	1.33	1.33	1.30	1.27	1.10	.77	
				1.30	1.30	1.19	1.05	.62	
			11	1.30	1.30	1.21	1.06	.65	
					1.23	1.16	.92		
				12	1.25	1.18	.98		
						1.10	.56		CALCULATED
					13	1.15	.62		MEASURED

Figure 11-78

SEQUOYAH 1 CYCLE 3 ASSEMBLY PEAK AXIAL POWER - CALCULATED VS MEASURED

292.04 EFPD 100(Z)FP CONTROL BANK D AT 216 STEPS WITHDRAWN

	H	G	F	E	D	C	B	A	
	1.23	1.22	1.28	1.32	1.27	1.26	1.12	.82	
8	1.24	1.23	1.28	1.33	1.29	1.26	1.14	.85	
	1.26	1.31	1.29	1.31	1.23	1.16	.87		
9	1.28	1.32	1.31	1.34	1.24	1.18	.89		
	1.29	1.31	1.26	1.25	1.08	.76			
10	1.31	1.32	1.28	1.27	1.11	.79			
	1.27	1.28	1.18	1.06	.64				
11	1.28	1.30	1.20	1.07	.66				
	1.21	1.17	.92						
12	1.24	1.19	.97						
	1.10	.57	CALCULATED						
13	1.15	.63	MEASURED						

Figure 11-79

SEQUOYAH 1 CYCLE 1 ASSEMBLY PEAK AXIAL POWER - CALCULATED VS MEASURED

378.92 EFPD 100(%)FP CONTROL BANK D AT 222 STEPS WITHDRAWN

	H	G	F	E	D	C	B	A	
	1.19	1.20	1.24	1.30	1.26	1.27	1.15	.86	
8	1.22	1.22	1.27	1.34	1.28	1.29	1.17	.90	
	1.23	1.29	1.26	1.30	1.23	1.19	.89		
9	1.26	1.33	1.30	1.34	1.25	1.22	.93		
	1.26	1.30	1.25	1.26	1.11	.80			
10	1.29	1.33	1.28	1.30	1.14	.84			
	1.26	1.28	1.20	1.09	.67				
11	1.28	1.32	1.23	1.11	.69				
	1.22	1.19	.94						
12	1.26	1.24	1.00						
	1.11	.59	CALCULATED						
13	1.19	.67	MEASURED						

Figure 11-80

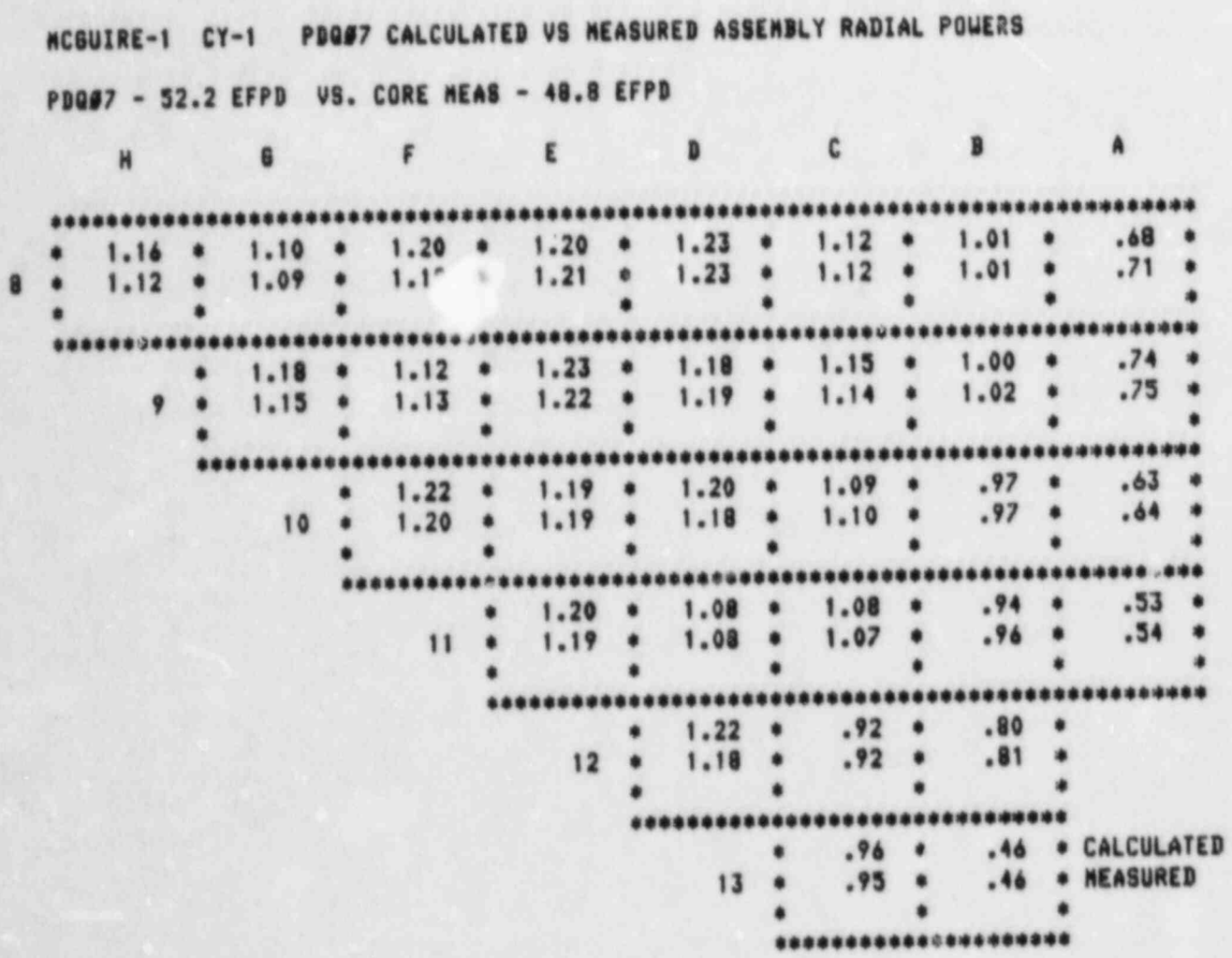
MCGUIRE-1 CY-1 PDQ#7 CALCULATED VS MEASURED ASSEMBLY RADIAL POWERS
PDQ#7 - 52.2 EFPD VS. CORE MEAS - 48.8 EFPD
H G F E D C B A
8 1.16 1.10 1.20 1.20 1.23 1.12 1.01 .68
1.12 1.09 1.1 1.21 1.23 1.12 1.01 .71
9 1.18 1.12 1.23 1.18 1.15 1.00 .74
1.15 1.13 1.22 1.19 1.14 1.02 .75
10 1.22 1.19 1.20 1.09 .97 .63
1.20 1.19 1.18 1.10 .97 .64
11 1.20 1.08 1.08 .94 .53
1.19 1.08 1.07 .96 .54
12 1.22 .92 .80
1.18 .92 .81
13 .96 .46 CALCULATED
.95 .46 MEASURED

Figure 11-81

MCGUIRE-1 CY-1 PDQ87 CALCULATED VS MEASURED ASSEMBLY RADIAL POWERS

PDQ87 - 104.4 EFPD VS. CORE MEAS - 100.5 EFPD

	H	G	F	E	D	C	B	A	
	1.17	1.13	1.19	1.20	1.20	1.12	1.00	.69	
8	1.15	1.15	1.19	1.23	1.19	1.12	1.00	.70	
	1.18	1.15	1.14	1.21	1.18	1.13	1.01	.74	
9	1.17	1.16	1.16	1.20	1.19	1.12	1.02	.74	
		1.20	1.19	1.18	1.09	.96	.64		
10		1.18	1.20	1.16	1.11	.96	.64		
			1.19	1.10	1.07	.94	.54		
11			1.17	1.11	1.07	.96	.53		
				1.21	.94	.80			
12				1.18	.94	.80			
					.96	.47		CALCULATED	
13					.94	.47		MEASURED	

Figure 11-82

MCGUIRE-1 CY-1 PDQ#7 CALCULATED VS MEASURED ASSEMBLY RADIAL POWERS

PDQ#7 - 156.7 EFPD VS. CORE MEAS - 150.2 EFPD

	H	G	F	E	D	C	B	A	
	1.17	1.15	1.18	1.19	1.17	1.12	1.00	.70	
8	1.15	1.17	1.17	1.21	1.17	1.13	1.00	.71	
		1.17	1.15	1.18	1.17	1.12	1.02	.75	
	9	1.15	1.17	1.17	1.19	1.10	1.03	.74	
			1.18	1.18	1.16	1.10	.96	.65	
		10	1.16	1.20	1.14	1.11	.95	.65	
				1.17	1.11	1.07	.95	.55	
			11	1.16	1.12	1.06	.96	.54	
					1.20	.96	.81		
				12	1.17	.97	.81		
						.96	.49		CALCULATED
					13	.95	.48		MEASURED

Figure 11-83

MCGUIRE-1 CY-1A PDQ07 CALCULATED VS MEASURED ASSEMBLY RADIAL POWERS

PDQ07 - 208.9 EFPD VS. CORE MEAS - 198.7 EFPD

	H	G	F	E	D	C	B	A
	1.10	1.22	1.08	1.17	1.05	1.16	.99	.78
8	1.08	1.23	1.09	1.19	1.06	1.18	.99	.79
	1.22	1.09	1.20	1.06	1.17	1.05	1.18	.76
9	1.22	1.08	1.20	1.06	1.18	1.05	1.17	.76
	1.07	1.19	1.06	1.18	1.06	1.16	.95	.72
10	1.07	1.19	1.06	1.19	1.06	1.16	.93	.72
	1.14	1.04	1.17	1.08	1.22	1.04	1.03	.54
11	1.17	1.04	1.18	1.08	1.22	1.04	1.03	.54
	.98	1.12	1.04	1.21	1.20	1.15	.83	
12	.99	1.13	1.04	1.21	1.17	1.13	.83	
	.96	.98	1.12	1.03	1.14	1.02	.58	
13	.99	.98	1.14	1.02	1.12	1.01	.58	
	.91	1.11	.91	1.01	.82	.58		
14	.91	1.11	.91	1.01	.82	.57		
	.73	.72	.69	.53	CALCULATED			
15	.74	.72	.70	.53	MEASURED			

Figure 11-84

SEQUOYAH-1 CY-1 PDQ#7 CALCULATED VS MEASURED ASSEMBLY RADIAL POWERS

PDQ#7 - 103.6 EFPD VS. CORE MEAS - 101.6 EFPD

	H	G	F	E	D	C	B	A	
	1.16	1.08	1.17	1.13	1.18	1.08	1.01	.71	
8	1.14	1.07	1.17	1.13	1.17	1.07	1.00	.71	
	1.17	1.12	1.19	1.17	1.17	1.14	1.02	.77	
9	1.16	1.12	1.19	1.17	1.17	1.13	1.01	.77	
		1.18	1.13	1.18	1.18	1.10	.97	.65	
	10	1.18	1.13	1.18	1.18	1.10	.98	.66	
			1.18	1.15	1.09	.91	.55		
		11	1.18	1.14	1.08	.92	.56		
				1.13	1.00	.84			
			12	1.11	1.00	.85			
					1.01	.50		CALCULATED	
				13	1.02	.51		MEASURED	

Figure 11-85

SEQUOYAH-1 CY-1 PDQ#7 CALCULATED VS MEASURED ASSEMBLY RADIAL POWERS

PDQ#7 - 155.5 EFPD VS. CORE MEAS - 133.3 EFPD

	H	G	F	E	D	C	B	A	
	1.17	1.11	1.18	1.16	1.17	1.09	1.00	.71	
8	1.13	1.09	1.18	1.16	1.15	1.08	.99	.71	
		1.18	1.16	1.19	1.18	1.12	1.02	.76	
	9	1.17	1.16	1.19	1.18	1.12	1.01	.77	
			1.19	1.16	1.17	1.10	.96	.65	
		10	1.19	1.16	1.17	1.10	.96	.66	
				1.17	1.15	1.07	.90	.55	
			11	1.16	1.14	1.06	.92	.56	
					1.11	1.00	.82		
				12	1.08	1.00	.84		
						.99	.50		CALCULATED
					13	1.00	.52		MEASURED

Figure 11-86

SEQUOYAH-1 CY-1 PDQ#7 CALCULATED VS MEASURED ASSEMBLY RADIAL POWERS

PDQ#7 - 362.7 EFPD VS. CORE MEAS - 378.9 EFPD

	H	G	F	E	D	C	B	A	
	1.04	1.04	1.09	1.15	1.11	1.13	1.01	.77	
8	1.03	1.04	1.09	1.14	1.09	1.10	1.01	.78	
	1.07	1.14	1.11	1.16	1.09	1.06	.80		
9	1.07	1.14	1.11	1.15	1.08	1.05	.81		
	1.11	1.15	1.11	1.12	.98	.72			
10	1.11	1.14	1.10	1.12	.99	.73			
	1.11	1.15	1.06	.95	.60				
11	1.10	1.13	1.05	.96	.61				
	1.08	1.05	.85						
12	1.07	1.07	.87						
	1.01	.57	CALCULATED						
13	1.03	.59	MEASURED						

12. References

1. Nuclear Associates International Corp., "Advanced Recycle Methodology Program System Documentation", CCM-3, (EPRI Confidential), September, 1977.

2. Studsvik Energiteknik AB, "CASMO-2 A Fuel Assembly Burnup Program," Studsvik/NR-81/3, 1981.

3. Duke Power Company, "Oconee Nuclear Station Reload Design Methodology," NFS-1001, Rev. 4, June 1981.

4. Bettis Atomic Power Laboratory, C. J. Pfeiffer, "PDQ-7 Reference Manual II," WAPD-TM-947(L), February 1971.

5. Rothleder, B. M., Fisher, J. R., "EPRI-NODE-P," EPRI-ARMP System Documentation, CCM-3, Part II, Chapter 14, September 1977.

6. Verbuk, P., Hoppe, N., "COMETHE-IIIJ A Computer for Predicting Mechanical and Thermal Behaviour of a Fuel Pin", BN 7609.1, Belgonucleaire S. A., March 1977.

7. TACO2 - Fuel Pin Performance Analysis, BAW-10141, Babcock & Wilcox, Lynchburg, Virginia, August 1979.

8. Cobb, W. R., Eich, W. J., Tivel, D. E., "EPRI-CELL Code Description," EPRI-ARMP System Documentation, CCM-3, Part II, Chapter 5, October 1978.

9. Edenius, M., Ekberg, K., Haggblom, H., "CASMO - THE DATA LIBRARY," Studsvik/K2-81/491, 1981.

10. Cobb, W. R., Tivel, D. E., "EPRI-CELL: GAM-THERMOS Library Descriptions," EPRI-ARMP System Documentation, CCM-3, Part II, Chapter 2, April 1976.

11. Rothleder, B. M., Poetschat, G. R., "NUPUNCHER Code Description," EPRI-ARMP System Documentation, CCM-3, Part II, Chapter 8, October 1975.

12. Duke Power Company, "MULTIFIT User Documentation," (Proprietary), February 1983.

13. Hebert, M. J., et., al., "PROGRAM C-HA-R-T CASMO to HARMONY Tableset Conversion Processor," YAEC-1313P, May 1982.

14. Rothleder, B. M. et. al., "PWR Core Modeling Procedures for Advanced Recycle Methodology Program," RP-976-1, August 1979.

15. Rothleder, B. M., Poetschat, G. R., "EPRI-FIT Code Description," EPRI-ARMP System Documentation, CCM-3, Part II, Chapter 10, October 14 1975.

16. Rothleder, B. M., Poetschat, G. R., "SUPERLINK-P Code Description," EPRI-ARMP System Documentation, CCM-3, Part II, Chapter 12, October 22 1975.

17. Smith, M. L., "PDQ7V2P7," (Proprietary), Virginia Electric and Power Company, December 1977.

18. McGuire Nuclear Station, Units 1 and 2, Final Safety Analysis Report, Docket Nos. 50-369,-370.

19. Catawba Nuclear Station, Units 1 and 2, Final Safety Analysis Report, Docket Nos. 50-413,-414.

20. Letter, W. O. Parker to H. R. Denton, "Oconee Reload Design Methodology Topical Report," Question 3, Docket Nos. 50-269,-270,-287, November 13 1980.

21. Duke Power Company, "Administrative Policy Manual for Nuclear Stations", Revision 21, August 1 1983.

22. Duke Power Company, "PDQEDIT User Documentation," (Proprietary), March 1982.

23. Morita, T., et al, "Topical Report Power Distribution Control and Load Following Procedures", WCAP-8385 (Proprietary), Westinghouse Electric Corporation, September 1974.

24. Duke Power Company, "Computer Code Users Manual for the NODE Utility Code (NUC) - Margins", Revision 2, (Proprietary), September 24 1982.

25. D. B. Owen, "Factors For One-Sided Tolerance Limits And For Variables Sampling Plans," SCR-607, Sandia Corporation Monograph, March 1963.

26. Shanstrom, R. T., et al, "CORE Codes for Operating Reactor Evaluation", SNA1617 (Proprietary), Shanstrom Nuclear Associates, April 1982.

27. American National Standards Institute, Inc., "Assessment of the Assumption of Normality (Employing Individual Observed Values)," ANSI N15.15-1974, 1974.

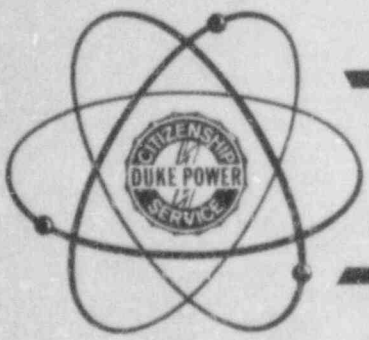
CITIZENSHIP
DUKE POWER
SERVICE